Image Cover Sheet

CLASSIFICATION UNCLASSIFIED	**SYSTEM NUMBER** 150979

TITLE

THE PACIFIC ECHO SEA TRIALS DREP.NRL: 1986-92

System Number:

Patron Number:

Requester:

Notes:

DSIS Use only:

Deliver to: FF

Defence Research
Establishment Pacific

Centre de recherches
pour la défense pacifique

DEFENSIO PER SCIENTIAM

[redacted]

DEFENCE RESEARCH ESTABLISHMENT PACIFIC
Research and Development Branch
Department of National Defence

Canada

[redacted]

Defence Research Establishment Pacific
Centre de recherches pour la défense pacifique

DEFENCE RESEARCH ESTABLISHMENT PACIFIC

CFB Esquimalt, FMO Victoria, B.C. VOS 1BO

Technical Memorandum 94- 151

THE PACIFIC ECHO SEA TRIALS
DREP/NRL: 1986-92

by

N.R. Chapman, J.A. Fawcett and M.L. Yeremy

December 1994

Approved by:

CHIEF

Research and Development Branch
Department of National Defence

Canada

Abstract

The PACIFIC ECHO sea trials comprised a series of collaborative experiments between the Defence Research Establishment Pacific and the Naval Research Laboratory from 1986-92. The general objective of the experiments was to investigate matched field processing for source localization and geoacoustic inversion. The experiments were carried out in thin sediment environments in the North Pacific. Much of the data analysis carried out at DREP over the years has been reported primarily at meetings of Technical Panel TTCP GTP-9, and has not been widely distributed. This report provides a brief summary of the PACIFIC ECHO sea trials, and includes the collection of DREP papers on the analysis of the PACIFIC ECHO data in appendices.

1. Introduction

The Ocean Acoustics Group at the Defence Research Establishment Pacific (DREP) collaborated with the Naval Research Laboratory (NRL), Washington, D.C., in a series of four sea trials known as PACIFIC ECHO during the period 1986-92. The general objective of the experiments was to investigate matched field source localization (MFSL) using vertical and horizontal line arrays at thin sediment sites in the North Pacific. Each laboratory made roughly equal contributions of assets and personnel to the sea trials, and carried out its own analysis of the data. Much of the data analysis carried out over the years at DREP has primarily been reported at meetings of TTCP Technical Panel GTP-9, but there has not been wide distribution of this work in the open literature. It is the purpose of this Technical Memorandum to provide a summary of the PACIFIC ECHO sea trials, and to present the collection of DREP papers that were given at the various meetings.

At the time that the collaborations were conceived, matched field processing (MFP) was in its infancy. There had been some initial research using simulations to determine the expected performance of MFP for source localization for various different processors[1-3], and there were generally high expectations among the believers. In order to promote the concept further, an experimental verification of the technique was needed. The PACIFIC ECHO sea trials were designed to provide an experimental demonstration of matched field source localization in the ocean.

The specific focus of the PACIFIC ECHO experiments was the performance of MFSL in thin sediment environments. This type of bottom is characteristic of large areas of the North Pacific (Figure 1). However, there was very sparse information about the geoacoustic properties of the thin sediment/upper crust environment, and the effect of this type of bottom on low frequency sound propagation in the ocean was not well understood. As a consequence, the PACIFIC ECHO experiments were carefully designed to acquire the necessary geoacoustic information for processing the source localization data at each site. The central focus of this aspect of the project was an investigation to determine the effect of geological age on the sound speed in upper oceanic crust (layer 2A).

In the remainder of this report, each of the four PACIFIC ECHO sea trials is described briefly, and the results are summarized in order to provide an overall picture of the collaborative experiments. At the end of the report, the DREP papers on the PACIFIC ECHO data analysis are reproduced in appendices. These include six papers on source localization:

Appendix A1: 'Low frequency propagation in a thin sediment North Pacific environment', N.R. Chapman and M.L. McKirdy, presented at the 18th Meeting of TTCP GTP-9, DREP, Victoria, B.C., Nov. 1989.

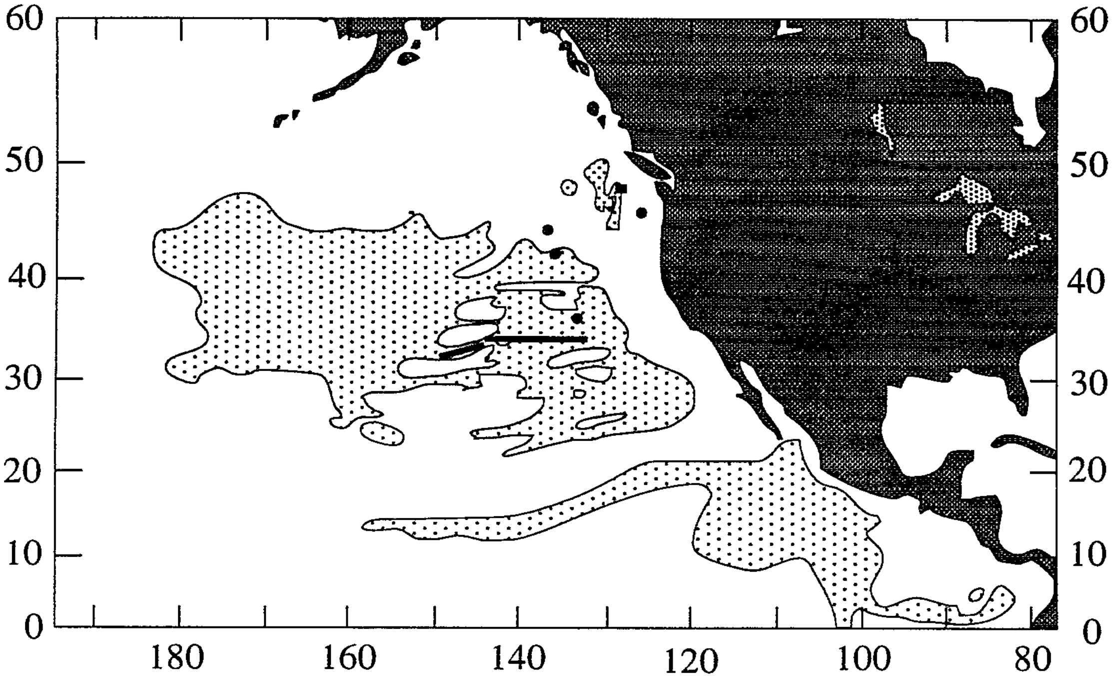

Figure 1. Distribution of thin sediment (< 70 m), shown by the dotted areas, in the North Pacific, and the locations of the sea trials: PACIFIC ECHO (closed circles), ECHO II (track at 34° N), ECHO III (closed square), and ECHO IV (track to 150° W).

Appendix A2: 'Matched field source localization in a deep ocean rough bottom environment', J.A. Fawcett, N.R. Chapman and M.L. McKirdy, presented at the 18th Meeting of TTCP GTP-9, DREP, Victoria, B.C., November, 1989.

Appendix A3: 'Matched field processing with PACIFIC ECHO sea trial data', J.A. Fawcett, N.R. Chapman and M.L. McKirdy, presented at 19th Meeting of TTCP GTP-9, DSTO, Adelaide, Australia, October, 1990.

Appendix A4: 'Matched field source localization using broadband shot data', N.R. Chapman and M.L. McKirdy, presented at 20th Meeting of TTCP GTP-9, NUSC, New London CT, October, 1991.

Appendix A5: 'Matched field source localization with a horizontal line array', N.R. Chapman and M.L. Yeremy, presented at 21st Meeting of TTCP GTP-9, ARE, Portland, UK, October, 1992.

Appendix A6: 'Low SNR matched field processing in a range dependent environment', J.A. Fawcett, M.L. Yeremy and N.R. Chapman, presented at 22nd Meeting of TTCP GTP-9, DREA, Dartmouth, NS, October, 1993.

In addition, two papers on matched field inversion for geoacoustic properties are also reproduced:

Appendix B1: 'Matched field inversion for geoacoustic profiles of upper oceanic crust', N.R. Chapman and M.L. Yeremy, presented at 2nd European Conference on Underwater Acoustics, Copenhagen, Denmark, July, 1994.

Appendix B2: 'Matched field inversion for geoacoustic properties of young ocean crust', N.R. Chapman and K.S. Ozard, presented at NATO conference on Full Field Inversion Methods in Ocean and Seismic Acoustics, La Spezia, Italy, June, 1994.

2. Pacific Echo Sea Trials

2.1 General Background

The major resource contribution from each laboratory was a research ship. DREP contributed its vessel, CFAV ENDEAVOUR, and NRL provided the USNS DESTEIGUER. The receivers used in all the experiments were the DREP research arrays COAMS (Canadian Ocean Acoustic Measurement System) and MEVA (Multi-Element Vertical Array). COAMS is a 128-channel towed horizontal line array (HLA), consisting of four nested arrays spanning the frequency range from 20 Hz (VLF) to 160 Hz. The VLF array, consisting of the full 1.5-km aperture with 40-channels, was used for all the PACIFIC ECHO data processing. There were two versions of MEVA, a 16-element, 675-m vertical line array (VLA) with 45-m element spacing, and a similar system with a total aperture of 45 m and 3-m spacing. (The latter array was only used in the first sea trial for MF (100-300 Hz) source localization experiments designed by NRL, and for downslope propagation experiments by DREP).

The arrays were deployed and monitored from CFAV ENDEAVOUR, which was designated as the receiving ship, and carried scientists from both DREP and NRL for the purposes of recording data for each laboratory. Only one array system was deployed at a time, either COAMS or MEVA. USNS DESTEIGUER was used as the source ship, and deployed the various sound sources that were used in the experiments. These included the MK-VI VLF and HLF-2 MF sound sources from NRL, and the moving coil projector VLF source from DREP. DESTEIGUER also deployed 0.8 kg SUS (Signals underwater Sound) charges for broadband sources in the propagation and localization experiments.

The Chief Scientist from DREP was Ross Chapman, who planned the experiments, in collaboration with the US scientists, and participated in all the sea trials. The entire effort was shared by all of the members of the Ocean Acoustics Group, and most of them participated in one or more sea trials. The DREP personnel included Dave Thomson, Gordon Ebbeson, Brian Maranda, John Fawcett, Garry Heard, Tony Hoffmann, Brian Burger, Carl Kelly, Bruce Freguson, Mark Rowsome, Tim Popoff, Maureen Yeremy and

Derek Hankel. The NRL group was led by Orest Diachok and Ron Dicus who proposed the original experiment, and participated in planning the others. NRL personnel who sailed on CFAV ENDEAVOUR included Ron Dicus, Dick Fizell, Basil Decina, Bob Lee, George Vermillion, John Schafer, John Wolf and Bob O'Connor.

2.2 PACIFIC ECHO: May-June 1986

The specific objective of this sea trial was to investigate MFSL performance with vertical and horizontal line arrays at a thin sediment site in the North Pacific. Because low frequency sound propagation had not been studied extensively at thin sediment/rough bottom environments, a thick sediment abyssal plain site, for which the propagation was better understood, was included in the exercise plan in order to provide a 'controlled' environment. The experiments were carried out using COAMS and both versions of MEVA as receiving arrays, and the MK-VI, the HLF-2 and SUS charges as sound sources. The sites are summarized in Table I.

Table I. PACIFIC ECHO sites.

Site Location	Description	Depth (m)
37° 30' N 133° W	Thin sediment/upper crust	5100
44° N 137° W	Abyssal Plain	4200
42° N 136° W	Thin sediment, abyssal hill	4400
45° N 127° W	Continental slope	2700

At each site, VLF source localization experiments were carried out at frequencies of 10 and 15 Hz, using the 675-m VLA which was suspended in the deep sound channel. Broadband shot runs were also performed in order to study the acoustic propagation at the site, in particular the interaction with the bottom. These data were used to derive geoacoustic models of the bottom for use in processing the MFSL data. A source localization experiment using the towed HLA in a pseudo-stationary geometry was carried out at the primary thin sediment site. In addition to these core experiments, NRL carried out broadband localization trials with the HLF-2 MF source, using the 45-m VLA.

An experimental approach using the HLA for measurement of the compressional wave critical angle in the upper crust was also investigated. Two trials were performed, one using a VLF FM sweep signal (at the primary thin sediment site), and another using broadband SUS charges (at the abyssal hills site). At the completion of the matched field experiments, DREP carried out broadband downslope propagation experiments using the 45-m VLA at the Cascadia Basin /continental slope site.

2.3 PACIFIC ECHO II: Oct-Nov 1988

The objective of the second PACIFIC ECHO sea trial was to investigate the effect of geological age on the properties of mid-age upper oceanic crust, 40-60 million years (m.y.), at selected thin sediment sites. The measurements were made using the COAMS HLA at 12 stations along 34° N from 130° W to 144° W. The bathymetry in this region is characterized by a series of low ridges 50-100 m high, with axes parallel to the spreading centre (roughly 346°, ~14° off true north). The site locations and environments are summarized in Table II. The method used was based on the broadband reflectivity measurement (BRM) technique which was investigated in the first sea trial. Two ships were used: CFAV ENDEAVOUR towed the HLA while USNS DESTEIGUER opened range on a course at approximately 35° to the ENDEAVOUR course (Figure 2). On the outbound leg, DESTEIGUER deployed SUS charges and on the inbound leg, the MK-VI sound source broadcast a tone at 15 Hz. The experimental geometry was designed so that the acoustic propagation path was parallel to the axes of the sea floor ridges. However, at two sites, additional runs were carried out to investigate the effect of propagation perpendicular to the ridges; these sites are indicated by an asterisk (*) in the table. In addition to these geoacoustic experiments, a pseudo-stationary source localization experiment was carried at one station.

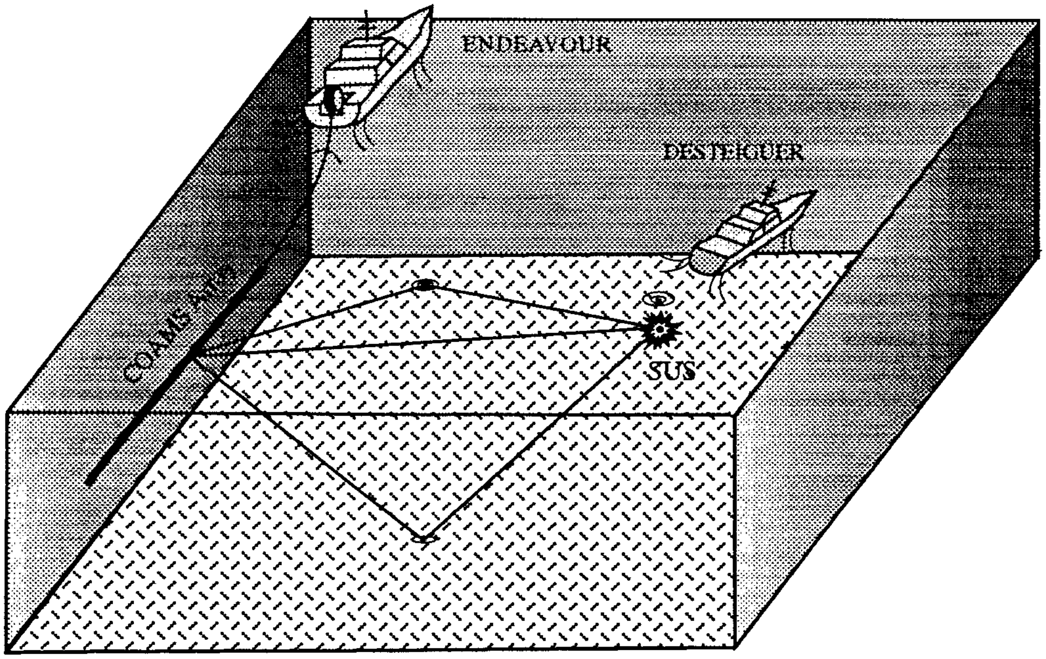

Figure 2. Geometry of the BRM shot runs.

Table II. PACIFIC ECHO II sites.

Site Location	**Age (m.y.)**	**Sediment Thickness (m)**	**Depth (m)**
* 34° N 130° 10' W	40	< 25	5030
34° N 131° 55' W	42	33	5100
34° N 136° 11' W	49	23	5010
34° N 137° 41' W	50	22	5050
34° N 138° 22' W	52	15	5080
* 34° N 138° 18' W	52	24	5080
34° N 138° 41' W	52	< 25	5180
34° N 140° 01' W	56	< 25	5145
34° N 141° 02' W	59	< 25	5030
34° N 142° 27' W	61	28	5300
34° N 143° 18' W	63	15	5540
34° N 144° 06' W	66	36	5360

2.4 PACIFIC ECHO III: July 1991

The objectives of this sea trial were threefold: to investigate the geoacoustic properties of very young crust; to investigate MFSL in complex bathymetric environments using the VLA; and to initiate a study of matched field inversion for geoacoustic properties. The experiments were carried out at three sites at the Juan de Fuca Ridge in the vicinity of the spreading centre (Table III), using the COAMS HLA and the 675-m VLA as receivers, and the DREP moving coil projector and SUS charges as sound sources.

Table III. PACIFIC ECHO III sites.

Site Location	**Age (m.y.)**	**Sediment Thickness (m)**	**Depth (m)**
47° 59' N 129° 8' W	0.1	< 5	2200
48° 3' N 129° 20' W	0.7	19	2400
47° 59' N 129° 33' W	1.5	22	2600

In addition to the BRM experiments, expanding spread profiles were carried out at each site using SUS charges and the HLA. This type of experiment is a standard technique used by marine geophysicists; it has the advantage that the reflection point for each shot is the same, whereas the BRM effectively measures average properties over the track of the experiment. Measurements were made at three thin sediment sites over which the crustal age increased from ~0.1 to 1.5 m.y.

At the oldest site, an experiment was carried out with the VLA using VLF tones to investigate the concept of environmental signal processing[4]. The idea is that a complex ocean environment can be exploited to provide an estimate of the source bearing for MFSL with a VLA, since the cylindrical symmetry of the sound propagation is broken. The VLF source was towed in a series of arcs from 5.5 to 102 km (Figure 3). The data from the close range arc was also used to investigate MF inversion. For this case, the experimental geometry is known and the acoustic field data were inverted for geoacoustic properties, using simulated annealing as an efficient global search technique.

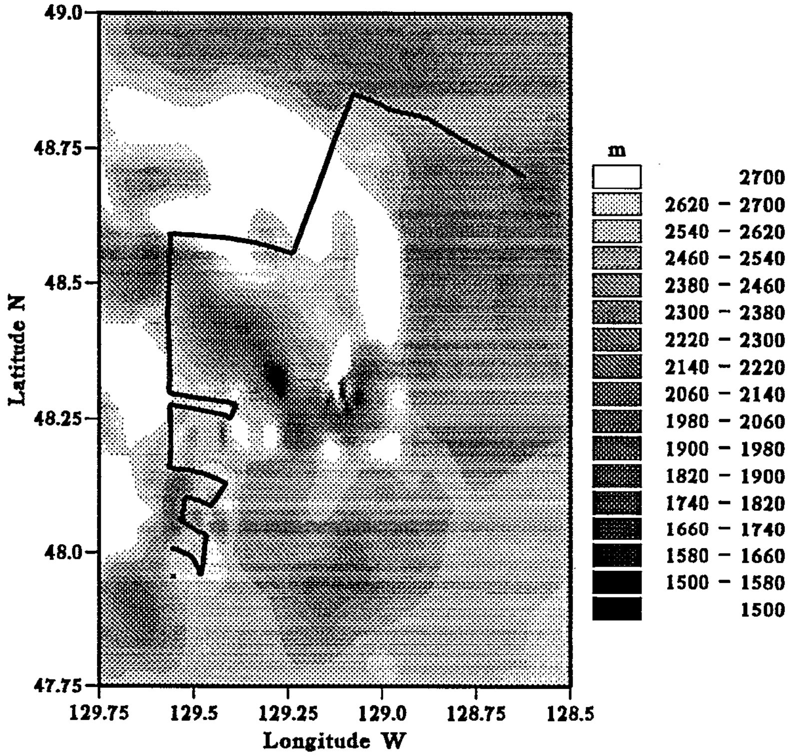

Figure 3. Source ship track and bathymetry for the VLA source localization experiments in PACIFIC ECHO III. The location of the VLA is indicated by the dot.

2.5 PACIFIC ECHO IV: May/June 1992

The objective of this sea trial was to extend the investigation of the effect of geological age to old oceanic crust. The experiments were carried out with the COAMS HLA, using the same geometries as in PACIFIC ECHO III, i.e. a BRM and an expanding spread profile at each site. In this sea trial, the source ship was the Canadian research vessel, CSS JOHN P. TULLY. After the ECHO experiments were completed, the Ocean Acoustics Group carried out additional DREP source tracking experiments with COAMS.

The analysis of data from PACIFIC ECHO II indicated a significant increase in the sound speed at the westernmost site along the track[5]. In consideration of this result, the ECHO IV experiments started at the end of the ECHO II track and continued along a track to the south west out to 148° 51' W, following a recent NRL/Scripps survey line. Five measurements were made at sites where the age of the crust increased from 66 to 78 m.y. These measurements concluded the investigation of the effect of geological age. The sites are described in Table IV.

Table IV. PACIFIC ECHO IV sites.

Site Location	**Age (m.y.)**	**Sediment Thickness (m)**	**Depth (m)**
33° 23' N 143° 56' W	66	39	5360
33° 7' N 145° 14' W	69	57	5500
32° 59' N 146° 4' W	72	49	5560
32° 48' N 146° 53' W	74	50	5600
32° 21' N 148° 51' W	78	44	5600

3. PACIFIC ECHO RESULTS

3.1 PACIFIC ECHO

The first PACIFIC ECHO sea trial provided a very rich data set that was analyzed throughout the entire program. The initial effort at DREP was concentrated on the environmental acoustics at the primary thin sediment site. The results of the analysis of the broadband propagation loss data carried out to obtain the geoacoustic model of the bottom for the thin sediment site are reproduced in Appendix A1. These data were recorded using the long VLA, and were processed to obtain the bottom reflection loss. The loss versus angle information was inverted using a non linear inversion algorithm to estimate the bottom properties, assuming a plane reflection boundary[6]. The initial analysis in Appendix A1 for the 25-Hz band obtained an estimate of 3.4 km/s for the compressional wave speed in the basalt. Subsequent analysis at lower frequencies, where the effects of scattering at the rough bottom were less significant, estimated a slightly lower value of 2.9 km/s[7]; the lower value was used in th MFP studies in Appendices A3-A5. The estimate obtained by NRL from the compressional wave critical angle measurement was intermediate between the two DREP results[8]. The effect of the rough bottom on MFP was investigated using simulations in the paper presented in Appendix A2.

Generally, good localization performance was obtained for all the experimental geometries at the thin sediment site. The first analysis of the narrowband VLA data is reproduced in Appendix A3; this paper demonstrated that MFSL was sensitive to the array tilt. Performance was improved by searching over the VLA tilt angles to obtain the highest MF correlation. An ambiguity surface for the 10-Hz data obtained using the Bartlett MF processor is shown in Figure 4; the maximum at 110 m depth and 36.5 km range is very close to the true source position. The MF correlation at the peak is 0.79. Broadband MFP was applied to the shot data that were obtained with the VLA. The analysis presented in Appendix A4 investigated the issue of frequency averaging in MFP, and the performance limits on the use of a restricted mode sum in calculating the replica fields. Source localization with a HLA is the subject of Appendix A5. This paper demonstrated that good performance was obtained using a pseudo-stationary source/receiver geometry, with the source near the aft endfire beam.

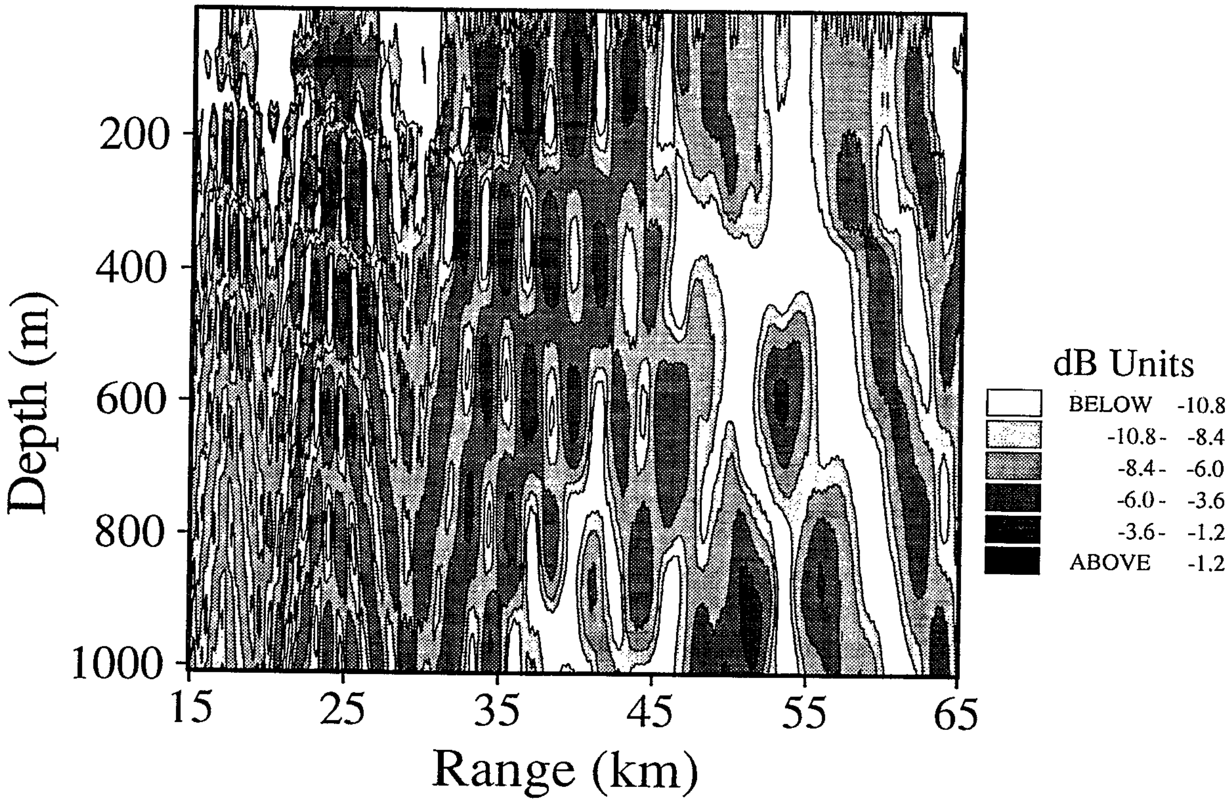

Figure 4. Range-depth ambiguity surface for a 3-minute data sample for the 10-Hz source. A tilt angle of 1° was used for the replica calculations. The true source position is at a range of 36.8 km and a depth of 100 m.

An initial investigation was carried out using the broadband shot data recorded on the VLA to develop a method for matched field inversion for geoacoustic properties. For a known experimental geometry, the properties of the waveguide can be inverted using MFP and an efficient global search technique to search the model parameter space[9-13]. In this study, presented in Appendix B1, the shot data for a bottom bounce range of 17 km were processed to obtain the spectral component at 20 Hz and inverted using MFP with simulated annealing. The results were consistent with expected values for basalt of similar age[14,15], and with the reflection coefficient inversions at the site[7,8]. The geoacoustic model, consisting of 13 parameters, that was inverted from the data is shown in Figure 5.

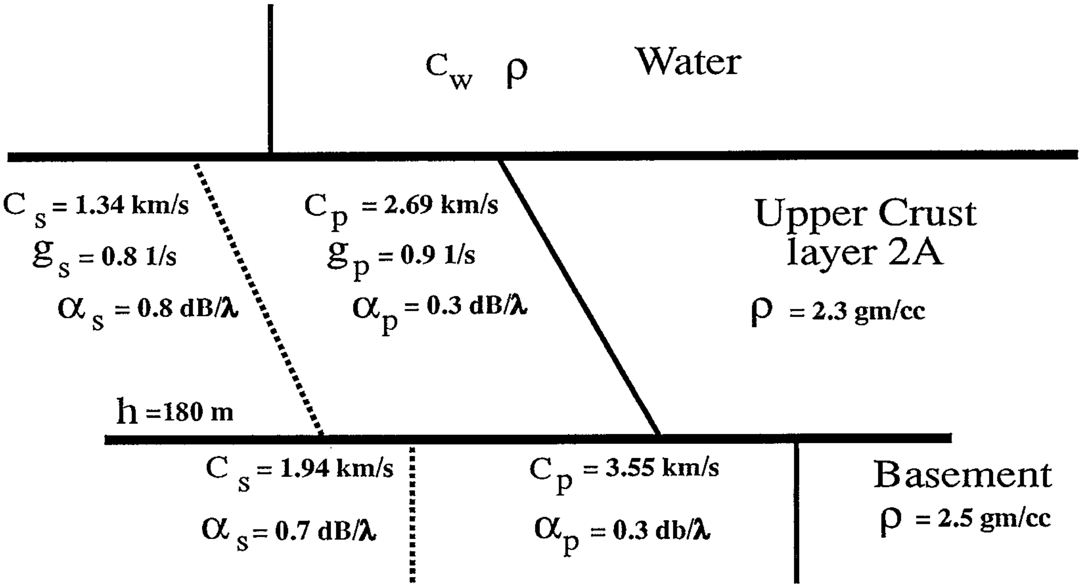

Figure 5. Estimated values for the geoacoustic model parameters of the upper crust model for the primary thin sediment site (PACIFIC ECHO).

3.2 PACIFIC ECHO II

The bottom reflectivity data were processed to obtain the reflection loss versus grazing angle in 1/3 octave bands from 8-128 Hz for sites 2 to 13 from 130° W to 144° W[16]. The age of the upper crust (Layer 2A) increased from 42 to 66 m.y. over this portion of the track. An example of the reflectivity data is shown in Figure 6 where the processed array beam time series for the 1/3 octave band at 128 Hz are plotted versus time; intensity is indicated by the gray shade. The effect of scattering from the rough bottom is evident in the large angular spread of the acoustic energy for the first and second bottom reflection paths. The reflection coefficient data for the 8-Hz band were inverted using a global search technique to estimate the compressional and shear speeds in the upper crust as a function of geological age[5,17]. The results are shown in Figure 7, where the sound speeds are plotted versus age of the crust. There is a moderate increase with age out to 63 m.y., followed by a significant change of ~1.5 km/s in the compressional speed at the final site at the end of the track. This behaviour supports the model that the aging process of hydrothermal circulation is continuing at thin sediment sites located at large distances from the spreading centre[14,15], out to at least 144° W.

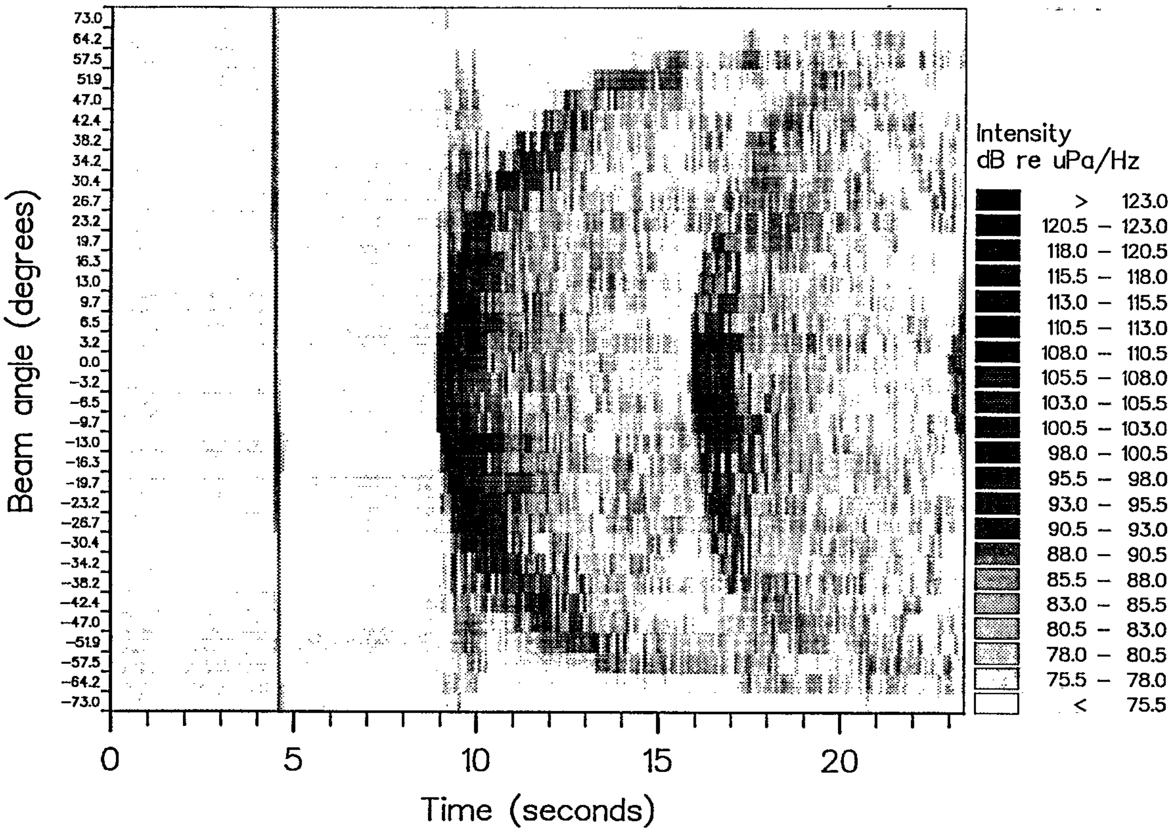

Figure 6. Array beam time series for the beams from forward (top) to aft (bottom) endfire. The first (9 s) and second (16 s) bottom reflections are shown for a shot at a range of 4.6 km. The direct path is at 4.8 s.

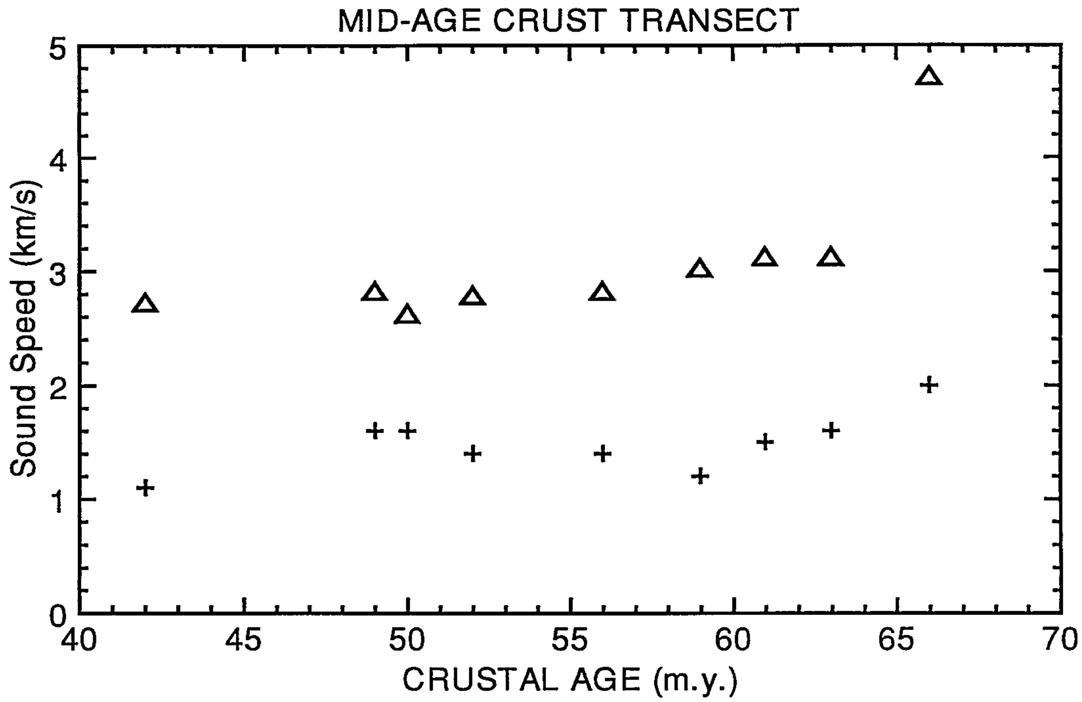

Figure 7. Layer 2A sound speeds (compressional Δ ; shear +) versus geological age for the mid-age transect at 34° N (PACIFIC ECHO II).

3.3 PACIFIC ECHO III

The investigation of the effect of crustal age continued with the analysis of the bottom reflectivity data from the expanding spread profiles[18]. These data were inverted using the global search algorithm to estimate the basalt sound speeds near the Juan de Fuca Ridge spreading centre. The results presented in Figure 8 indicate that there is a significant increase in sound speed, particularly for the shear speed, over the first one or two million years. Coupled with the behaviour shown in Figure 7, the PACIFIC ECHO data suggest that a significant change occurs at very young ages (0-2 m.y.) as the large cracks in the newly formed rock are filled by hydrothermal deposition. This is followed by a slower increase with age until the hydrothermal circulation effectively ceases at the older sites where the sediment layer is thicker (> 50 m) and there is no further exchange with the ocean. The sound speeds for these sites are characteristic of mature crustal layers (4-5 km/s).

The analysis of the VLF source localization data to estimate bearing as well as range and depth for a VLA is presented in Appendix A6. The data from this experiment provided the first experimental verification of the concept of Environmental Signal Processing in MFP. The results are shown in Figure 9 where the range-bearing ambiguity surface is plotted for a data set from the 38-km arc. As can be seen in Figure 3, there is significant bathymetric variation between the array and the various source positions for the differennt azimuths along this portion of the track. There is a broad peak at a bearing of ~5°, very close to the true bearing of 6.2°.

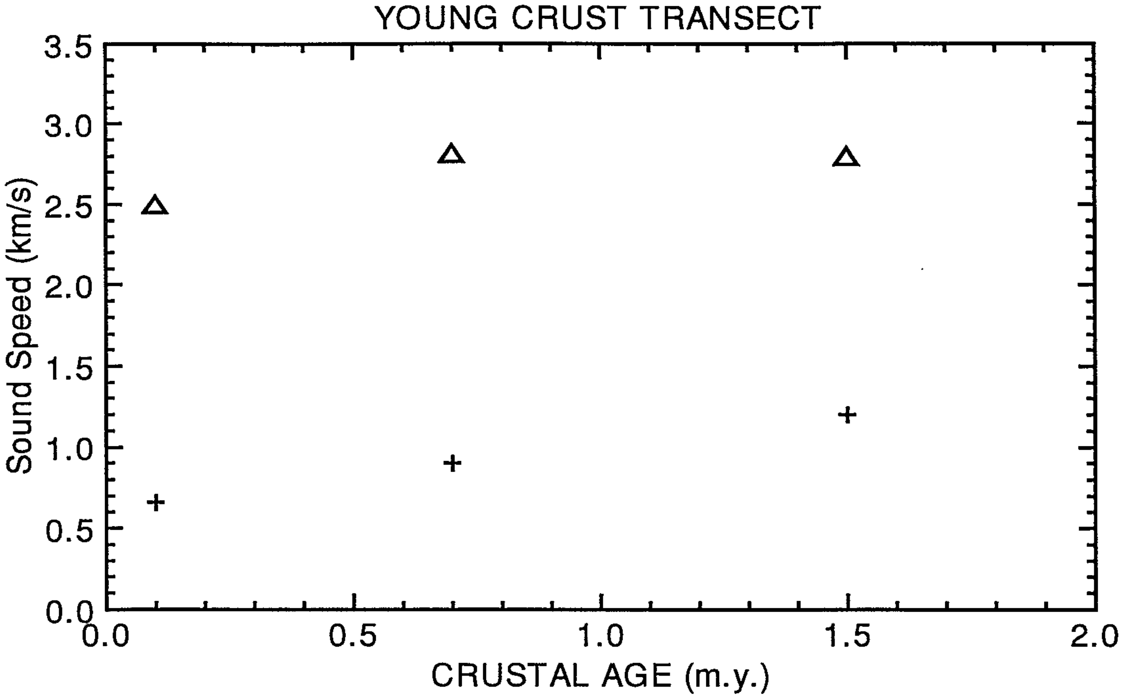

Figure 8. Layer 2A sound speeds (compressional Δ ; shear +) versus geological age for the young age transect at the Juan de Fuca Ridge, 48° N (PACIFIC ECHO III).

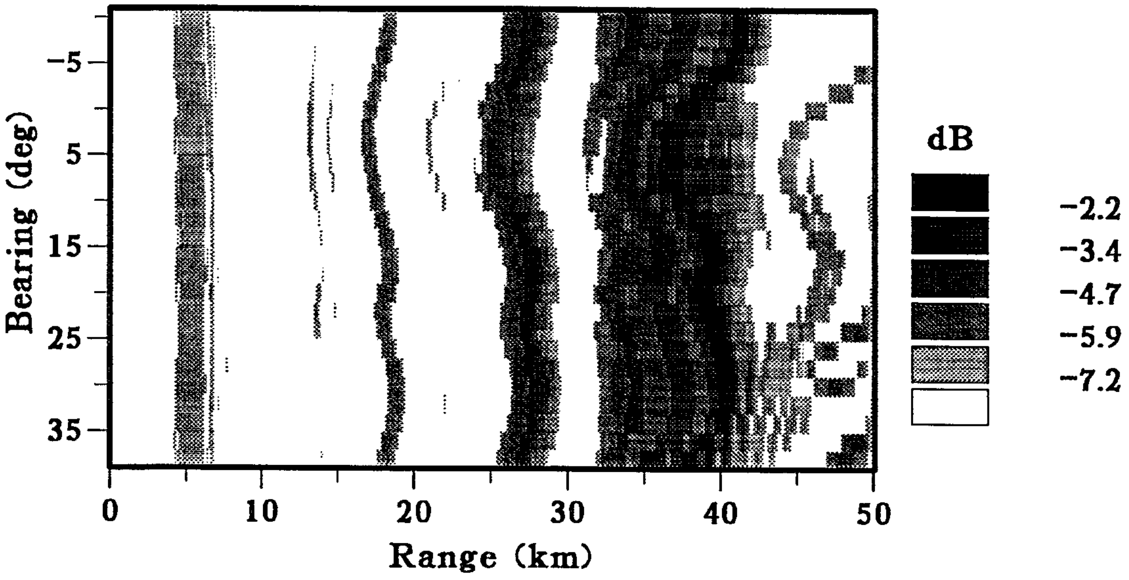

Figure 9. Range-bearing ambiguity surface for the 38 km arc. The surface is obtained for a one-minute data sample.

The data from the 5.5 km arc were inverted using MFP with simulated annealing as the global search technique to estimate the geoacoustic properties of the bottom. The analysis is presented in Appendix B2. The results were in good agreement with the estimates from the reflection coefficient inversion for the data from this site[18]. The inversion method demonstrated an effective use of the concept of focalization[19] to account for uncertainty in the experimental geometry.

3.4 PACIFIC ECHO IV

The data from the BRM and the expanding spread profiles were processed to obtain the reflection coefficient at each site[20]. This data set provided a useful comparison of the two experimental techniques. The reflection coefficient data were generally of better quality for the expanding spread experiments. Although the BRM method is an efficient survey technique, it suffers the disadvantage that the reflection point is different for each shot, and the bathymetry may vary extensively over the track of the measurement. Preliminary results for inverting the expanding spread data indicate compressional speeds from 4.0 - 5.5 km/s, consistent with the result from the last site in ECHO II.

4. Summary

The PACIFIC ECHO collaboration was a highly successful project that provided an extensive and unique data set for investigating the performance of matched field processing in real ocean environments. Both laboratories, DREP and NRL, acquired high quality data for the advancement of their research programs in matched field processing, and achieved considerable cost savings in the experiments by pooling their resources. The PACIFIC ECHO data provided the first experimental demonstrations of MFSL with vertical and horizontal arrays in the ocean, and the results provided a clear indication of the potential advantages of MFP in advanced sonar design. New concepts such as environmental signal processing and focalization were tested experimentally, and the results showed that a knowledge of the features of a complex ocean environment could be exploited to achieve further advantages with MFP. In addition, the investigation of the effect of geological age in thin sediment bottom environments provided significant new geophysical information on the evolution of the upper oceanic crust. This report presents a brief summary of the collaboration, and includes in the appendices a collection of DREP PACIFIC ECHO papers that have not previously been widely circulated.

Acknowledgement

The Ocean Acoustics Group wishes to acknowledge the asssitance of Bob Chappell from the Applied Technology Section, DREP. His contributions initially in the design of the data acquisition systems for both COAMS and MEVA, and his continued support throughout PACIFIC ECHO in preparing and setting up the electronic systems for the sea trials were critical to the ultimate succes of the project. It is also a pleasure to acknowledge the insight, enthusiasm and cooperation of the NRL scientists, in particular Orest Diachok, Ron Dicus, Basil Decina and John Wolf, throughout the entire project.

References

1. H.P Bucker, 'Use of calculated sound fields and matched-field detection to locate sound sources in shallow water', J. Acoust. Soc. Am., **59**, 368-373, 1976.
2. R.G. Fizell, 'Application of high resolution processing to range and depth estimation using ambiguity function methods', J. Acoust. Soc. Am., **82**, 606-613, 1987.
3. M.B. Porter, R.L. Dicus and R.G. Fizell, 'Simulations of matched field processing in a deep water Pacific environment', IEEE J. Oceanic Eng., **12**, 173-187, 1987.
4. W.A. Kuperman, M.B. Porter, J.S. Perkins and R.B. Evans, 'Rapid computation of acoustic fields in three dimensional ocean environments', J. Acoust. Soc. Am., **89**, 1801-1819, 1991.
5. D.E. Hannay and N.R. Chapman, 'Estimation of the geoacoustic properties of the upper oceanic crust from bottom reflection loss measurements', J. Acoust. Soc. Am., **92**, 2303, 1992.
6. N.R. Chapman, K. Stinson, S. Levy, J. Cabrera and D.W. Oldenburg, 'Estimation of the elastic properties of sea floor sediments by inversion of precritical reflection data', IEEE J. Oceanic Eng., **13**, 215-221, 1988.
7. N.R. Chapman and M.L. Yeremy, 'Inversion of geoacoustic properties in upper oceanic crust by matched field processing of acoustic field data', EOS supplement, 1992 Spring Meeting, p274, 1992.
8. P.L. Gruber and R.L Dicus, 'Low frequency measurements of bottom reflectivity at a thin sediment site in the North Pacific', J. Acoust. Soc. Am., **85**, S87, 1989.
9. M.D. Collins, W.A. Kuperman and H. Schmidt, 'Nonlinear inversion for ocean bottom properties', J. Acoust. Soc. Am., **92**, 2770-2783, 1992.
10. S.E. Dosso, M.L. Yeremy, J.M. Ozard and N.R. Chapman, 'Estimation of Ocean bottom properties by matched field processing of acoustic field data', IEEE J. Oceanic Eng., **18**, 232-239, 1993.
11. C.E. Lindsay and N.R. Chapman,'Matched field inversion for geoacoustic model parameters using adaptive simulated annealing', IEEE J. Oceanic Eng., **18**, 221-231, 1992.
12. P. Gerstoft, 'Inversion of seismoacoustic data using genetic algorithms and *aposteriori* probability distributions', J. Acoust. Soc. Am., **95**, 770-782, 1993.
13. N.R. Chapman and M.L. Yeremy, 'Estimation of seismoacoustic properties of the ocean bottom by matched field inversion', J. Acoust. Soc. Am., **93**, 2399, 1993.

14. O.I. Diachok, S. Wales, and R.L. Dicus, 'Compressional and shear wave velocities in the upper crust', in *Shear Waves in Marine Sediments*, J. M Hovem, M.D. Richardson and R.D. Stoll, editors, Kluwer Academic Publishers, Dordrecht, pp387-394, 1991.
15. N.R. Chapman and D.E. Hannay, 'Seismic velocities of upper oceanic crust', Geophys. Res. Lett., Oct 15, 1994.
16. D.E. Hannay, 'Bottom loss processing of the PACIFIC ECHO II experimental data', DREP Contractors Report 92-31, Sept. 1992.
17. D.E. Hannay and N.R. Chapman, 'Inversion of geoacoustic properties in thin-sediment environments from ocean bottom reflection loss data', Oceans 93, Vol III, 381-386, 1993.
18. D.E. Hannay, 'Bottom loss processing of the PACIFIC ECHO III experimental data', DREP Contractors Report 93-32, May, 1993.
19. M.D. Collins and W.A. Kuperman, 'Focalization: environmental focusing and source localization', J. Acoust. Soc. Am., **90**, 1410-1422, 1991.
20. D.E. Hannay, 'Bottom loss measurements from the PACIFIC ECHO IV experiment', DREP Contractors Report 94-62, April, 1994.

Low Frequency Sound Propagation in a Thin-sediment North Pacific Environment.

N.R. Chapman and M. McKirdy
Defence Research Establishment Pacific
FMO Victoria, B.C. V0S 1B0

Abstract

Measurements of propagation loss at low frequencies were obtained at a thin-sediment deep water site in the northeast Pacific. The sediment layer was of variable thickness, between 5 and 40 m over the track of the experiment, and beneath the material was upper oceanic crust. The relatively large values of propagation loss observed at ranges between 10 and 40 km can be explained as losses due to shear wave propagation in the basalt crust, using a simple model of plane wave reflection from an elastic solid bottom. The bottom reflection coefficient data were inverted using a non-linear inversion method based on the plane wave model in order to estimate the model parameters. The values obtained for the compressional and shear wave speeds and the density were in reasonable agreement with other values reported for basalt of similar geological age.

Introduction

The interaction of low frequency sound with the ocean bottom sediments has been recognized as an important aspect of sound propagation in abyssal plains and deep ocean basins, and the physics of the process is well understood[1,2]. The seabed in these regions is a layered system of sediment material which can be of the order of one kilometre in thickness. Low frequency sound penetrates this structure to a considerable depth and is refracted by the strong gradients in the sediment column. By contrast, the sea floor in regions of thin sediment cover is generally rough, with outcrops of basement rock and varying thicknesses of sediment material. The interaction of sound with this type of bottom is dominated by the reflection at the ocean basement, and the conversion of acoustic energy into shear waves in the basalt must be taken into account in modeling the propagation.

In June 1986 the Defence Research Establishment Pacific (DREP) collaborated with the Naval Research Laboratory (NRL) in the joint sea trial Pacific Echo, one of a series of experiments designed to investigate the effect of a thin-sediment bottom on the performance of matched field source localization methods. We report in this paper the results of an experiment carried out during Pacific Echo to study the interaction of low frequency sound with the bottom at a thin sediment site. Experimental measurements of the propagation loss for bottom-interacting paths were used to infer the ocean bottom reflection coefficient. A geoacoustic profile was estimated from this information, assuming that the bottom was an elastic solid representing the basalt oceanic crust. This model provides the basis for describing the bottom interaction at low frequencies. The model parameters were obtained by inverting the reflection coefficient versus angle information using a nonlinear parametric inversion technique[3].

The paper is organized in the following way. In the next two sections we describe the ocean environment at the thin sediment site, and outline the experimental method and the data processing scheme. Then the propagation loss measurements and the bottom reflection coefficient derived from these data are presented. Following this, the inversion technique is described, and we present the geoacoustic profile estimated from the data. We then investigate the sensitivity of the model to the attenuation of the compressional (P) and shear (S) waves in the oceanic basement, and also discuss the effect of the sediment layer. In the last section we summarize the results of the experiment.

Acoustic Environment

The experiment was carried out at a site in a region of abyssal hills at the eastern boundary of the Pacific plate about 900 km west of San Francisco. The water depth at the site is 5200 m, and the bottom rises about 200 m over 40 km with undulations of less than 50 m. The bathymetry measured over the track of the experiment is shown in Figure 1. The sediment layer is known to consist of deep sea clay material, and the thickness of the layer is variable with a maximum value of less than 80 m[4]. Our own estimates of the layer thickness based on the acoustic data indicate a range of values from 5 to 40 m. This layer overlies a basement substrate of ~40 million year old basalt crust. The basalt interface is a rugged surface, and the upper portion of the layer consists of pillow lavas interspersed with sediments and water. This material was generated at the ocean ridge and has subsequently been transported away from the spreading centre over periods of millions of years. It is expected that since the geophysical properties of the material have changed over this period of time, the acoustic velocities depend on the age of the basalt[5].

The sound speed profile in the water which was measured at the site is shown in Figure 2. The depth of the sound channel is about 600 m at this latitude. The acoustic field for a 25 Hz source at 244 m has been calculated for this profile using the parabolic equation method[6], and the result is shown in Figure 3. The bottom is assumed to be totally absorbing in the calculation and the range dependence has been removed in this display. For a receiver at 480 m, there is a shadow zone from about 8 to 35 km. This region is insonified by bottom reflections in a realistic bottom environment.

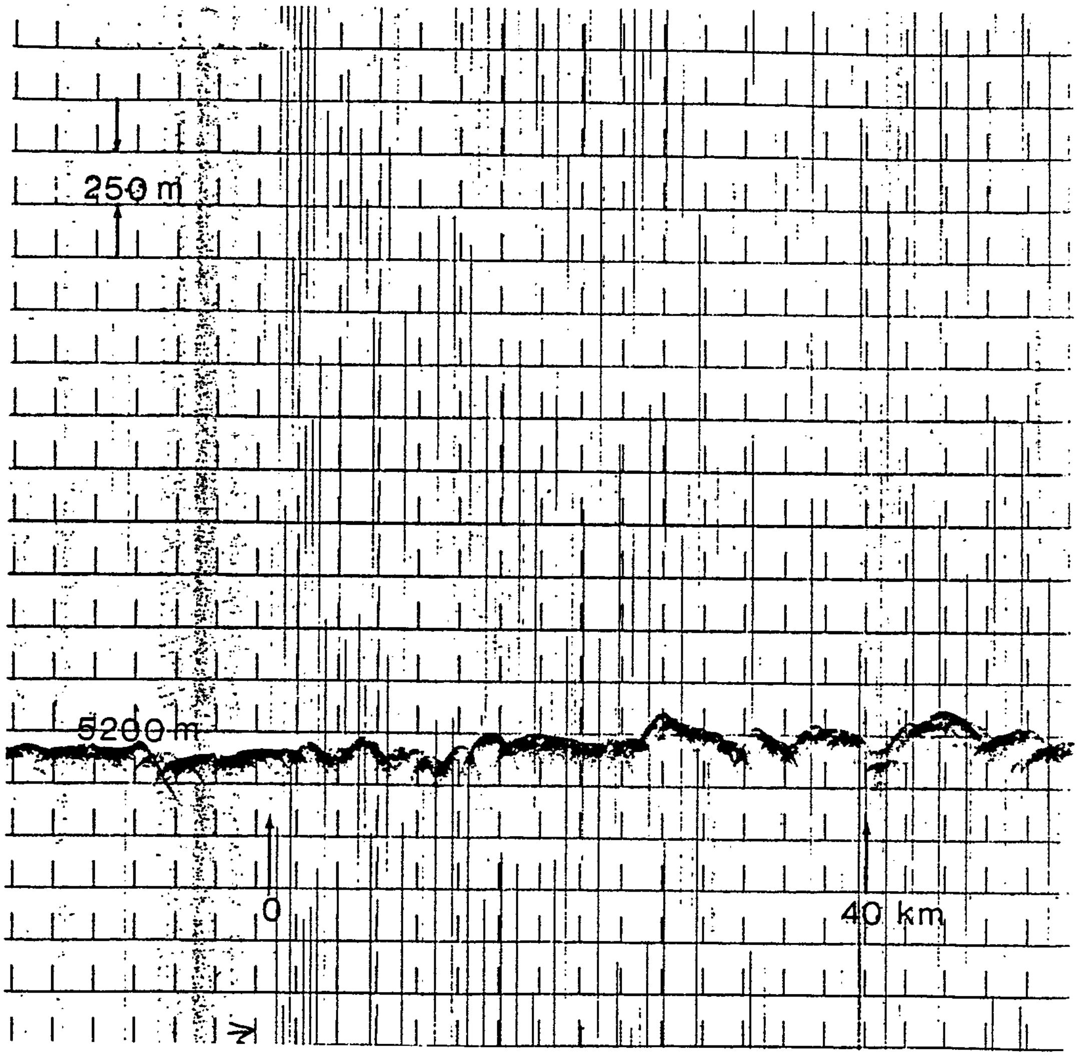

Figure 1. Bathymetry measured over the track of the experiment, using a 3.5 kHz profiler. The depth scale is 250m/division, and the average depth is 5200 m.

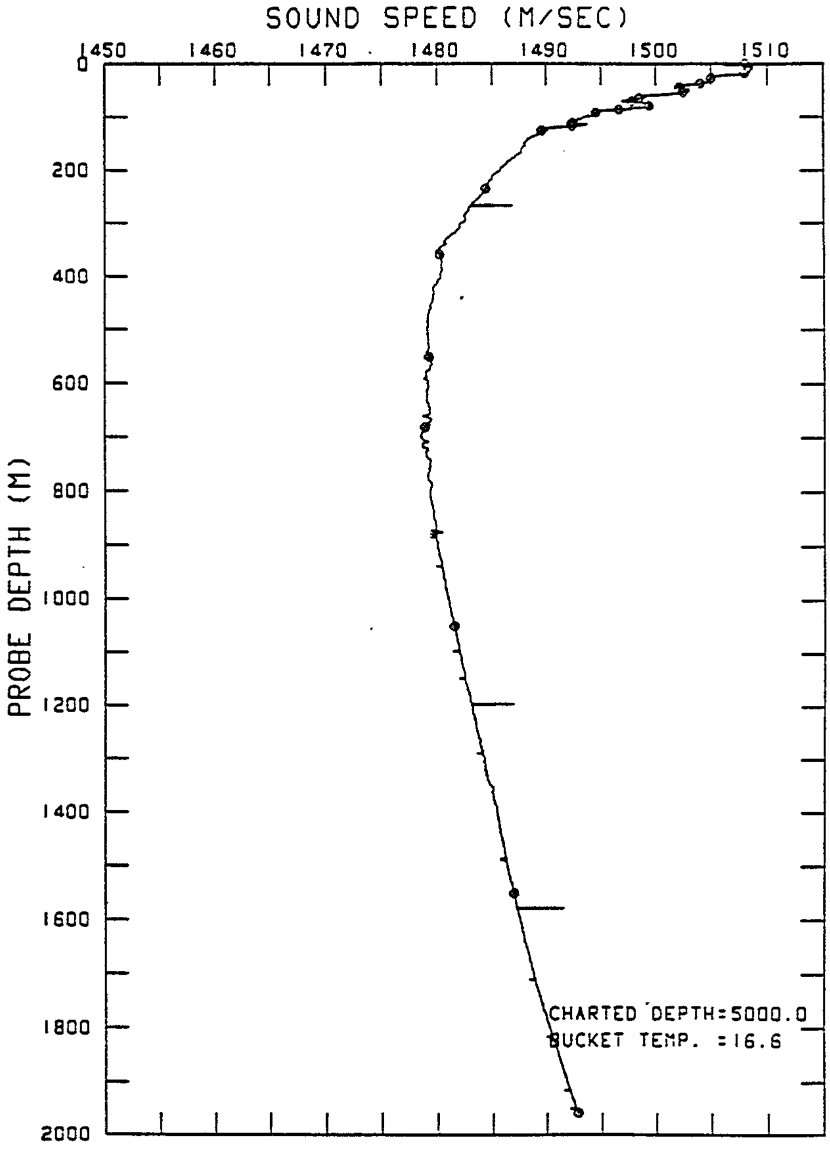

Figure 2. Sound speed profile at the site, measured with an expendable sound velocity probe. For depths greater than 2000 m, the values were obtained from archival data.

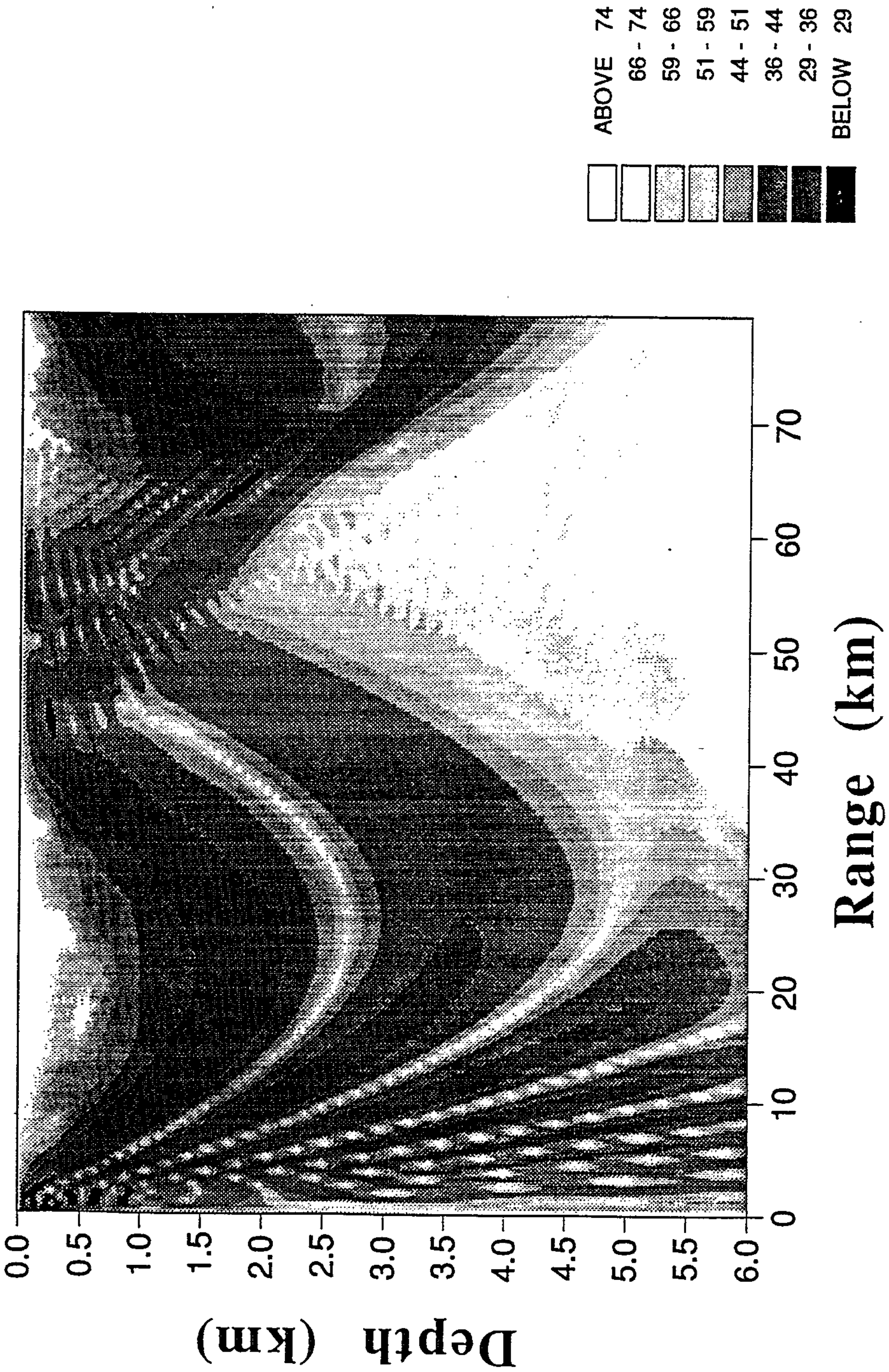

Figure 3. Sound pressure field for a source depth of 244 m calculated by the wide-angle parabolic equation method.

Experiment

The data were obtained in a shot run carried out with two ships, CFAV ENDEAVOUR (DREP) and USNS DESTEIGUER (NRL), to measure the propagation loss out to a range of about 40 km. DESTEIGUER opened range deploying 0.8 kg SUS charges at depths of 244 m at a spacing designed to provide a measurement of the reflectivity at 2° intervals from normal to near-grazing incidence. Ranges between the ships were measured with a trisponder system for each shot deployment. The transient signals from the shots were received by a 16-element vertical line array which was monitored by DREP and NRL personnel on ENDEAVOUR. The array was suspended in the sound channel, and the analysis is described here for a hydrophone at 480 m. The bathymetry along the track of the shot run was recorded using a 3.5 kHz profiler on DESTEIGUER. Measurements of the sound speed profile in the water were made from both ships during the run, using expendable sound velocity probes.

The multipath propagation loss was measured in 1/3 octave bands from 12.5-400 Hz for the direct path and the first and second bottom bounce components of the transient signal. The source levels used in the data analysis were obtained from previous work[7]. Estimates of the reflection coefficient were inferred from these data by scaling the measured loss for the bottom reflections with a ray theory calculation of the geometric spreading loss along the ray path. The ray calculation, which was based on the sound speed profile measured at the site, also provided the values of the angles at the sea floor for each shot range.

Multipath Propagation Loss

The multipath propagation loss measurements for the 1/3 octave band at 25 Hz are shown in Figure 4. The total loss and the first and second bottom bounce components are plotted out to a range of 40 km. Direct path propagation is dominant out to a range of 6 km and the loss increases sharply to a level of about 80 dB. Beyond this range there is an acoustic shadow for the direct path, and the propagation is dominated by bottom interacting paths. The propagation loss increases to a roughly constant level of 86 dB, and the loss for the first bottom bounce component is within 3 dB of the total loss over this range. These data show that the nature of the bottom interaction must be understood in order to determine the performance of sonar detection systems operating at short ranges in thin sediment regions. Processes such as scattering at the rugged basalt interface and shear wave propagation in the oceanic crust are expected to play a significant role in low frequency sound propagation in these areas.

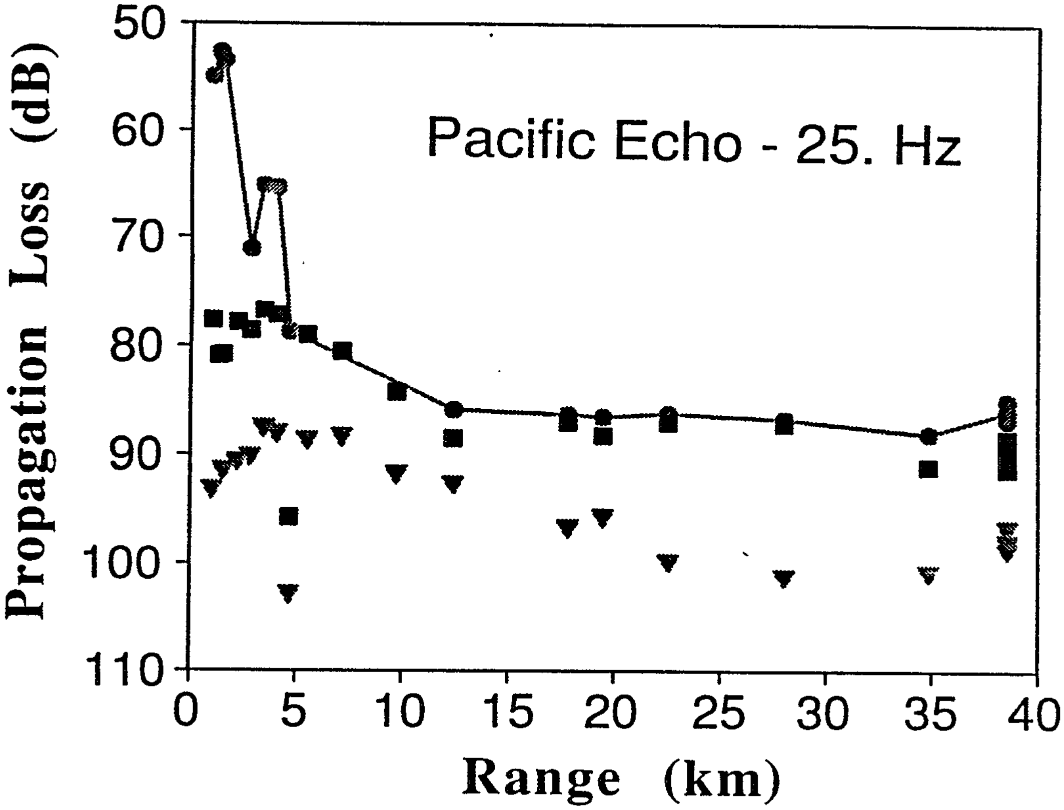

Figure 4. Multipath propagation loss for the 1/3-octave band at 25 Hz. The total loss (●), the first bottom bounce component (■), and the second bottom bounce component (▼) are plotted versus range.

Reflection Coefficient

The reflection coefficent derived from the propagation loss data for the first and second bottom bounce paths is shown for the 25 Hz band in Figure 5, where the results are plotted versus angle of incidence. The reflectivity decreases at large angles of around 75° and reaches a minimum value at a mid-range of angles. At smaller angles there is a local maximum around 25°, with a decrease to a constant level near normal incidence. In contrast to the behaviour in thick sediments, the reflectivity is weaker at the mid-range of angles from 30-70°. This result is a consequence of the strong interaction with the elastic basement, with the excitation of shear wave propagation in the basalt.

Geoacoustic bottom model

The reflectivity data presented in Figure 5 have been interpreted in terms of a plane wave reflection model in order to estimate a geoacoustic profile of the bottom. In this analysis we have restricted our attention to very low frequencies (< 30 Hz), and have made several assumptions for simplification. We require first that the source and receiver are large distances (at least five wavelenths) from the bottom. Since the sediment layer is thin (generally less than one wavelength at 30 Hz) and of variable thickness along the track of the experiment, we will neglect the presence of the sediment layer in the inversion of the data. We also assume that the roughness of the basalt interface is small and can be ignored for the very low frequency band. It is clear that these assumptions are consistent with the design of the experiment and also with the known geophysical information for the region. The degree to which this approach is successful for estimating material properties of the bottom will be determined by comparison of model predictions with the data.

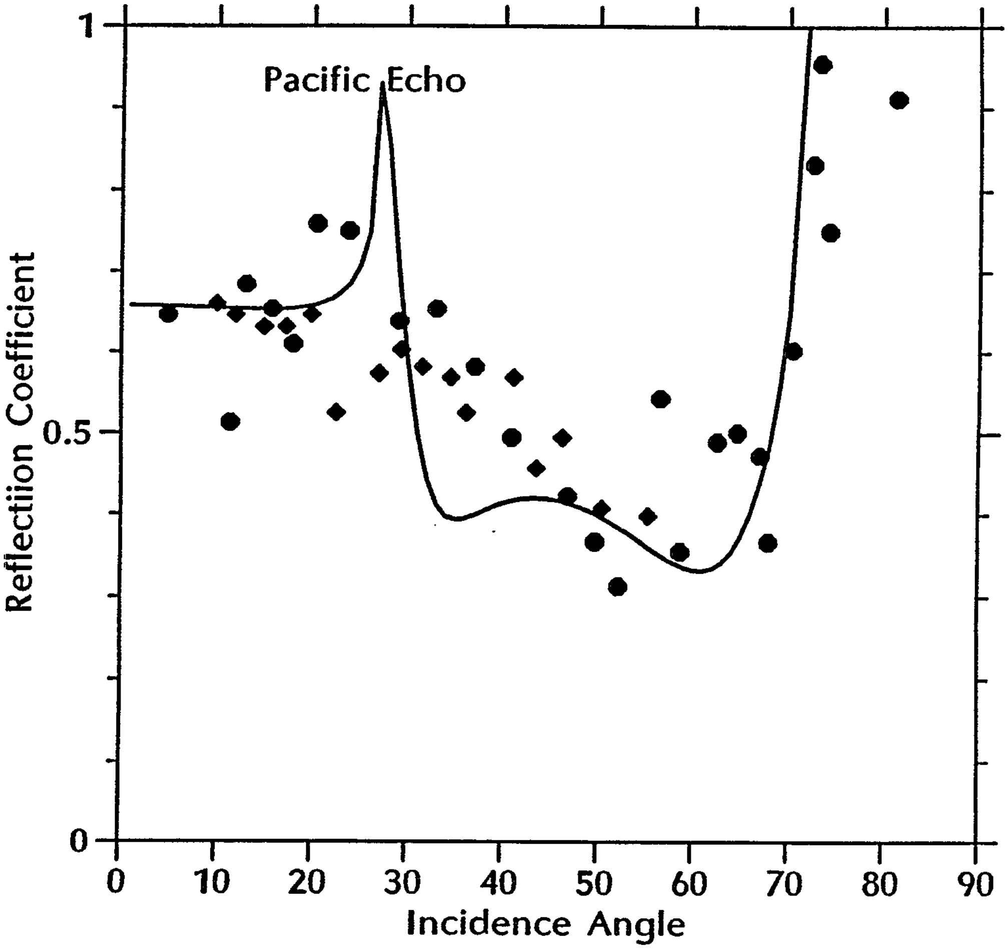

Figure 5. Reflection coefficient for the 25 Hz 1/3-octave band. The first and second bottom bounce data are shown by ● , and ◆. The smooth curve is modelled using $v_2 = 3.4$ km/s, $\beta_2 = 1.58$ km/s, and $\rho_2 = 2.5$ g/cm^3.

Under these conditions, we have modelled the bottom as an elastic solid and assumed that the bottom interaction can be described by the plane wave reflection coefficient, V. This relationship is given in terms of the ray parameter, $p = \cos\theta_1/v_1$, by[8]

$$V(p) = (mx + my - z)/(mx + my + z) \qquad (1)$$

where $m = \rho_2/\rho_1$,

$$x = v_2 \sin^2\phi_2/v_1\sin\theta_2,$$

$$y = \beta_2 \cos^2\phi_2/v_1\sin\theta_2,$$

and $z = 1/\sin\theta_1$.

For this simple model, shown in Figure 6, the bottom is described by three parameters: the density, ρ_2, and the compressional, v_2, and shear wave, β_2, speeds of the oceanic basement. The values of these parameters are obtained by inverting the reflection coefficient versus angle information, using a nonlinear inversion technique. The method proceeds by rewriting Equation 1 as

$$m(1 - V)(x + y) = (1 + V)z \qquad (2)$$

It is clear that the new expression involves only a single unknown if x and y are specified. From a set of N observations of the reflection coefficient at known angles, Equation 2 can be solved to obtain a solution for m and an associated pair of values for v_2 and β_2 which fits the data optimally in a least squares sense. The solution is found by systematically searching over a set of values for the P- and S- wave sound speeds. Further details about the method, and the sensitivity of the inversion to each parameter, can be found in Reference 3.

For the data in Figure 5, the search range for the P-wave speed was 2.5-4.0 km/s, and 0.0-0.6 for the ratio of S to P-wave speed. These values spanned a range that could realistically be expected for the elastic properties of fairly young basalt. The results of the inversion were 3.4 + 0.3 km/s for the P-wave speed, 1.6 + 0.1 km/s for the S-wave speed, and 2.5 + 0.2 g/cm^3 for the density. These values are consistent with other results reported for basalt of similar geological age. Diachok et al.[5] report values of 3.5 km/s for the P-wave speed of 30 million year basalt, and indicate a range of values for the S-wave speed from 1.5-2.0 km/s. Hamilton[9] reports a range of values for the density between 2.4 and 2.8 g/cm^3. The model prediction for the reflectivity, using the parameter values listed above, is indicated by the smooth curve in Figure 5. As can be seen in the figure, despite the relative simplicity of the geoacoustic model, the fit to the data is good.

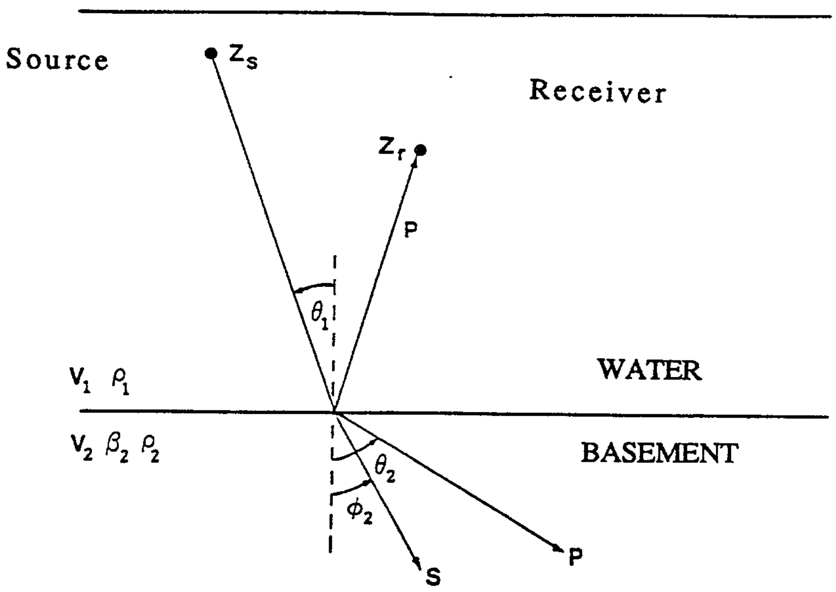

Figure 6. Diagram of the experiment geometry and the geoacoustic bottom model used to interpret the data. The angle of incidence of the sound wave in water with speed v_1 is θ_1.

Discussion of Results

In the remainder of the paper, we will assess the impact on the reflectivity of specific aspects of the bottom interaction which were not included in the geoacoustic model that was used to interpret the data. These effects include the attenuation in the oceanic basement, the presence of the sediment layer, and the bottom roughness. Attenuation can be introduced in the model (Equation 1) by making the wave vectors for the basement P and S waves complex, i.e.

$$k = k' + i\alpha, \tag{3}$$

with $k = \omega/c$.

The effect of attenuation for each type of wave is manifested at angles greater than the respective critical angles, where propagating waves can now be excited in the substrate medium. The results for P and S-wave attenuations of 0.1, 1.0, and 10.0 dB/m/kHz, shown in Figure 7, indicate that the effect is indeed negligible near the P-wave critical angle. For S-waves, there is a significant effect only for the largest value. Since this value is at least an order of magnitude greater than the attenuation expected for S-waves in basalt[9], it is clear that this effect can be ignored in the inversion.

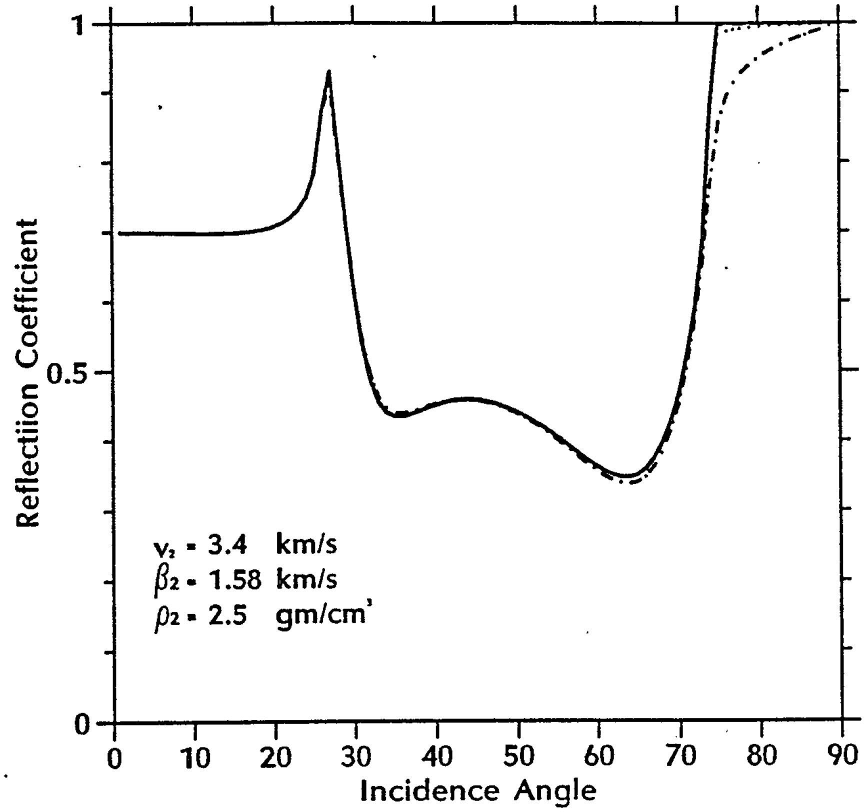

Figure 7. Effect of P and S-wave attenuation on the reflection coefficient. Attenuations of 0.0 (——), 0.1 (-----), 1.0 (······), and 10.0 (·----) are used in the calculation.

The presence of the sediment layer introduces the effect of interference between reflections from the water/sediment and sediment/basement interfaces. For thin sediments, Vidmar[10] has shown that the sediment must be modelled as an elastic solid in order to include the contribution from doubly-converted P-waves that are generated by S-waves reflected at the sediment/basement interface. This effect has been shown to be important in shallow water propagation over thin-sediment bottoms, where the interference between the doubly-converted P-waves and reflected P-waves has been observed in experiments[11]. However, the impact of this effect on our results is likely diminished owing to the frequency averaging in the 1/3-octave band. In addition, there is significant spatial averaging of the interference pattern because the thickness of the sediment layer varies greatly over the track of the shot run, with estimated values mostly around 5 m and some as great as 40 m. It is beyond the scope of this paper to carry out a detailed analysis of the effect of shear waves excited in the sediment layer; our intention instead is to determine the usefulness of a relatively simple model for the bottom. However, we can indicate the expected behaviour using a specific example. We have used Safari[12] model calculations of the reflection coefficient averaged in a 1/3 octave band to determine the bottom loss. This quantity is related to the reflection coefficient, V, by the expression -20 Log V. The bottom loss for a 5-m solid layer of deep sea clay overlying basalt is compared to that for unsedimented basalt in Figure 8. The overall magnitude is changed slightly from the unsedimented case, but the transitions at the basalt S- and P-wave critical angles are essentially unaffected. Consequently we can argue that the inversion of the P and S-wave speeds is not greatly affected, although there may be an effect on the density, since the density inversion is more sensitive to the overall magnitude of the reflection coefficient. However, the values obtained for the density are quite reasonable compared to other values reported in the literature.

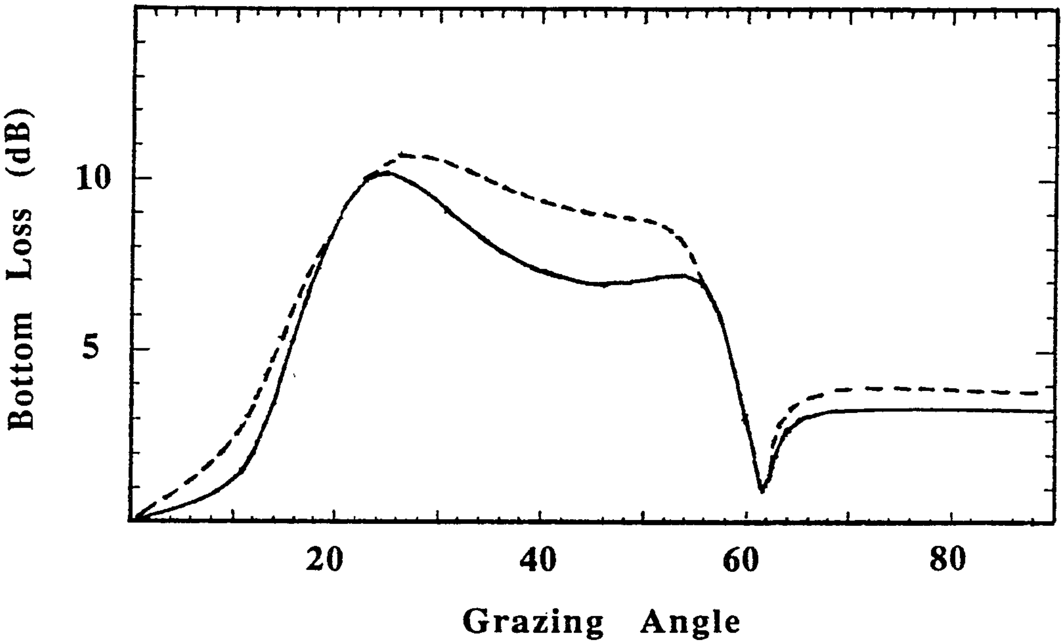

Figure 8. Effect of frequency averaging in the 1/3-octave band at 25 Hz. The averaged bottom loss for a 5-m solid sediment layer overlying basalt is shown by the broken curve, and that for the unsedimented basalt by the solid curve.

The effect of scattering at a rough basalt bottom has been studied by Diachok et al[5]. The issue is not well understood because, at higher angles, the process includes the scattering of shear waves excited in the basalt. In our case, since the shear wave speed is approximately equal to the sound speed in water, the scattering behaviour will be similar for both types of waves. For small rms roughness (compared to a wavelength), Diachok et al conclude that the effect on bottom reflectivity is small, less than 1 dB over the entire range of angles. Although it is difficult to estimate the rms roughness from our bathymetric data, a value of 3-5 m is generally accurate for fairly young basalt. A roughness scale of this magnitude is not expected to have a serious effect on our results for 25 Hz.

Summary

Propagation loss data obtained at a thin sediment site indicate that the loss increases sharply to a relatively large value of about 86 dB after 8 km, and remains constant out to nearly 40 km. A simple model of the reflectivity based on plane wave reflection from an elastic solid bottom predicts that the large losses over this range are due to shear wave propagation in the basalt bottom. The reflection coefficient data were interpreted using this model and the model parameters were estimated with a non-linear inversion technique. The values obtained were in reasonable agreement with values reported in the literature for relatively young basalt. It is unlikely that these results are sensitive to the bottom roughness or the presence of a thin layer of sediment at the sea floor.

References

1. R.L. Dicus and R.S. Anderson and O.I. Diachok, Effective low frequency geoacoustic properties of ocean sediments inferred from acoustic reflectivity measurements and corresponding regional geological data, *J. Acoust. Soc. Am.*, **60**, S97(A), (1976).
2. C.W. Spofford, Inference of geoacoustic properties from bottom loss data, in *Bottom-interacting Ocean Acoustics*, W.A. Kuperman and F.B. Jensen, editors, 159-172, Plenum Press, New York, (1980).
3. N. R. Chapman, Estimation of the elastic properties of sea floor sediments, in *Oceans '89 Proceedings*, 1071-1075, (1989).
4. W. T. Morton and A. Lowrie, Regional geological maps of the Northeast Pacific, Naval Oceanographic Office, NOO RP 16, (1978).
5. O. I. Diachok, R. L. Dicus and S. W. Wales, Elements of a geoacoustic model of the upper crust, *J. Acoust. Soc. Am.*, **75**, 324-334, (1984).
6. D. J. Thomson and N. R. Chapman, A wide-angle split-step algorithm for the parabolic equation, *J. Acoust. Soc. Am.*, **74**, 1848-1854, (1983).
7. N. R. Chapman, Source levels of shallow explosive charges, *J. Acoust. Soc. Am.*, **84**, 697-702, (1988).
8. L.M. Brekhovskikh, *Waves in Layered Media*, Academic Press, New York, 1980.

9 E.L. Hamilton, Geoacoustic modeling of the sea floor, *J. Acoust. Soc. Am.*, 68, 1313-1340, (1980).

10. P.J. Vidmar, A ray path analysis of sediment shear wave effects on bottom reflection loss, *J. Acoust. Soc. Am.*, **68**, 639-648, (1980)
11. P.R. Staal, S.J. Hughes, D.D. Ellis and D.M.F. Chapman, Shallow water acoustics on the Canadian east coast continental shelf, *J. Acoust. Soc. Am.*, **84**, S150(A), (1988).
12. H. Schmidt, SAFARI User's Guide, Saclantcen Report SR-113, (1988).

MATCHED FIELD PROCESSING IN A ROUGH BOTTOM, DEEP OCEAN ENVIRONMENT

John A. Fawcett, N. Ross Chapman, and Maureen McKirdy

Defence Research Establishment Pacific

Victoria, B.C., Canada

ABSTRACT

The effects of rough bottom bathymetry upon the performance of a matched field processing algorithm are investigated. Monte Carlo simulations with respect to stochastic bottom models are used to quantify statistically the localization errors incurred in matched field processing algorithms by assuming a flat bottom for the propagation model.

INTRODUCTION

Matched Field processing (MFP) attempts to localize a target in an oceanic waveguide by finding the source position which produces the "best" match of modelled pressure values with the measurements at an array. Matched field processing can also be thought of in terms of beamforming; instead of using plane waves with different direction cosines as steering vectors, the steering vectors are the modelled complex pressure field at the array as a function of source depth, range, and perhaps bearing. As with plane-wave beamforming it is possible to derive high-resolution methods which for sufficiently high SNRs will give well resolved estimates of source position[1].

An important issue in MFP is the sensitivity of the algorithms to incorrect knowledge of the oceanic environment. Various authors have considered the effects of different types of environmental mismatch (sound speed profile mismatch[2], bottom depth mismatch[3], etc.) on MFP. This paper addresses the effects of bottom bathymetry. The pressure field measured at an array may undergo interactions with a rough bottom during propagation from the source. If the bathymetry is known, a range-dependent acoustic model may be used in the matched-field algorithm[4]. In this paper, however, it is assumed that, at best, only a statistical description of the bottom is available and the effect of using a flat-bottom model in the MFP method is assessed.

There are 3 major sections in this paper. First, Monte Carlo simulations with respect to a stochastic model of the bottom bathymetry are used with a range-dependent Parabolic Equation[5] (PE) method to investigate the statistics of scattering in the waveguide. The second section investigates the effects of the bathymetric scattering on the performance of a Minimum Variance[1] MFP estimator. The simulations are done for three different bottom models and three different frequencies. Finally, two possible methods of improving MFP results for a rough bottom environment are discussed; reducing the cone angle for the PE computation of the model pressure vectors and averaging cross-spectral matrices of the data for a moving source.

MODELLING OF PRESSURE IN A ROUGH-BOTTOM OCEANIC ENVIRONMENT

Propagation in a penetrable oceanic waveguide for a stationary harmonic source with frequency ω is described mathematically by the reduced wave equation

$$\rho(x,y,z)\nabla\cdot(\rho^{-1}(x,y,z)\nabla P)+\omega^2 n^2(z)P(x,y,z)=\delta(z-z_S)\delta(r) \qquad (1)$$

where the source is at depth z_S and range $r=0$. The density of the acoustic medium is denoted by ρ and the refractive index by n. The pressure, p, vanishes at the upper surface $z=0$ and must satisfy outgoing or decaying radiation conditions at ∞. In this paper there is a surface z_I which is the interface between the water column and a lower half-space. The sound speed and the density may be discontinuous at this interface (although numerically the density variation may be smoothed somewhat). The surface z_I is described in the form

$$z_I = (5200 + f(r))m \tag{2}$$

where r is the range from the origin. There are three types of surface considered in this paper,

$$f(r) = \begin{cases} 25 \times \cos(\frac{2\pi x}{1000} + \phi) & (3a) \\ 50 \times \cos(\frac{2\pi x}{2000} + \phi) & (3b) \\ \sum_{i=-N'}^{N} a_i \cos(ik_{min}r + \phi_i). & (3c) \end{cases}$$

The sum in Eq.(3c) does not include the constant Fourier component corresponding to $i = 0$. These surface types will be referred to as Model 1, Model 2, and Model 3 respectively in the remainder of this paper. Model 3 is one used in the paper of Baer et al[6] in their study of bathymetric scattering. The coefficients a_i of Eq.(3c) are chosen so that the power spectrum $S(k)$ has a k^{-5} roll-off for large k and the resulting surface z_I has a correlation length of 1 km. The parameter N is equal to 400 and k_{min} is set to 200 m. In all three models the phase ϕ has a uniform distribution between $-\pi$ and π. A single realization of Model 3 is shown in Figure 1.

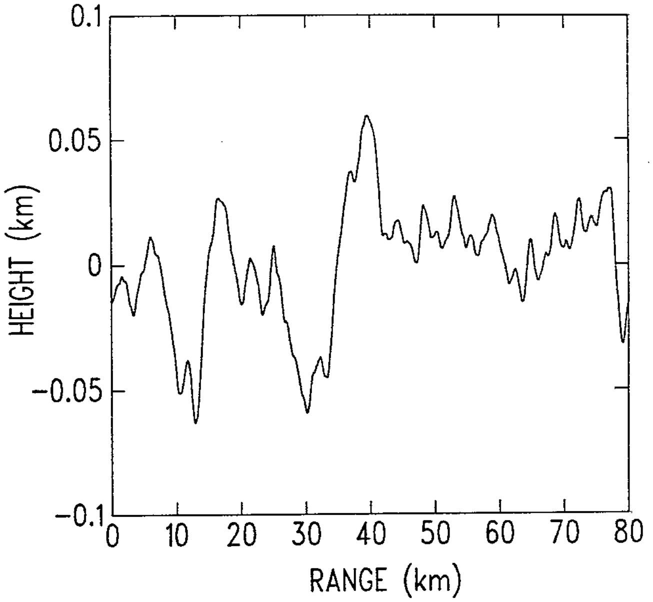

Figure 1. A Single Realization of Model 3 Bathymetry

The wide-angle split-step Parabolic Equation (PE)[5] method is used to model propagation through the waveguide with the range-dependent bathymetry described by one of the three models. Three frequencies, 10, 15, and 25 Hz are considered and the PE computations of this paper are done with either 4096 vertical steps of $\Delta z = 2m$ or 8192 steps of $\Delta z = 1m$. The fields were computed out to a range of 100 km with either $\Delta r = 50m$ or $\Delta r = 25m$. The finer range step was used for all 25-Hz computations and the finer range and depth steps were used for all the frequencies with Model 3. The PE model was selected for the computations because it can treat range-dependant environments with moderate impedance mismatch at the bottom. In analyzing cases with high compressional speeds in the bottom, where steeper-angle propagation is supported in the waveguide, a different range-dependant modelling scheme would have to be used.

The Northeast Pacific sound speed profile used in the computations of this paper is shown in Figure 2.

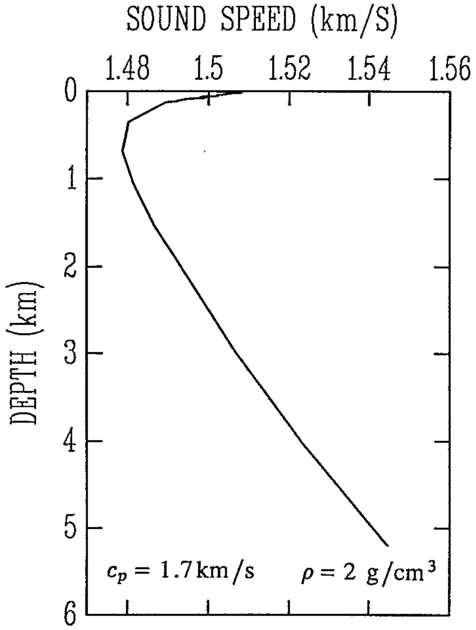

Figure 2. Sound Speed Profile Used in Computations

In Figure 3 the propagation loss for a flat bottom waveguide is shown as a function of depth and range for a 15-Hz source at 270 m.

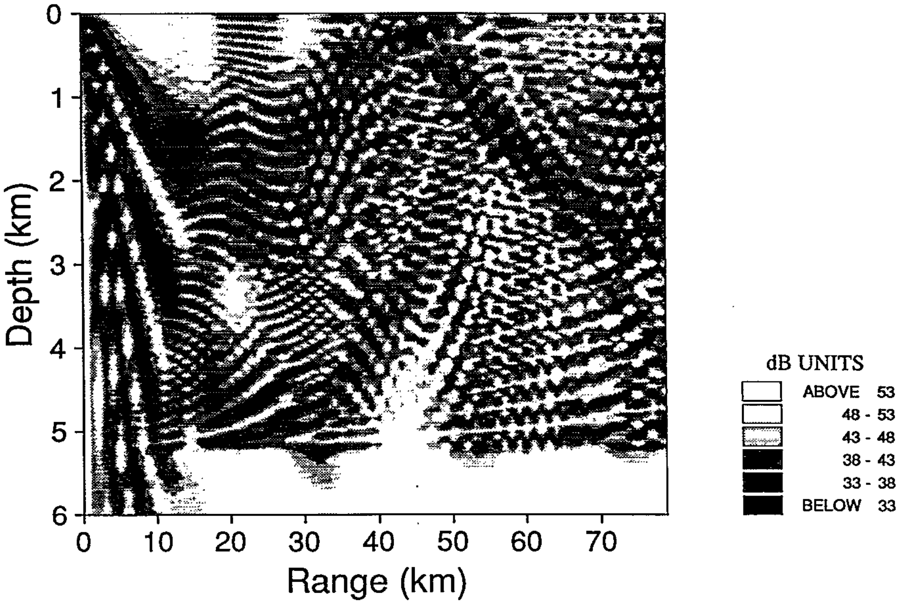

Figure 3. Propagation loss for flat-bottom waveguide; 15-Hz source at 270m depth

Statistics of the stochastic acoustic field are computed by appropriately ensemble averaging the two-dimensional range-depth grids of complex pressure values. In Figure 4a the modulus of the difference between the expected pressure field (i.e., the ensemble averaged field) and the field computed for a flat bottom is shown for Model 1 and a 25-Hz source at a depth of 270 m. The difference between these two fields has been normalized by the modulus of the flat field. In Figure 4b the standard deviation of the pressure amplitude (normalized by the squared amplitude of the flat-bottom pressure field) is shown for the same source. For this particular example it can be seen from Figure 4a and 4b that there is strong scattering (relative to the flat-bottom field) near the surface for regions near 20 km and 65 km. However, the overall performance of the Matched Field processors depends not only upon the scattered pressure field, but also on the sensitivity of the processor to deviations of the pressure field from the flat-bottom values. This sensitivity varies with the range and depth. Also, although Figures 4a and 4b show the relative amount of scattering in the waveguide they do not indicate the correlation-structure of the scattered field.

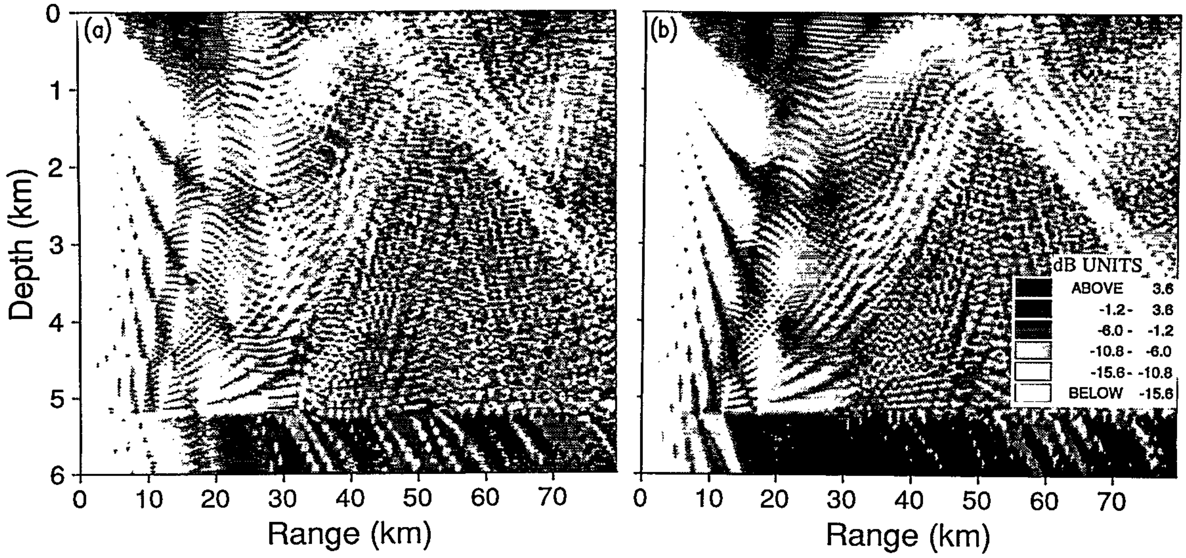

Figure 4. (a) relative difference between expected pressure field and flat-bottom field for Model 2 and a 25-Hz source at a depth of 270 m. (b) the relative standard deviation of the scattered field.

The pressure data at a vertical array can also be generated for each realization of the bottom type. The vertical array used in this paper consists of 16 hydrophones spaced 44 m apart with the first hydrophone at 404 m (this value was used to simulate the array depth during an actual sea experiment). The vertical array outputs are computed for ranges of 15, 20, 30, 50, and 80 km. At the ranges of 15 and 20 km a significant amount of the acoustic energy received at the array has interacted with the bottom; the array at 50 km receives mostly energy which has not interacted with the bottom and the arrays at 30 and 80 km receive a mixture of both direct and bottom-interacting energy. By using ensemble averaging over the realizations of a model type, it is possible to compute the expected cross-correlation of the pressure field at an array. In Figure 5 the values of the relative correlation

$$C_{i,j} \equiv \frac{| < p_i^* p_j > - p_{i,f}^* p_{j,f} |}{\sqrt{\sum_{j=1}^{16} |p_{i,f} p_{j,f}|^2 / 16}} \qquad (4)$$

from a 15-Hz source at 270 m depth are plotted across the vertical array at the 5 ranges with $i = 1$. Model 2 was used as the bottom type. The subscript f in Eq.(4) refers to the flat-bottom waveguide values. The quantity $C_{i,j}$ represents the expected relative "noise" in the j'th element of the i'th row of the cross-spectral matrix R_{ij} due to the scattering from the rough bottom.

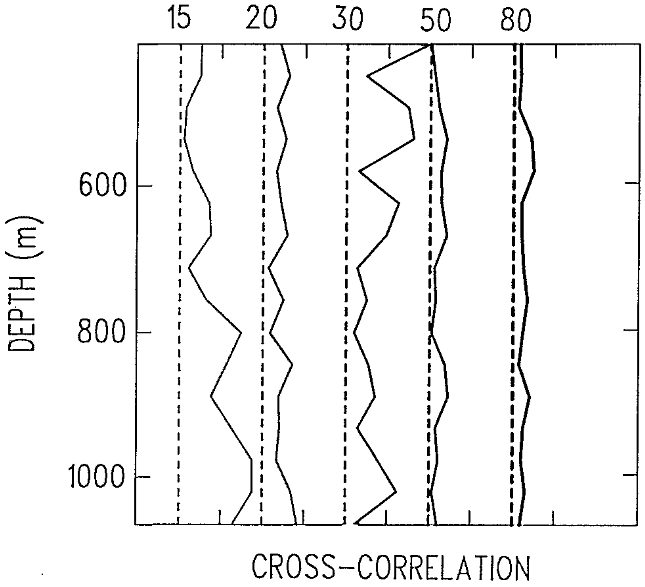

Figure 5. Normalized cross-correlation of "noise" created by scattering from bottom bathymetry for Model 2 with a 15-Hz source at 270m depth

In other words, $C_{i,j}$ represents the portion of the cross-spectral matrix element R_{ij} which cannot be modelled correctly by a flat-bottom model. As can be seen, the magnitude and structure of the relative correlation noise varies significantly with range. Various theories[7,8] have been proposed for the prediction of the correlation of pressure across an array. A comparison of these theories and the ensemble results of this paper should be an area of interesting research.

MATCHED FIELD PROCESSING

The Matched Field algorithm used for the study of this paper is the Minimum Variance estimator. For this estimator the Matched Field ambiguity surface is computed from

$$E(r,z) = \sum_{i=1,\, j=1}^{NH} (\hat{p}_i^*(r,z) \mathrm{R}_{\mathrm{ij}}^{-1} \hat{p}_j(r,z))^{-1} \tag{5}$$

where **R** is the cross-spectral matrix given by

$$\mathrm{R}_{\mathrm{ij}} = d_i d_j^*, \tag{6}$$

NH is the number of hydrophones in the array, d_i is the observed complex pressure value at the i'th hydrophone and $\hat{p}_i(r,z)$ is the modelled complex pressure value at the i'th hydrophone for a source at range r and depth z. This value is normalized so that the vector of pressures across the array, **p** , has unit length. In this paper **p** is modelled by the Parabolic Equation method assuming a flat bottom. For computational efficiency, 16 matrices of discrete range-depth values are computed for a source located at each of the hydrophone depths (instead of doing a PE run for each different source position). These matrices contain the PE pressure fields subsampled at grid spacings of $\Delta r = 50m$ and $\Delta z = 22m$ for the 10 and 15-Hz computations and with $\Delta r = 25m$ for the 25 Hz computations. The appropriate pressure values, using the theory of reciprocity, can be accessed from these grids to obtain the values of $\mathbf{p}(r_i, z_j)$.

The vertical array data at one of the 5 studied ranges (15, 20, 30, 50, 80 km) are used to form the cross-spectral matrix **R** for a particular bottom realization and the ambiguity surface is generated from Eq.(5) using the precomputed array described above for **p**. The maximum peak can then be located within the discrete ambiguity surface. By repeating these calculations for a large number of different realizations of the bottom, the expected error and the the standard deviation of the range and depth estimates are calculated and an average ambiguity surface is computed.

In Figure 6a a single ambiguity surface is shown for a 15-Hz source at a range of 80 km and depth of 270 m. Here the "data" are generated with a flat bottom model so that the matched field estimate is very good with little ambiguity. For Figure 6b the data are generated for the same source location as for Figure 6a but now a realization of the second model is used. As can be seen the location of the source is now much more ambiguous. There are now two possible areas of localization corresponding to approximately 40 km and 80 km ranges.

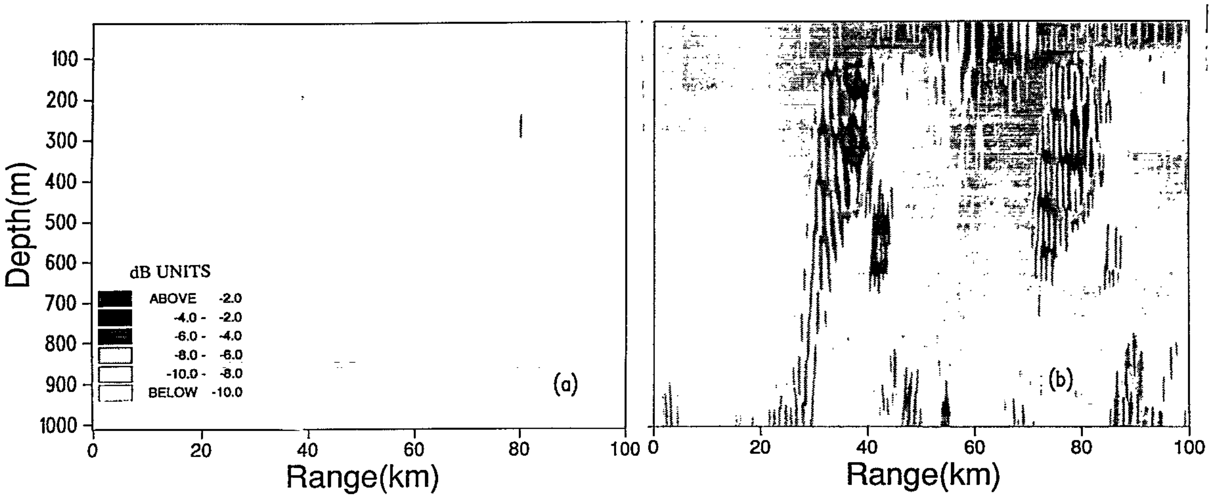

Figure 6. Ambiguity surfaces for a 15-Hz source at range of 80 km, and a depth of 270m when (a) both data and matching field are generated with a flat-bottom model; (b) the data are generated from a single realization of Model 2.

In this and the following examples a very small amount (approximately -10 dB) of white noise is added to the hydrophone data in order that the matrix, $\mathbf{R}_{ij}$, of Eq.(6) may be inverted. The resulting averaged ambiguity surfaces (using 50 simulations) are shown for different source ranges, model types, and frequencies in Figures 7a-7d.

In Table 1 the statistics of range estimation are summarized for the various Monte Carlo simulations. The computed bias and standard deviation of the range estimates are computed for true source ranges of 15, 20, 30, 50 and 80 km and with each of the bottom types. The statistics are computed using only those simulations for which the maximum peak of the ambiguity surface lies within 20 km of the true range. The statistic N_A indicates the number of simulations for which the estimated range was within this window. This statistical windowing was necessary in order that statistical outliers would not greatly affect the computed bias and standard deviation of the estimator. Typically, range estimates fall outside of the window if the maximum peak is located within the wrong cycling zone.

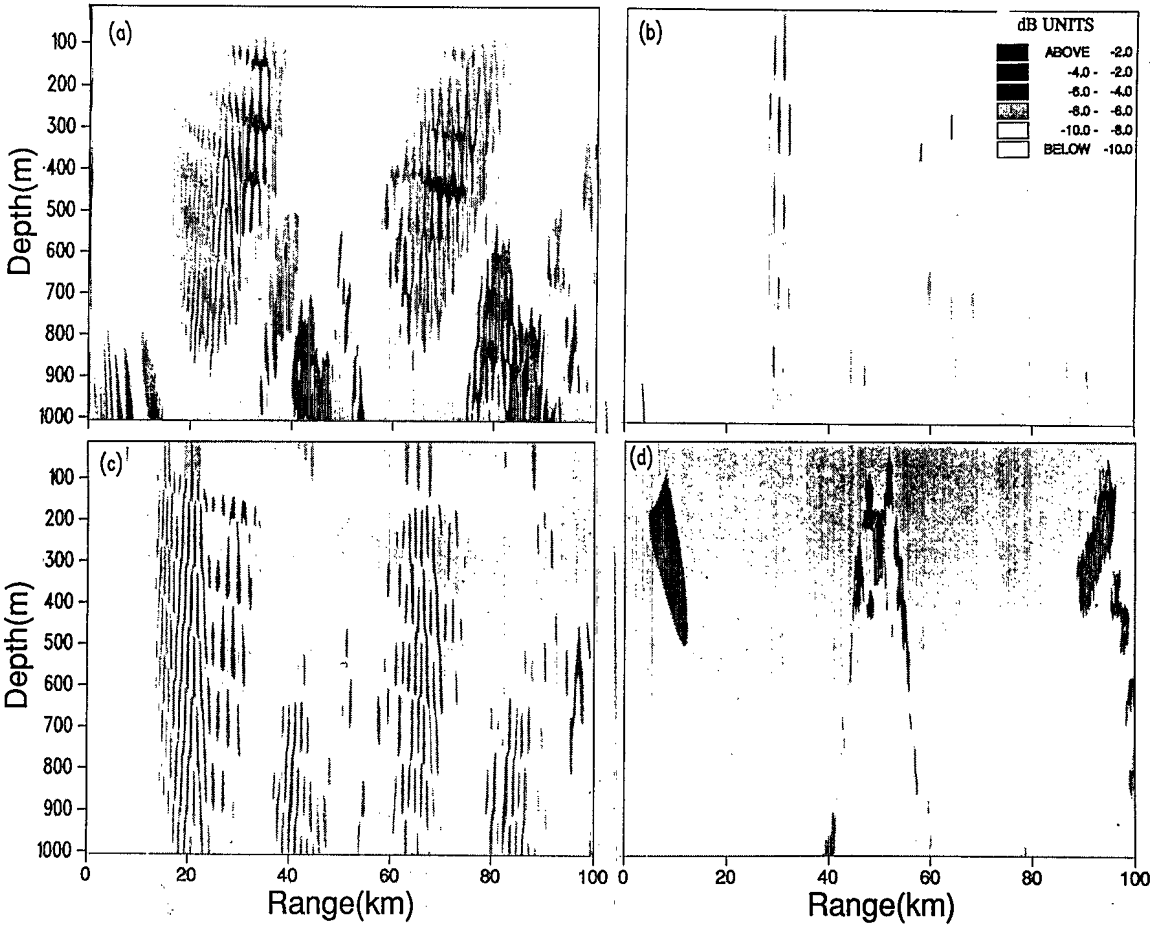

Figure 7 Averaged ambiguity surfaces for a source depth of 270 m and (a) range = 30 km, frequency = 15 Hz, Model 1; (b) range = 30 km, frequency = 10 Hz, Model 3; (c) range = 20 km, frequency = 10 Hz, Model 1; (d) range = 50 km, frequency = 25 Hz, Model 2.

Table 1. Statistics of MFP range estimates

Model		1	2	3	1	2	3	1	2	3
		10 Hz	10 Hz	10 Hz	15 Hz	15 Hz	15 Hz	25 Hz	25 Hz	25 Hz
15 km	bias	0.90	0.44	0.17	-0.06	-0.50	0.20	-0.38	-0.28	-0.05
	σ	1.25	2.04	0.67	2.05	1.37	0.51	1.48	1.16	0.47
	N_A	50	50	50	50	50	50	50	50	50
20 km	bias	2×10^{-3}	-2.23	0.12	-0.21	-1.64	1×10^{-3}	-1.42	-4.26	0.01
	σ	0.40	3.19	0.67	0.42	2.31	0.57	6.80	6.14	0.64
	N_A	41	44	50	50	50	50	50	50	50
30 km	bias	0.05	0.48	-0.02	-0.05	-0.97	0.19	-0.56	0.04	0.39
	σ	1×10^{-5}	1.62	0.60	0.84	0.24	0.89	0.89	1.08	0.86
	N_A	50	48	49	50	5	45	50	6	49
50 km	bias	0.05	0.08	0.09	0.05	0.10	0.04	0.06	0.04	0.01
	σ	7×10^{-3}	4×10^{-2}	0.75	3×10^{-5}	0.22	3.5×10^{-2}	4×10^{-2}	7×10^{-2}	0.14
	N_A	50	50	50	50	50	50	50	50	50
80 km	bias	0.06	-0.59	0.07	0.04	-0.48	-0.07	0.09	-0.09	-0.24
	σ	0.02	0.86	0.52	0.05	0.60	0.60	0.08	0.49	0.58
	N_A	50	37	37	38	42	33	50	40	46

In this paper the cycling zones of a particular location (r, z) in the waveguide are defined as those regions where the interference structure of the pressure field is essentially the same as that at range r and depth z. For example, the cycling zones of a convergence zone are the other convergence zones. For a location where first bottom-bounce energy is dominant, its cycling zones might be regions where second or third bottom bounce energy is dominant.

These results show that in general the rough bottoms do not have a "disastrous" effect on the matched field performance. At the closer ranges of 15 and 20 km the range estimates show a fair amount of variation, especially for bottom model 2. At 30 and 80 km the maximum peak is often found in the wrong cycling zone. However, within the proper cycling zone the estimates are accurate. At a range of 50 km, where the water-borne energy is predominant, the effect of the bottom is minimal for all model types and frequencies. However, the effect seems to be greatest for model type 3 in this case.

POSSIBLE IMPROVEMENTS TO THE MATCHED FIELD PROCESSING

In this section two possible variations of the Matched Field Processing problem discussed above are considered. First, the effect of modelling only waterborne energy with the PE code is considered. Second, the effect of averaging the cross-spectral matrices obtained from a source moving over the rough bottom is investigated.

Other authors[2] have discussed using only the totally water-borne energy in the computation of the pressure vector **p**. This is often done with a modal method since it is straightforward to exclude the bottom-interacting modes from the modal sum. In this paper the same effect is achieved by reducing the cone-angle used in the PE computations for the flat bottom model from 45° to 17°. However the data for the rough bottoms are computed as before with a 45° cone angle. The averaged ambiguity surfaces are shown in Figures 8a and 8b for source ranges of 15 and 30 km with bottom model 2 and a frequency of 15 Hz. The surfaces are smoother than the same ambiguity surfaces computed with the 45° cone angle. The ambiguity surface for the 20 km range (not shown) is entirely black when plotted , reflecting the fact that the energy reflected from the bottom is essential in this case in order to obtain useful matched field processing results. The ambiguity surface for the 50 km source is only slightly affected.

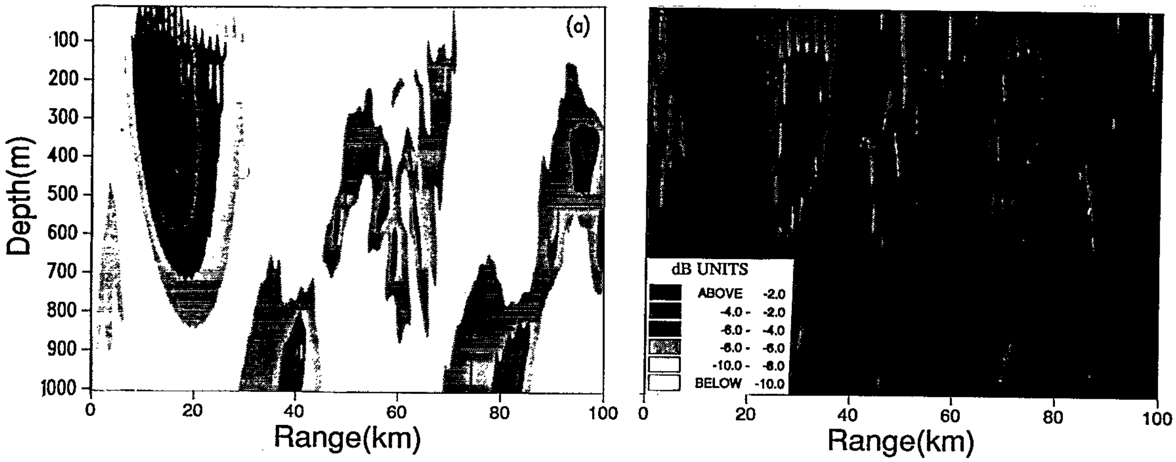

Figure 8 Averaged ambiguity surfaces for 15 Hz source at depth 270 m and bottom Model 2, with 17° cone-angle for matching pressure field with (a) range = 15 km; (b) range = 30 km.

For the bottom model and frequency considered here, there is no significant improvement obtained by restricting the cone angle.

A simulation is shown to illustrate the effect of averaging the cross-spectral matrices obtained from a source moving over a rough bottom. A 15 Hz source, initially at a range of 30 km, moves radially with a speed of 5 m/s over the Model 1 bottom type. The array pressure values are then generated for a single realization of a bottom for the ranges at 20 second intervals. The cross-spectral matrices obtained from these intervals are averaged to produce an average cross-spectral matrix for use in MFP. The section of the bottom bathymetry which is "illuminated" by the energy of the moving source changes as the range changes. Hence, by averaging the cross-spectral matrices the various phase mismatches that are introduced by the bottom roughness may be averaged out. This method of simulating a moving source is very simplified as the changes in phase due to the doppler shift are ignored. The ambiguity surface for a single cross-spectral matrix is shown in Figure 9a. In Figure 9b the ambiguity surface is shown for a cross-spectral matrix which has been formed by averaging 41 cross-spectral matrices (corresponding to a 4 km change in source range over the time interval).

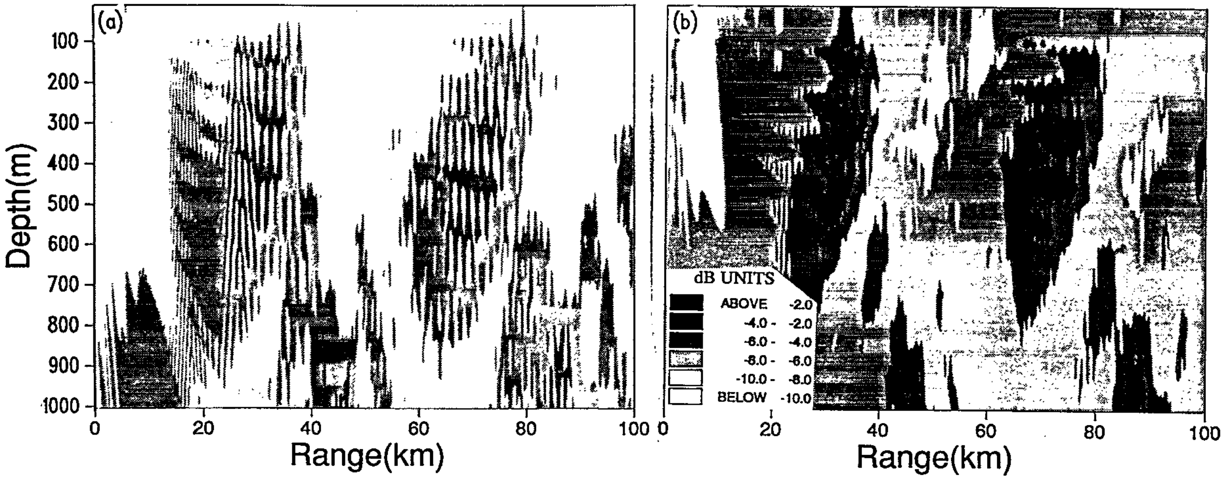

Figure 9. Ambiguity surfaces for a moving (5 m/s) 15 Hz source over Model 1 (initial range = 30 km) with (a) first cross-spectral matrix; (b) averaging 40 cross-spectral matrices.

As can be seen the ambiguity surface is now simpler in structure and the range and depth estimates are fairly accurate. The computed range estimate of 33.45 km and depth of 286 m compares favorably with the expected values of 32 km and 270m. However, for this example, the computed peak corresponds to a secondary maximum. The global maximum is in the wrong cycling zone.

SUMMARY

This paper has investigated the effect of bottom scattering on Matched Field Processing. Different bottom models, frequencies and source ranges were used in the simulations. It was shown that the models of this paper introduced substantial relative scattering within the waveguide and produced very correlated "noise" (with respect to flat-bottom predictions) at a vertical array. However, the overall performance of the MFP estimator depends not only on the amount of "noise" that the rough bottom introduces to the system but also on the sensitivity of the estimator for a particular scenario.

In general, the minimum variance Matched Field processor still performed well even with substantial bottom roughness. The MFP range estimates for true source ranges of 15 and 20 km seemed to show the most variation. In the environment examined these are ranges where first bottom bounce energy is significant. The ambiguity surfaces for true source ranges at 30 and 80 km had main power lobes near the true range and also at the next cycling range. However, within the correct cycling region the estimates are fairly accurate. The MFP results are most accurate and unambiguous for the true source range of 50 km, where, for the flat-bottom waveguide, the relative amount of bottom interacting energy is small.

It was shown that restricting the cone angle of the PE model in order to compute only water-borne energy did not seem particularly useful for the examples considered. It is very detrimental for the source range of 20 km where bottom bounce energy is dominant. When the source is moving in the rough waveguide, the averaging of the resulting cross- spectral matrices may be useful. This is an area which warrants further research.

REFERENCES

1. A.B. Baggeroer, W.A. Kuperman, and H. Schmidt, "Matched field processing: Source localization in correlated noise as an optimum parameter estimation problem", *J. Acoust. Soc. Am.*, **83**, 571-587 (1988).
2. A. Tolstoy, "Sensitivity of matched field processing to sound-speed profile mismatch for vertical arrays in a deep water Pacific environment", *J. Acoust. Soc. Am.*, **85**, 2394-2404 (1989).
3. D. R. Del Balzo, C. Feuillade, and M. M. Rowe, "Effects of water-depth mismatch on matched-field localization in shallow water", *J. Acoust. Soc. Am.*, **83**, 2180-2185 (1988).
4. C.A. Zala and J.M. Ozard, "Matched field processing in a range-dependent environment" *in proceedings of IEEE Pacific Rim Conference on Communications, Computers, and Signal Processing*, pp.566-569, Victoria, B.C., 1989.
5. D.J. Thomson and N.R. Chapman, "A wide-angle split-step algorithm for the parabolic equation", *J. Acoust. Soc. Am.*, **74**, 1848-1854 (1983).
6. R.N. Baer, J.S. Perkins, and D.H. Berman, "Bathymetric scattering by Parabolic Equation simulation", pp.227-240, *in Computational Acoustics; Algorithms and Applications, Proceedings of the 1st IMACS Symposium on Computational Acoustics* , New Haven, ed. by D. Lee, R. Sternberg, and M. Schultz, North Holland, Amsterdam (1986).
7. C.S. Clay, "Effect of a slightly irregular boundary on the Coherence of Waveguide Propagation", *J. Acoust. Soc. Am* , **36**, 833-837 (1964).
8. W.A. Kinney and C.S. Clay, "The spatial coherence of sound scattered from a wind-driven surface: Comparison between experiment, Eckart theory, and the facet-ensemble method", *J. Acoust. Soc. Am*, **75**, 145-148 (1984).

MATCHED FIELD PROCESSING EXPERIMENTS WITH PACIFIC ECHO SEA-TRIAL DATA

by

John A. Fawcett, N. Ross Chapman, and Maureen L. McKirdy
Defence Research Establishment Pacific
FMO Victoria, B.C., Canada V0S 1B0

Abstract

In this paper Matched Field results obtained using sea-trial data are presented. In spite of environmental uncertainties, Matched Field Processing provided good localization estimates. The effects of varying the number of modes and the roughness of the bottom in Matched Field Processing are considered. Also, it is shown that source position estimates are improved if the tilt of the vertical array is modelled.

I. INTRODUCTION

During May-June 1986 the Defence Research Establishment Pacific (DREP) participated in the first Pacific Echo sea-trial experiments with the U.S. Naval Research Laboratory (NRL). These experiments were designed to study various aspects of matched field source localization at selected sites in the Northeast Pacific which were chosen to provide examples of typical bottom conditions in this part of the ocean. This paper studies the performance of Matched Field localization algorithms with the experimental data obtained using a vertical line array at a thin-sediment site south of the Pioneer Fracture Zone (see Figure 1). Pacific Echo data from a thick sediment site in the Tufts Abyssal Plain have been previously analyzed by NRL[1].

Matched field Processing (MFP) attempts to localize a target by finding the source location within the oceanic waveguide which produces the "best" match between the measured field at the array and modelled replicas of the field: the replicas are calculated using propagation models such as the Parabolic Equation method, modal methods, or Fast Field programs such as SAFARI[2]. This paper will employ the KRAKENC

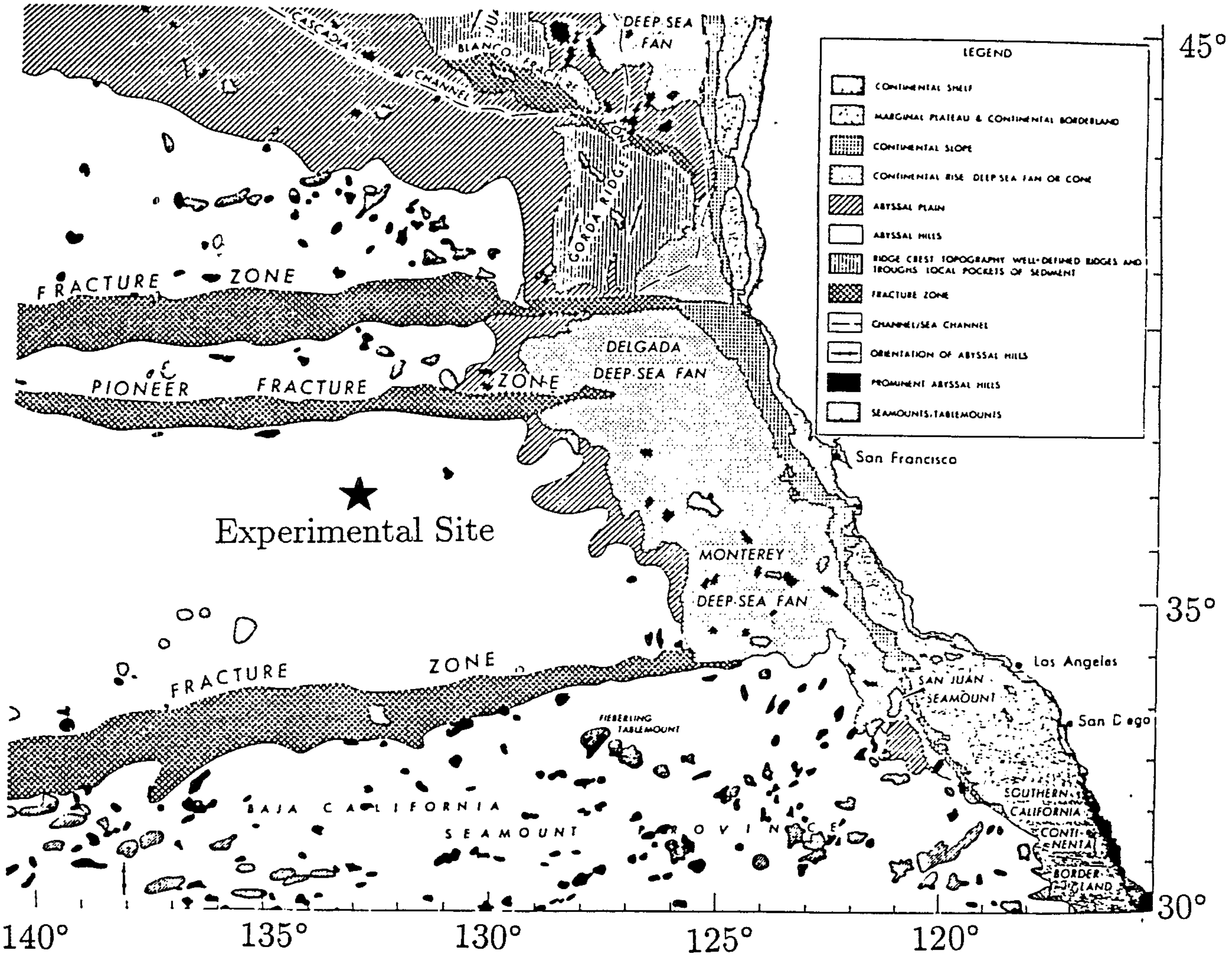

Figure 1. Location of MFP experiment

modal code due to M. Porter[3].

One area of current research in MFP is the robustness of MFP algorithms to inaccuracies in environmental knowledge. For example, if the oceanic sound speed profile used in modelling the acoustic field is slightly inaccurate, how will this affect MFP localization estimates? This type of question has been investigated previously by other authors for environmental factors such as sound speed profile mismatch[4], bottom roughness[5], and water depth mismatch[6].

The questions of environmental mismatch arise with the Pacific Echo experiments analyzed in this report. Uncertainties exist in both the sound speed profile in the water and in the geoacoustic properties of the bottom; however, the experiments were designed to minimize the impact of these uncertainities on source localization. The sound speed profile was measured at the receiver and at several points along the source ship track during the experiment, so there is likely only a small degree of uncertainty in this parameter for the relatively short ranges in the experiment. The uncertainties in the description of the bottom are of greater concern. The bottom in this region consisted of a thin sediment layer overlying a basalt basement, however the thickness of the sediment was variable. The sea floor in the vicinity was rough and the bottom geoacoustic properties such as the compressional and shear speeds and attenuations, were not known a priori but were estimated from bottom reflectivity data obtained during the experiment[7]. An attempt was made to compensate for the bottom model uncertainties by choosing the source ranges so that the receiver was in the direct path, where the knowledge of the bottom is not as critical, or was in the region preceding the first convergence zone, where the bottom interacting paths penetrate only to relatively shallow depths in the basement. For these conditions, we have used the measured sound speed profiles and a relatively simple geoacoustic model based on the properties of the basalt basement, and have studied the effect of the bottom on source localization by restricting the number of modes used to calculate the replica pressure fields.

In addition to the uncertainties in the environmental model, there is also the question of mismatch due to uncertainty in the receiver position, which arose in this experiment due to the tilt of the vertical line array. We have investigated this effect by varying the tilt angle while using the best estimate of the environment model in the propagation modelling.

In this report four sets of data are used. A CW projector transmitting a tone at 15 Hz was towed on a circular arc at ranges of approximately 6 and 38 km from the vertical line array. These experiments were repeated using a frequency of 10 Hz. Ambiguity surfaces using both the Minimum Variance estimator and the Bartlett estimator[8] were generated for the four data sets using different numbers of modes in calculating the replica fields, and using flat and rough bottom geoacoustic models. Finally, we present the analysis of the effect of array tilt on the MFP results.

II THEORY

The Matched Field algorithms used for the study of this report are the Bartlett estimator,

$$S(r,z) = \sum_{i=1,j=1}^{N_H} (\hat{p}_i^*(r,z)\mathbf{R}_{ij}\hat{p}_i(r,z)) \qquad (1)$$

and the Minimum Variance estimator

$$S(r,z) = \sum_{i=1,j=1}^{N_H} (\hat{p}_i^*(r,z)\mathbf{R}_{ij}^{-1}\hat{p}_i(r,z))^{-1} \qquad (2)$$

where $\mathbf{R}$ is the cross-spectral matrix given by

$$\mathbf{R}_{ij} = \frac{1}{N_{AVE}} \sum_{k=1}^{N_{AVE}} d_i(f)d_j^*(f). \qquad (3)$$

In Eqs.(1) and (2), N_H is the number of hydrophones in the array and $\hat{p}_i(r,z)$ is the modelled complex pressure value at the ith hydrophone for a source at range r and depth z. This value is normalized so that the vector of pressures across the array, $\mathbf{p}$, has unit length. In Eq.(3) d_i is the spectral value (frequency f) of the data at the ith hydrophone.

There are a variety of possible algorithms for modelling the propagation of acoustic pressure in an oceanic waveguide in order to generate the model pressure vector $\mathbf{p}$ at the vertical array. For this work the normal mode model, KRAKENC[3], was used to model propagation in a flat oceanic waveguide with elastic bottom layers. This model computes the pressure field from the sum

$$p_i(r,z) = \sum_{n=1}^{N} \phi_n(z_i)\phi_n(z)\frac{e^{-ik_n r}}{\sqrt{k_n r}} \qquad (4)$$

where z_i is the depth of the ith hydrophone. KRAKENC also computes leaky modes, allowing an approximation to the continuous spectrum (or branch-line integral) portion of the pressure field's spectrum. Unlike other modal programs which only approximate the effects of attenuation on the propagation of the modes, the modal code KRAKENC uses a complex root finder to locate the discrete, complex, wavenumbers corresponding to the modes of an elastic solid waveguide. However, we know that the oceanic waveguide of this experiment is range-dependent and that the range-independent assumptions of modal theory are not correct. Unfortunately, we do not know the deterministic form of the ocean bottom bathymetry and can only model it in a stochastic sense. The effects of bottom interface roughness were modelled by computing effective modal attenuation coefficients using a stochastic model in KRAKENC due to Kuperman and Ingenito[9].

As mentioned in the Introduction another source of mismatch in MFP is the assumption that an array is perfectly vertical when, in reality, it is tilted. If the array has a vertical angle of ψ and a horizontal angle of ϕ, (see Figure 2) then the ranges of the individual hydrophones from the source are given by,

$$r_i = r_0 - (i-1) d \sin\theta \cos\phi \tag{5a}$$

and the depths are given by

$$d_i = d(i-1)\cos\theta + d_0 \tag{5b}$$

where i is the hydrophone index, d is the distance between hydrophones,

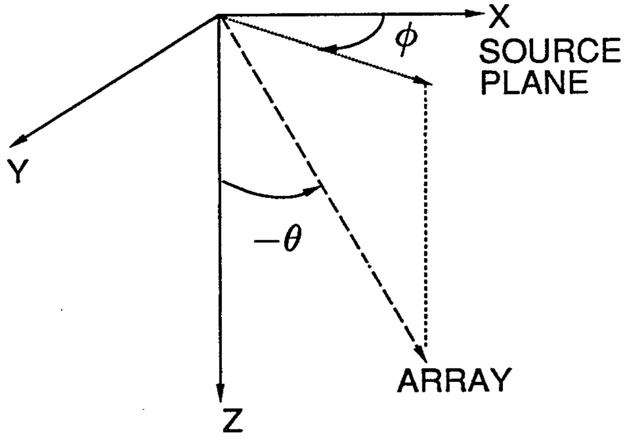

Figure 2. Geometry of tilted array

r_0 is the horizontal range from the first (top) hydrophone and d_0 is the depth of the first hydrophone.

III. DESCRIPTION OF THE EXPERIMENT

The data for this report were collected during June 1986 in the area of 37°30′N, 133°00′W. The NRL Mark VI projector was towed by USNS DeSteigeur on short- and long-range circular arcs at a depth of about 100m. The source depth was monitored on board the towship during the experiments. The 10- and 15-Hz lines were turned on for different portions of the arcs. The range of the USNS DeSteigeur from the vertical array was determined using an inter-ship trisponder system. The range for the long range 15-Hz arc was estimated to be 38 km, and for the 10-Hz experiment the range estimated to be 36 km. For the short range experiments the range was estimated to be 5.5 km in both cases. Because of the experimental geometry the source had very little radial speed with respect to the array, and consequently doppler effects were ignored in the data analysis. The DREP vertical line array MEVA (Multi-Element Vertical Array) was deployed from CFAV ENDEAVOUR. This array consists of 16 hydrophones at 45-m spacing, with the first hydrophone located at a depth of 396.7 m in the water column. The hydrophone data were sampled at a rate of 1500 Hz. Analysis of these data indicated that the second and sixteenth hydrophones were faulty during the experiment and these receivers were not used in the MFP analysis.

The sound speed profile shown in Figure 3 was obtained from CFAV ENDEAVOUR during the experiment. The values for depths greater than 2000 m were obtained by merging the measured profile with a generic profile for this area. In conjunction with the MFP data obtained during the Pacific Echo experiments, bottom reflectivity experiments were carried out. By computing the reflection coefficient of the bottom as a function of grazing angle it was possible to estimate the geoacoustic parameters using a nonlinear inversion technique[7]. The basement model used for this paper is also shown in Figure 3. In reality, there was probably a thin sediment layer with range-dependent thickness in this region. However, it was found that including a sediment layer of constant thickness in the MFP modelling did not improve the subsequent MFP results. A typical bathymetry profile is also shown for this area in Figure 4. As can be seen the bottom is rugged, with a mean depth of 5000 m and rms roughness of about 25 m.

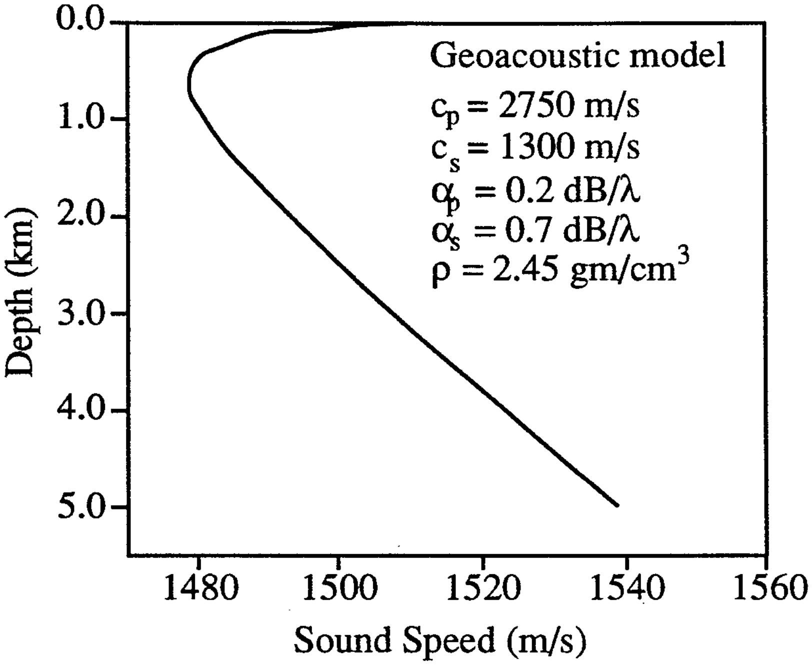

Figure 3. Sound speed profile at experimental site

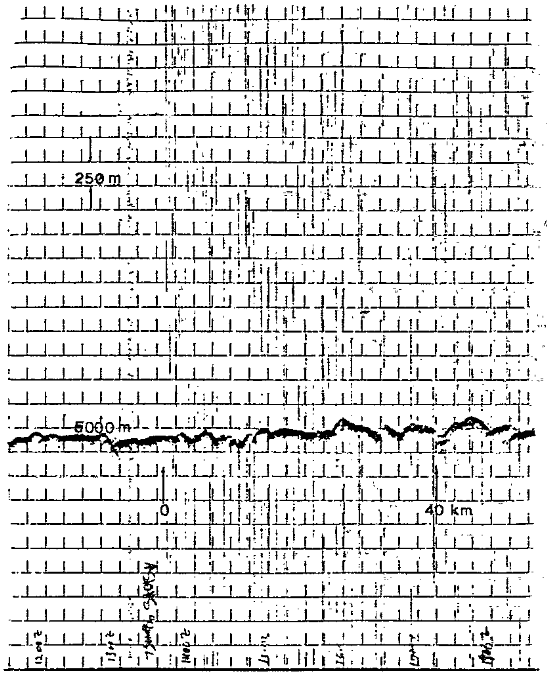

Figure 4. Typical bathymetric profile

IV. PROPAGATION MODELLING

A two-dimensional plot of propagation loss as computed by the KRAKENC computer code for the sound speed profile of Figure 3 and a 15-Hz source at a depth of 100 m, is shown in Figure 5. To illustrate the accuracy of the KRAKENC code the propagation losses computed by the SAFARI, KRAKENC, and KRAKEN codes as a function of range for a 15-Hz source at a depth of 100 m and a receiver at 486.7 m (the third hydrophone of the MEVA array) are shown in Figure 6. As can be seen the KRAKENC and SAFARI curves show excellent agreement even at short ranges where the continuous spectrum is important. The KRAKEN results are in fair agreement with the other two methods. This figure also indicates that, for the long range ($\approx$ 38 km) arc, there is a strong contribution from water column propagation paths. This was confirmed by an analysis of the multipath propagation loss which showed that the losses for the water column and all the bottom bounce contributions were roughly equal[7].

V. DATA PROCESSING

In this section examples of the spectral data used in the MFP are shown. In Figures 7a - 7b the power spectra resulting from 4096 point (2.73 sec) FFT for the 15-Hz line are shown for Channel 3 using 64 averages. The SNR was estimated to be 20 dB and 30 dB for the long range and short range 15-Hz experiments respectively. Similarly, in Figures 8a - 8b the power spectra for the 10-Hz line are shown. The estimated SNRs for these two cases are 12 dB and 27 dB. It should be noted that the programmable array gain was set 12 dB higher during the long range experiments than it was set during the short range ones and hence the peak spectral levels in Figures 7 and 8 appear almost equal for the long and short range cases.

The hydrophone data were also beamformed over the vertical array using 64 averages of the cross-spectral matrix with 4096 pt FFTs. The vertical beampower as a function of vertical arrival angle is shown in Figures 9a-d for the 10-Hz short-range, 10-Hz long-range, the 15-Hz short-range and the 15-Hz long-range data. In these plots 0° represents horizontally propagating energy, negative angles represent energy arriving from below the horizontal. For the short range data sets it can be seen that the dominant energy is almost totally direct, whereas for the 38 km data there are vertical arrival angles corresponding to deep refracted arrivals, bottom interacting arrivals, and surface interacting arrivals.

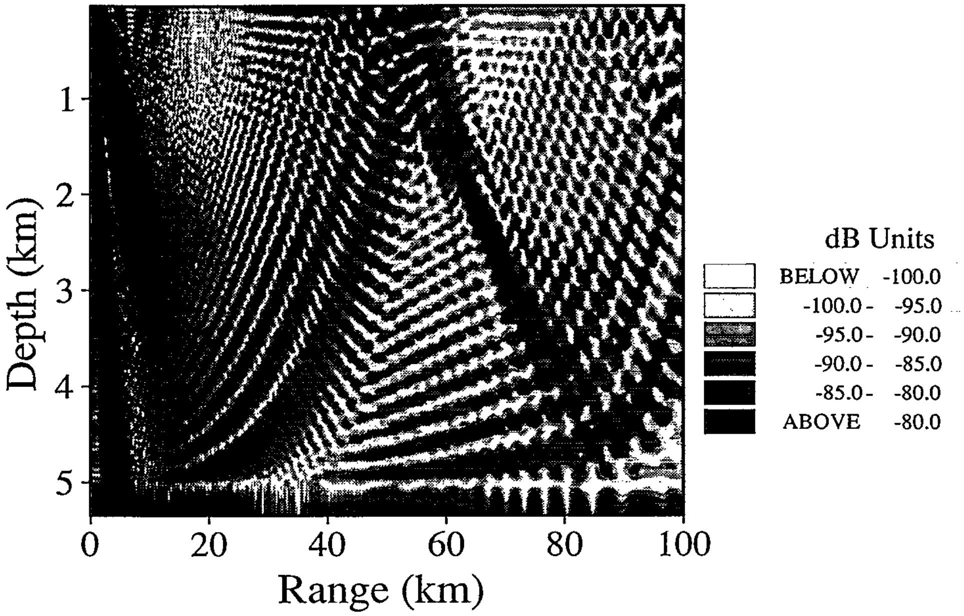

Figure 5. Propagation loss for 15-Hz source at 100-m depth

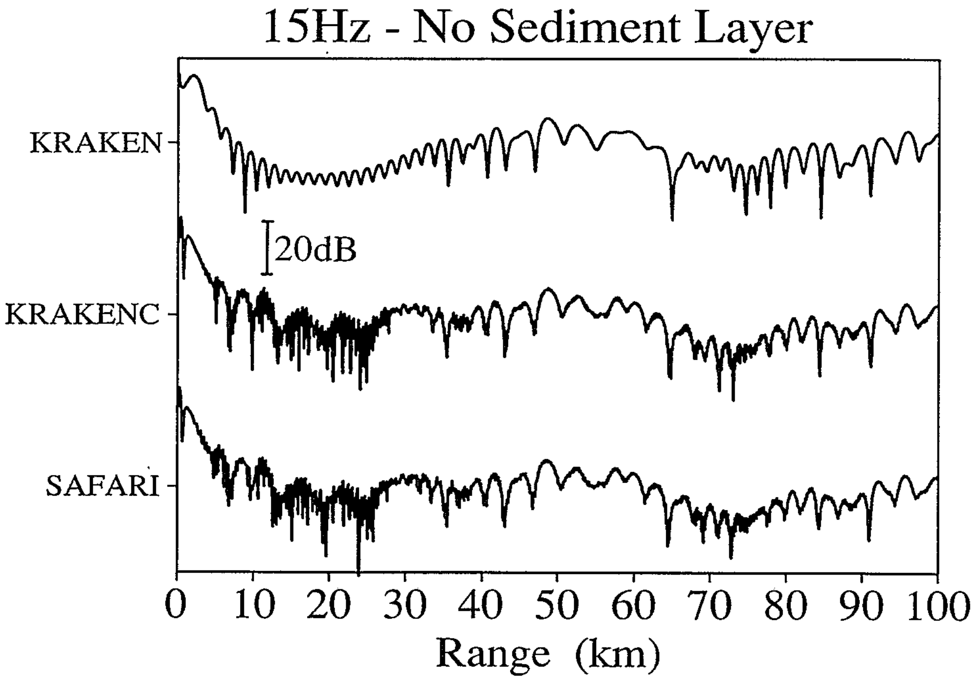

Figure 6. Comparison of SAFARI, KRAKEN, and KRAKENC propagation loss computations for the third hydrophone from a 15-Hz source at 100-m depth

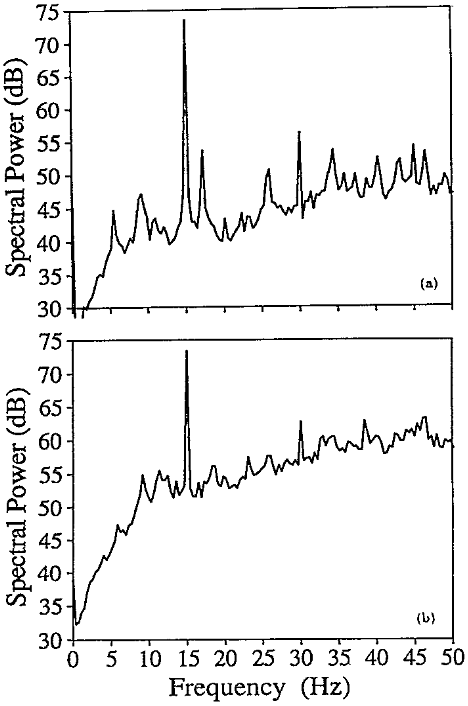

Figure 7. Power spectra from 4096 point FFT (64 averages) for 15-Hz source at (a) short range (b) long range

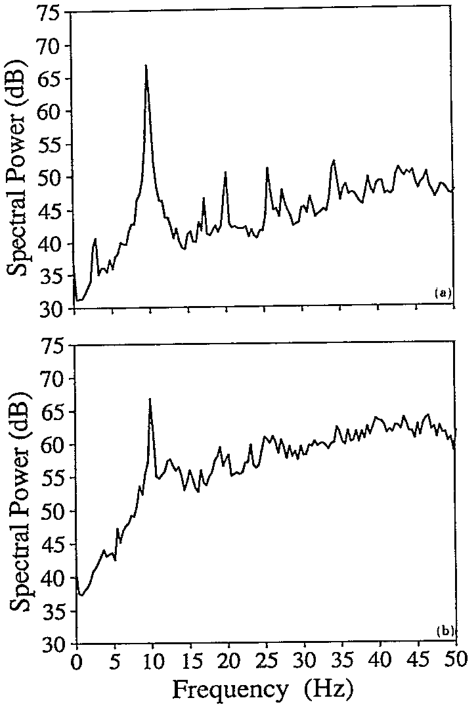

Figure 8. Power spectra from 4096 point FFT (64 averages) for 10-Hz source at (a) short range (b) long range

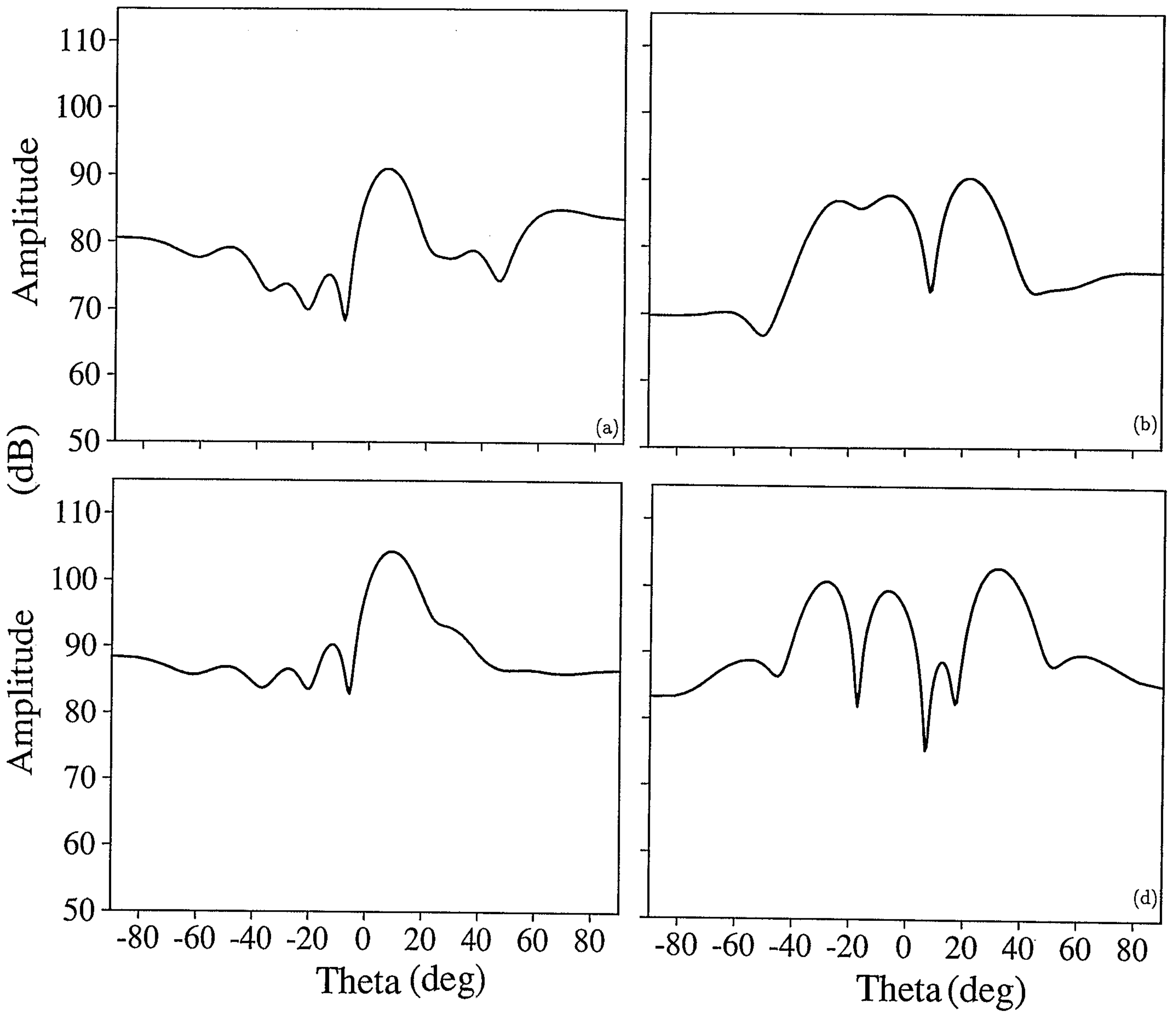

Figure 9. Plane-wave vertically beamformed power for (a) 10-Hz/short-range source (b) 10-Hz/long-range source (c) 15-Hz/short-range source (d) 15-Hz/long-range source

In Figures 10 a-b the modulus of the eigenvalues of the averaged cross-spectral matrix (64 averages) are plotted in dB for a 4096 point FFT, for the 10- and 15-Hz short-range lines.

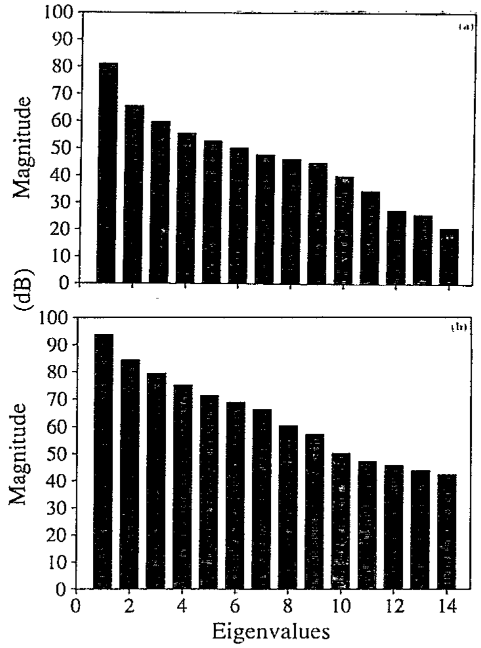

Figure 10. Modulus of eiegenvalues of averaged cross-spectral matrix (4096 point FFT, 64 averages) for (a) 10-Hz/short-range (b) 15-Hz/short-range

As can be seen there is a dynamic range of about 50 dB between the largest and smallest eigenvalue. Because of the very small eigenvalues it is necessary to add a small quantity to the diagonal of the cross-spectral matrix when inverting it to avoid numerical problems. In fact, it was found that the Minimum Variance estimator performed best with a significant percentage of the signal power added to the diagonal (e.g., 10%).

VII. COMPUTATION OF AMBIGUITY SURFACES

A. The effect of number of modes used in propagation modelling

Previous authors (for example, reference 4) have restricted the modes used in the computation of replica fields to those corresponding to water-borne energy. In this manner the energy which has interacted with the uncertain geoacoustic bottom is not considered in the "matching" process of MFP. However, for source locations where bottom-interacting energy is dominant this may make the resulting MFP estimates very ambiguous. Thus, there are trade-offs to be considered in the modelling of the bottom-interacting energy.

KRAKENC has the ability to simulate the continuous spectrum which can be important in the modelling of the acoustic field from a source in the first bottom-bounce region. Below, we consider the effects of using all modes in computing the replica fields, the effect of using only the discrete normal modes, and the effect of using all modes with a rough-bottom model. The rough-bottom model computes attenuation coefficients for the modes in order to account for the attenuation of the coherent pressure field due to the scattering from the rough surface.

A total of 94 modes were computed by KRAKENC of which only 31 are discrete modes for the 15-Hz case, and 63 modes of which only 21 are discrete for the 10-Hz case. In Figures 11a-d the Minimum Variance ambiguity surfaces for the data sets 10-Hz/short-range, 10-Hz/long-range, 15-Hz/short-range, and 15-Hz/long-range are shown using all the computed modes and assuming that the bottom was flat in calculating the replica fields. For comparison, the ambiguity surfaces shown in Figures 12a-d result from using only the discrete modes in the calculations. As can be seen the ambiguity surfaces are now smoother in structure. In Figures 13a-d the ambiguity surfaces are shown for all the computed modes but with a roughness of 25m in the Kuperman-Ingenito roughness model. As can be seen the ambiguity surfaces are smoother than those of Figure 11, but not as smooth as those of Figure 12. The depth and range estimates resulting from the peak location are shown in Table I for the three different propagation models and the four scenarios.

Table I. Location estimates for the three propagation models

	All Modes	Propagating	Rough	True
SR 10 Hz	(7.45km,170m)	(7.5km,210m)	(7.65km,10m)	(5.5km,100m)
SR 15 Hz	(7.3km,250m)	(7.1km,170m)	(7.35km,210m)	(5.5km,100m)
LR 10 Hz	(25.45km,250m)	(40.4km,10m)	(36.95km,90m)	(36.0km, 100m)
LR 15 Hz	(36.65km,50m)	(38.8km,10m)	(36.45km,70m)	(38.0km,100m)

The estimates from the discrete modes and rough-bottom models are better than those (in particular, for the long-range 10-Hz scenario) obtained by using all modes with a flat bottom. The former two cases also have smoother and more readily interpretable ambiguity surfaces. The rough-bottom model effectively attenuates higher-angle propagation because the associated modes have higher attenuation coefficients; thus, even though all modes have been used in the computation of the replica fields the resulting ambiguity surfaces are similar to those obtained by using only the discrete modes. The estimation results of Table I are good but can certainly be improved upon, particularly for the short-range scenarios. This improvement will be obtained below by considering the effect of array tilt.

B. The Effect of Array Tilt

Thus far in this paper, it has been assumed that the array is perfectly vertical. However, it is possible to compute the ranges and depths of the individual hydrophones for a given tilt angle by using Eqs.(5a) and (5b). The effect of tilt angle on the hydrophone depths is second order in θ so that this correction term is ignored. The tilt angle, θ, is now varied between −6° and 6° assuming that $\phi = 0$ in Eq.(5a); if, in fact, ϕ is not equal to zero then θ corresponds to an effective tilt angle in the plane of the source.

In order to simultaneously estimate the array tilt and localize the source we adopt the following strategy. We assume that we have a good apriori estimate of the source position; we then define a window about this location and as the hypothesized tilt of the array is varied the position of maximum power is located. The tilt angle which gives the maximum of these powers can then be obtained. For the short (long) range examples a window, 10-210m in depth by 4.5 to 6.5 km (34 to 40 km) in range is defined. For these ambiguity surfaces the rough bottom model was used. In Figures 14a-d the maximum power within the allowed window is plotted as a function of the tilt angle for the 10-Hz/short-range, 10-Hz/long-range, 15-Hz/short-range, and 15-Hz/long-range scenarios.

In Table II the depth and range estimates are given for the optimal tilt angle. As can be seen, including the array tilt angle in the model has improved the location estimates, particularly for the short range scenario.

Finally, in Figures 15a-b the MFP ambiguity surfaces for the 10-Hz short range example are shown for tilt angles of 0° and the optimal value of −3°. As can be seen the ambiguity surface for the −3° tilt is slightly less ambiguous.

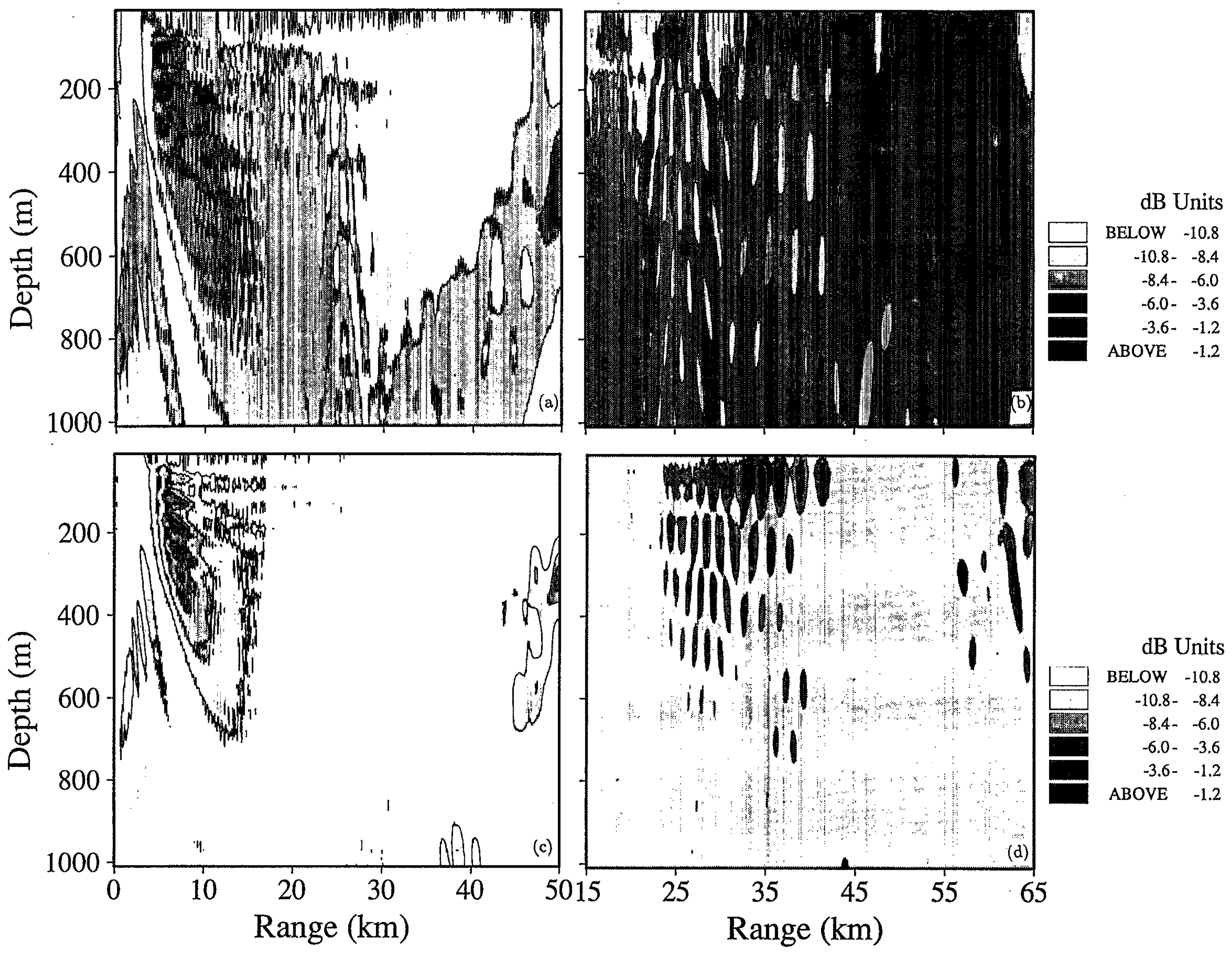

Figure 11. Minimum variance ambiguity surfaces using all computed modes for (a) 10-Hz/short-range source (b) 10-Hz/long-range source (c) 15-Hz/short-range source (d) 15-Hz/long-range source

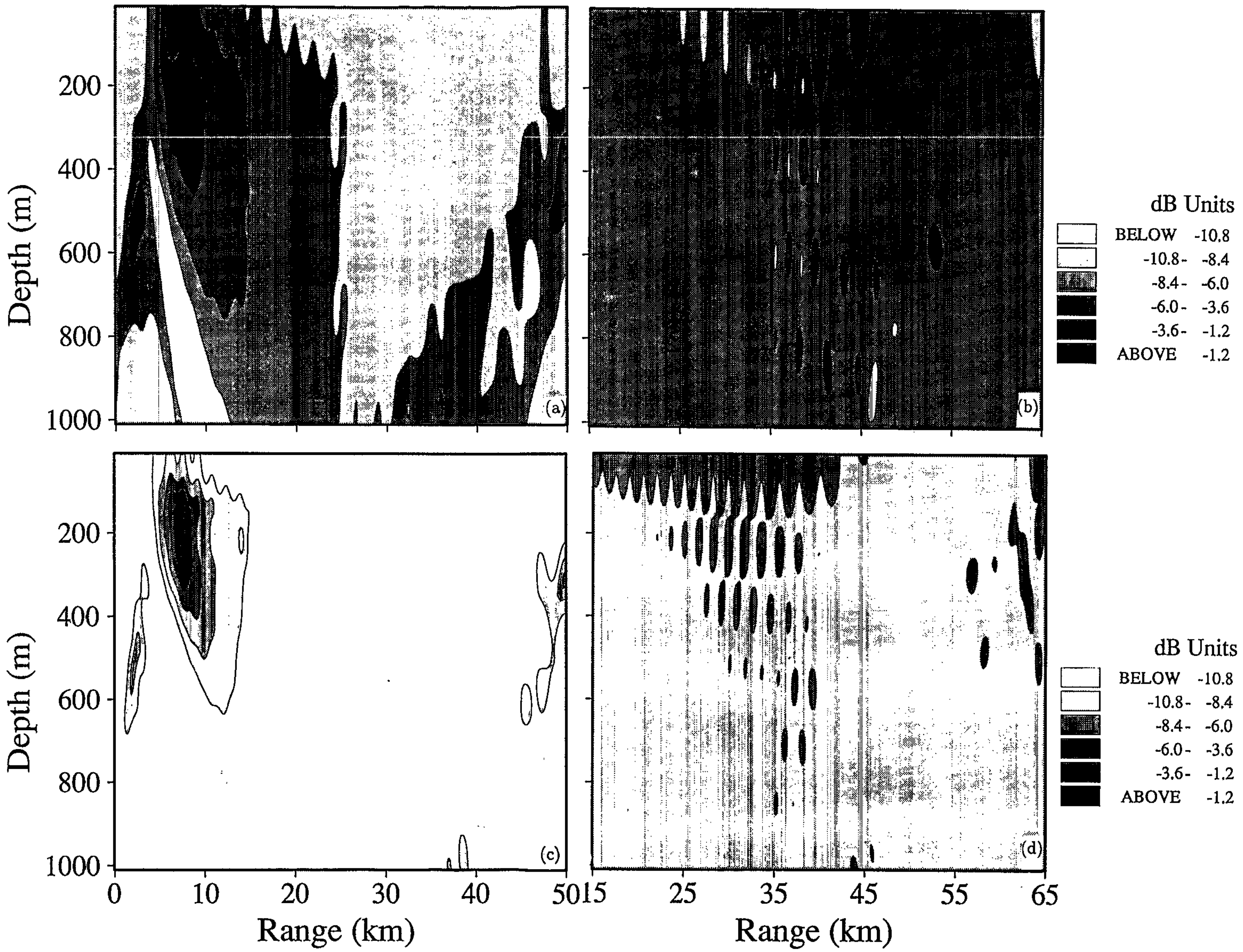

Figure 12. Minimum variance ambiguity surfaces using only discrete propagating modes for (a) 10-Hz/short-range source (b) 10-Hz/long-range source (c) 15-Hz/short-range source (d) 15-Hz long-range source

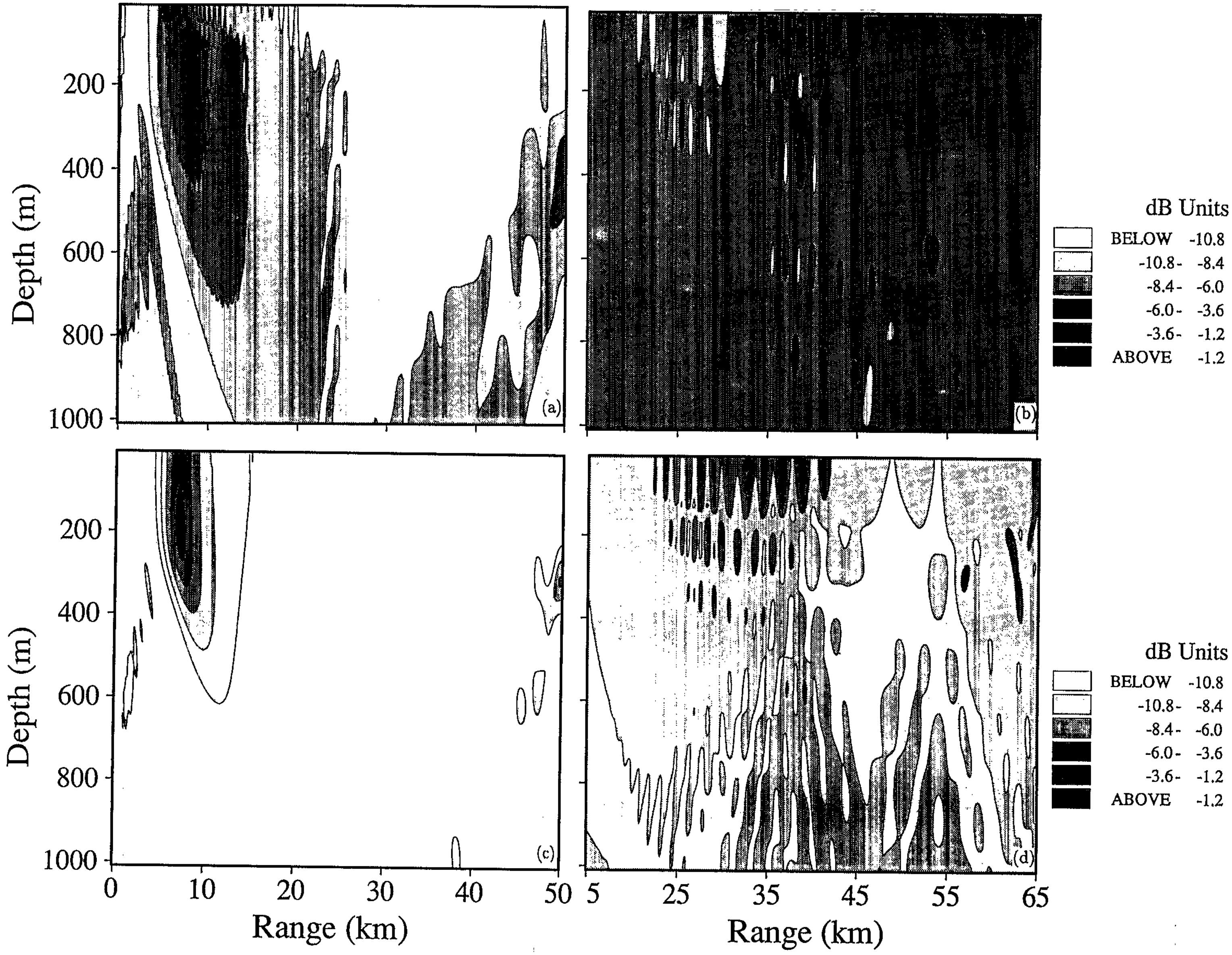

Figure 13. Minimum variance ambiguity surfaces using all computed modes with Kuperman-Ingineto roughness model for (a) 10-Hz/short-range source (b) 10-Hz/long-range source (c) 15-Hz/short-range source (d) 15-Hz/long-range source

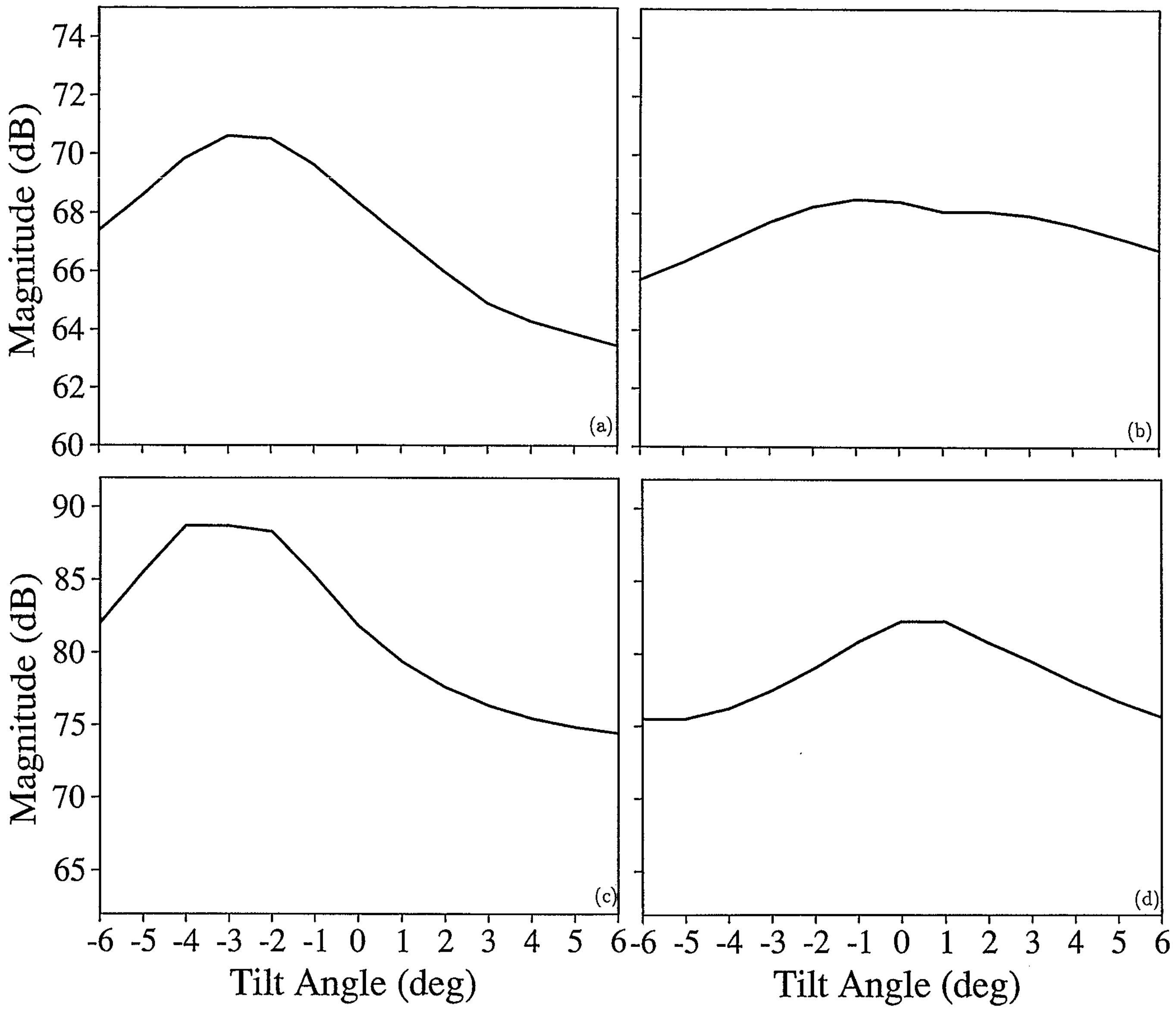

Figure 14. Maximum Minimum Variance power (rough bottom model) as a function of tilt angle for (a) 10-Hz/short-range source (b) 10-Hz/long-range source (c) 15-Hz/short-range source (d) 15-Hz/long-range source

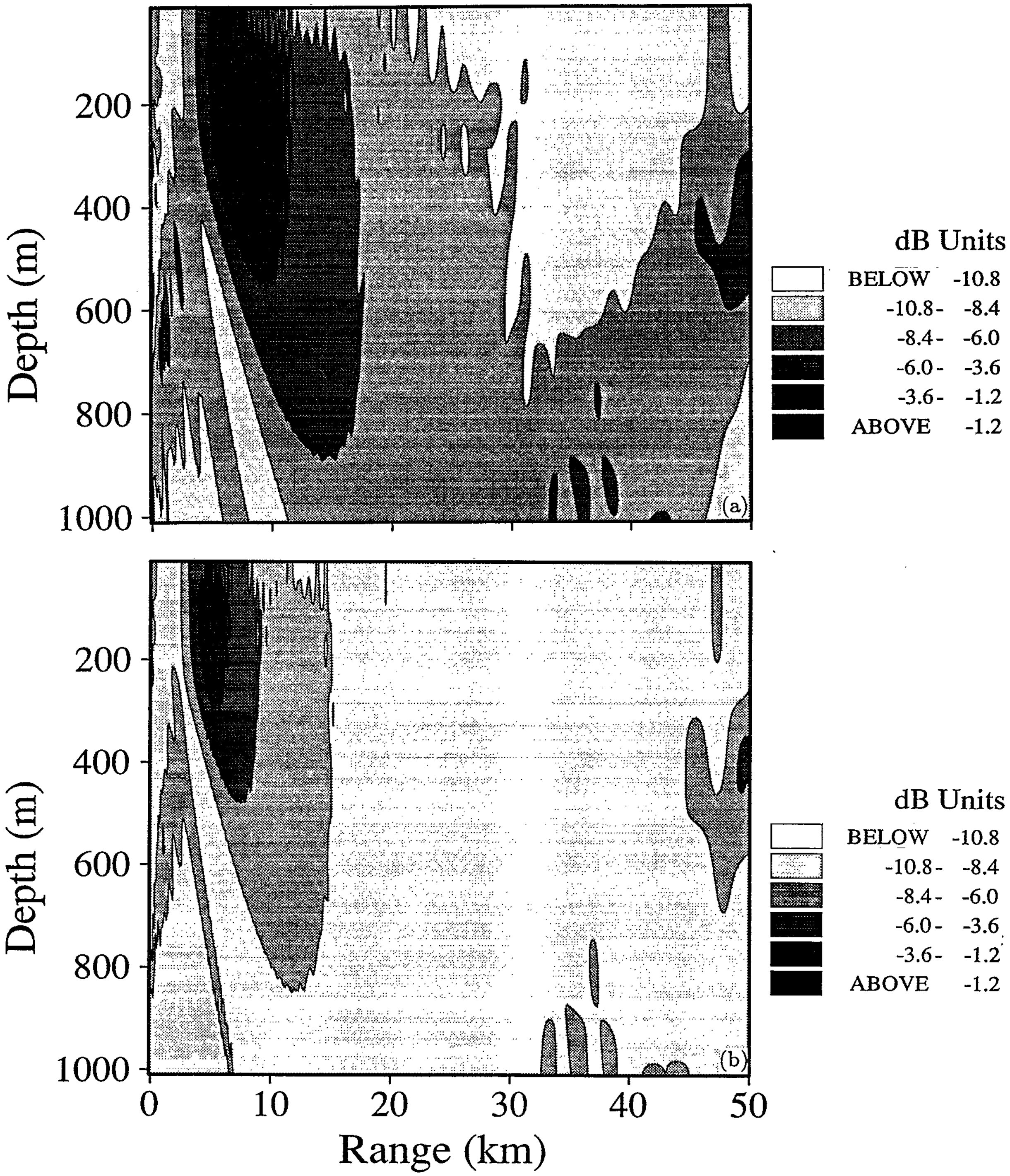

Figure 15. Minimum Variance ambiguity surfaces for 10-Hz short-range source for (a) −3° tilt angle (b) 0° tilt angle.

Table II. Location estimates for the optimal tilt angles

	Range(km)	Depth(m)	Tilt(°)
SR 10 Hz	5.2	50	-3
SR 15 Hz	4.5	10	-4
LR 10 Hz	37.1	90	-1
LR 15 Hz	36.4	70	0

C. The Bartlett Estimator

In the examples considered so far, we have considered only the Minimum Variance estimator. In Figures 16a-16d we show the ambiguity surfaces obtained from the Bartlett estimator for the four data sets using all computed modes with the rough bottom model and a 0° array tilt angle. As can be seen the ambiguity surfaces from the Bartlett estimator are more diffuse than those of the Minimum Variance estimator; however, the peak locations are very close to the corresponding Minimum Variance estimates.

VIII. SUMMARY

In this report the ability of MFP algorithms to localize an acoustic source with respect to range and depth has been demonstrated. This was done with both a 10- and 15-Hz source. The range estimation errors were usually smaller than 2 km and the depth error smaller than 100 m. The SNR of the data was very high for these experiments and was not an issue in the results; rather, the lack of knowledge about the oceanic environment and the receiver positions were probably the greatest sources of errors. It is encouraging that with the many assumptions which were made about the ocean environment, including range independence (which is clearly not true for the experiment) and the estimated values of the basement elastic parameters, the MFP results are still useful.

Restricting the higher order mode contributions, either directly or through a roughness model resulted in smoother and somewhat more interpretable ambiguity surfaces.

Finally, it was demonstrated that the tilt angle of the array could be determined from the data itself (given a good apriori knowledge of the source location) and that incorporating the tilt angle in the model did, in fact, improve the MFP results.

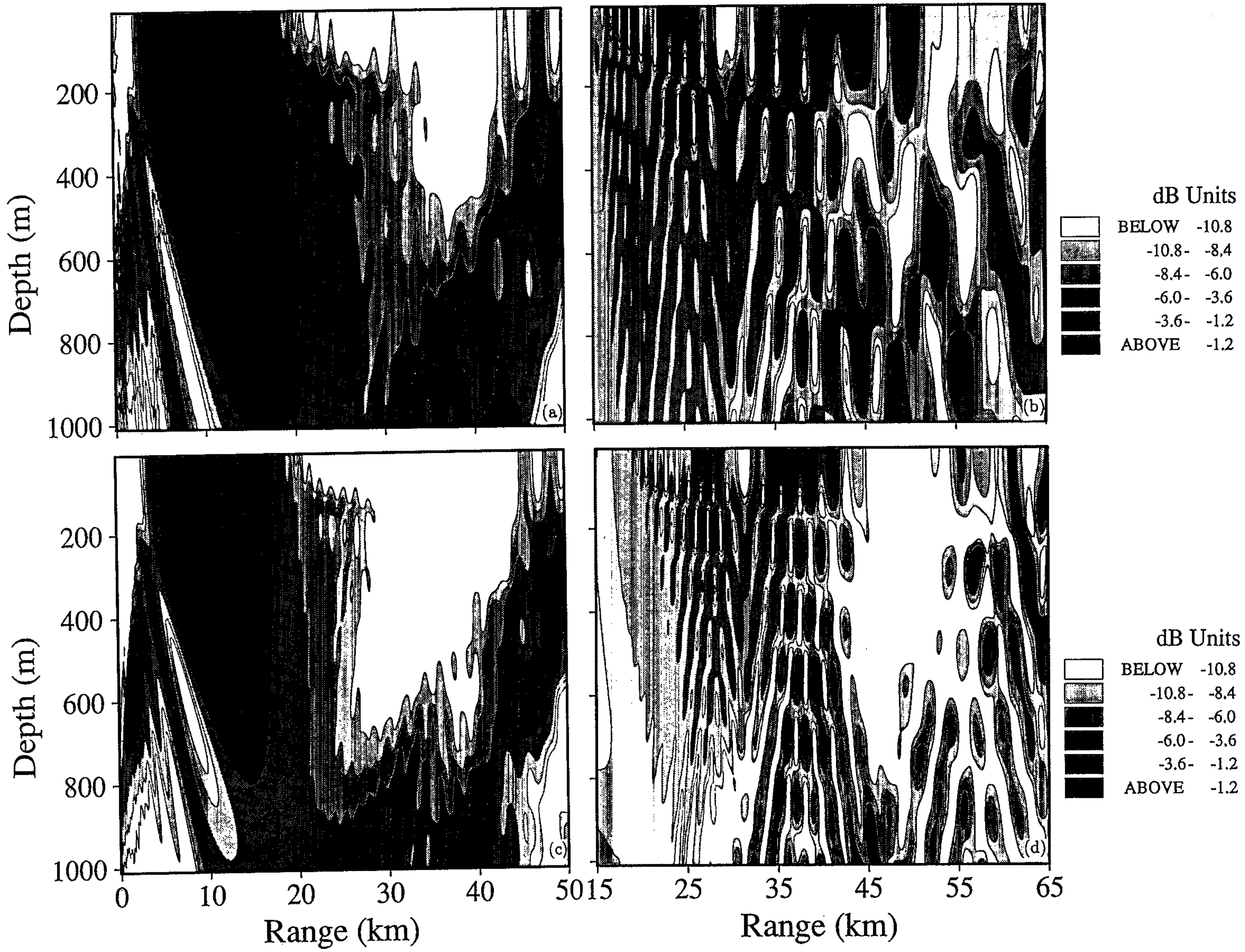

Figure 16. Bartlett ambiguity surfaces with rough bottom model for (a) 10-Hz/short-range source (b) 10-Hz/long-range source (c) 15-Hz/short-range source (d) 15-Hz/long-range source

REFERENCES

1. R. G.Fizell, R. L. Dicus, and O. I. Diachok, "Experimental applications of matched-field processing in the North Pacific", submitted to J. Acoust. Soc. Am., 1990.
2. H. Schmidt. "SAFARI: Seismo-Acoustic fast field algorithm for range-independent environments - user's guide.", SACLANTCEN Report SR-113, SACLANT Undersea Research Centre, Italy, September 1988.
3. M. B. Porter, "The KRAKEN Normal Mode Program ", SACLANT Undersea Research Centre, Italy, preprint, July, 1989.
4. A. Tolstoy, "Sensitivity of matched field processing to sound-speed profile mismatch for vertical arrays in a deep water Pacific environment", *J. Acoust. Soc. Am.*, **85**, 2394-2404 (1989).
5. J. A. Fawcett, N.R. Chapman, and M. McKirdy, "Matched field processing in a rough bottom, deep ocean environment", in Proceedings of 18th Meeting, TTCP Technical Panel, GTP-9, Victoria, October 1989.
6. D. R. Del Balzo, C. Feuillade, and M. M. Rowe, "Effects of water-depth mismatch on matched-field localization in shallow water", *J. Acoust. Soc. Am.*, **83**, 2180-2185 (1988).
7. N.R. Chapman and M. McKirdy, "Low Frequency Propagation in a Thin-Sediment North Pacific Environment", in proceedings of the 18th Meeting, TTCP Technical Panel, GTP-9, Victoria, October 1989.
8. A. B. Baggeroer, W. A. Kuperman, and H. Schmidt, "Matched field processing: Source localization in correlated noise as an optimum parameter estimation problem", *J. Acoust. Soc. Am.*, **83**, 571-587 (1988).
9. W.A. Kuperman and F. Ingenito, "Attenuation of the coherent component of sound propagating in shallow water with rough boundaries," J. Acoust. Soc. Am, **61**, 1178-1187 (1977).

MATCHED FIELD SOURCE LOCALIZATION USING BROADBAND SHOT DATA

N.R. Chapman and M.L. McKirdy
Defence Research Establishment Pacific
FMO Victoria B.C.
V0S 1B0

ABSTRACT

A method is described for matched field source localization using broadband shot data. The processing was carried out in the frequency domain, using an FFT to obtain the spectral components of shot signals received on a vertical line array. A Bartlett processor was used to correlate the measured fields at the array with replica fields calculated with a normal mode model. Several issues were investigated to determine methods for improving the matched field localization performance. These included frequency averaging of range/depth ambiguity surfaces, and processing with a restricted mode sum or with a partial multipath signal. The sensitivity to mismatch in sound speed profile was also investigated. These effects are analyzed in case studies using shot data from the first PACIFIC ECHO experiment carried out in the North Pacific.

INTRODUCTION

Matched field processing (MFP) has become a well-established method in underwater acoustics for estimating the range and depth of a sound source. In simple terms, MFP is a model-based signal processing technique in which the acoustic fields measured at an array of hydrophones are correlated with replica fields at the array calculated using realistic models of the ocean environment. Both horizontal and vertical arrays have been considered in MFP studies. An extensive amount of research has been carried out over the past few years to determine the sensitivity of various MF processors to uncertainties in knowledge of the environment and the experimental geometry. Much of the attention has been focussed on MFP with CW sources. However, broadband sources offer considerable promise for applications in tomography and inversion of environmental properties, as well as in source localization.

A number of approaches to MFP for broadband data have appeared in the literature. Clay and Li have discussed the formulation of broadband source localization in the time domain[1]. Hodgkiss and Brienzo[2], and Mignerey[3] have developed methods for broadband localization by processing the impulse response of explosive charge signals. In this paper, we describe source localization of broadband data using standard full-wavefield processing techniques that have been applied successfully to CW data. There are several types of broadband sources available; we restrict our attention to a specific type, namely explosive charges or shots. For these sources, the signal measured at a deep-ocean hydrophone consists of a series of pulses corresponding to specific propagation paths in the ocean waveguide. Depending on the geometry of the experiment, the multipath signals are generally well-resolved in time. We present an investigation of methods for processing the data which exploit the unique features of shot signals in order to improve the MF localization performance. These include frequency averaging of range/depth ambiguity surfaces, and the related effects of partial mode summation and partial multipath. An example is also presented to demonstrate the effect of mismatch in the sound speed profile. These effects are analyzed in case studies using deep-ocean shot data obtained in the first PACIFIC ECHO sea trial.

The paper is organized as follows. The next section provides a brief background for the PACIFIC ECHO experiments from which the data were taken. Then we describe the MF processor and the signal processing issues that were considered. Following this, case studies of two data sets are presented to demonstrate the effects of frequency averaging, partial mode spectra/partial multipath, and mismatch in sound speed profile on MFP with broadband shot sources.

PACIFIC ECHO BACKGROUND

The first PACIFIC ECHO sea trial was a collaborative exercise carried out by the Defence Research Establishment Pacific and the US Naval Research Laboratory to study MF source localization in a thin-sediment deep-water environment. The experiment described in this report was carried out at a site near 37° 30 N 133° W in the Northeast Pacific Ocean, where the water depth was 5000 m, and the bottom consisted of a thin sediment layer of at most 40 m overlying basalt. The properties of the bottom were determined from bottom reflectivity measurements at the site[4]; the geoacoustic model is shown in Figure 1. The most significant feature of the model is the elastic basalt basement; for this environment, it was necessary to account for the conversion of acoustic energy into shear waves in modelling the propagation.

The broadband localization data were obtained using a 16-element, 675-m vertical line array (VLA) that was suspended in the deep sound channel. The depth of the uppermost array hydrophone was 378 m. In the experiment, the array was monitored by CFAV ENDEAVOUR, while 0.82-kg SUS charges were deployed from USNS DESTEIGUER in a radial shot run out to the first convergence zone. The shot depth was nominally 244 m, and the spacing was designed to provide data at 2-degree grazing angle intervals. Ranges were measured with a ship-to-ship trisponder system; these values were corrected for the actual array position using radar navigation data to measure the range and bearing of the array surface buoy from CFAV ENDEAVOUR. The expected error in a range measurement was ± 200 m. The sound speed profile in the water was measured with expendable sound velocity probes (XSVs) deployed from the shooting ship at range intervals of about 10 km during the run, and from the array ship immediately before and after the experiment. These measurments provided information for the upper 2000 m of the water column, where the temporal and spatial variation in sound speed is greatest. A CTD measurment was also made at the site in order to extend the sound speed profile to the ocean bottom.

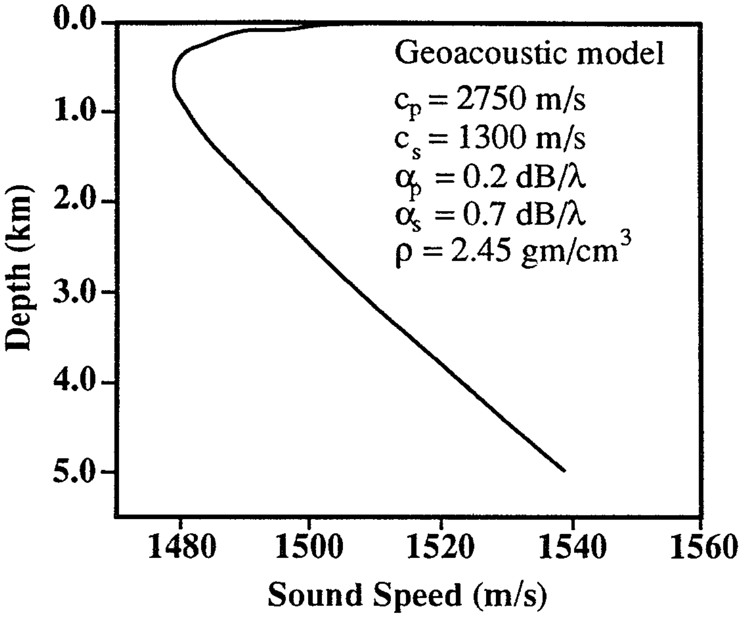

Figure 1. The environment model for the site, including a water column sound speed profile measured at the array and the geoacoustic parameters of the basalt[4].

DATA PROCESSING ISSUES

1. The MF Processor

The approach taken for MFP of the broadband shot data was to determine the spectral components of the shot signal, and then apply processing methods that have been used successfully with single frequency data. Accordingly, the shot time series was transformed to the frequency domain using an FFT. A Bartlett or linear processor was then used to compute ambiguity surfaces in range and depth for specific spectral components. This processor is defined as

$$B(r,z) = \sum_{i=1,j=1}^{N} p_i^*(r,z) R_{ij} p_j(r,z)$$

where $R_{ij} = X_i^* X_j$ is the expected value of the cross-spectral matrix of the spectral components, X, of the field at the ith and jth sensors, and $p_i(r,z)$ is the replica field at the ith sensor calculated for a point source in the environment determined for the site. The calculated pressures are normalized so that the vector of pressures across the array has unit length. If the acoustic environment has been modelled accurately, it can be shown that the MFP Bartlett processor achieves the maximum possible signal gain, 10 log N, for an array of N hydrophones[5].

For this work we have restricted the analysis to very low frequencies, a 1/6-octave band centred at 20 Hz, in order to minimize the error due to uncertainty in hydrophone position. As a rule of thumb for MFP, errors in the hydrophone positions should be much less than 1/3 of the wavelength of the processing frequency. The spectral level at 20 Hz was 15 to 18 dB below the peak value at about 60 Hz, and the actual signal-to-noise ratio (SNR) was strongly dependent on the shot range. For the shots deployed in the shadow zone (from 8 to 30 km) SNR values were generally less than 10 dB, whereas at convergence zone ranges (> 35 km) the SNRs were 20 to 25 dB.

There are a number of methods for modelling the acoustic pressure in order to generate the replica fields at the VLA. For this work the normal mode model KRAKENC[6] was used to model the propagation in a flat oceanic waveguide with elastic bottom layers. This model computes the pressure field from the sum

$$p_i(r,z) = \alpha \sum_{m=1}^{M} \Phi_m(z_i)\Phi_m(z)\frac{e^{-ik_m r}}{\sqrt{k_m r}}$$

where z_i is the depth of the ith sensor, M is the number of modes, and α is a constant. Unlike other modal codes which only approximate the effects of attenuation, KRAKENC uses a complex root finder to locate the discrete, complex wavenumbers corresponding to the modes of an elastic waveguide. KRAKENC also computes leaky modes, allowing an approximation to the continuous spectrum (or branch-line integral) portion of the field. For the ocean environment at this site there are 118 modes at 20 Hz, 28 of which are water column modes and the rest are bottom-interacting modes associated with the relatively large sound speeds in the basalt.

2. Broadband Source Localization

The unique features of broadband shot signals can be exploited in processing the data to obtain improved MF localization performance. These advantages are not available with CW data. In this paper we investigate the effect of three issues in processing broadband shot data. The first issue is averaging the range/depth ambiguity surfaces for different frequencies in a specific band. This procedure reinforces the peak associated with the true source position and averages out the sidelobes, which occur at different positions for each frequency. Frequency averaging is potentially important for low SNR data for which it is not possible to localize the source with a single frequency component. Such a condition arises in processing data at very low frequencies from relatively deep shots. Baggeroer et al. have demonstrated improvements in localization performance using frequency-averaged simulated data[7]. We present a similar analysis with deep-water shot data measured in the acoustic shadow zone where the dominant propagation paths are bottom reflections. Both dB and linear averages are considered in the analysis.

The second issue includes the related effects of processing a partial multipath signal and using a partial mode sum in calculating the replica fields. This is an important consideration for data where one propagation path is dominant, such as for sound sources (and arrays) in the deep sound channel where the propagation is primarily via convergence zone or SOFAR paths. There is potentially a great saving in the computing time necessary to process the data if smaller data segments and fewer modes can be used. Our analysis considers the questions of what components of the multipath signal, and what portion of the mode spectrum are required for localizing the source. We present the results of processing a shot deployed in the deep sound channel at a range of about one convergence zone.

The last effect that we consider is the mismatch of the sound speed profile in the water. The magnitude of the error introduced by this effect depends strongly on the sound speed gradients at relatively shallow depths near the source, and the problem has been studied extensively for a Pacific profile by Tolstoy[8]. We present a case study which demonstrates the effect of mismatch, using a PACIFIC ECHO shot which was processed with two sound speed profiles. One profile was taken near the array at the beginning of the shot run, approximately two hours before the shot was deployed, and the other was measured by the shooting ship within a few minutes of the shot time.

CASE STUDIES

1. Frequency Averaging

The effect of frequency averaging of the ambiguity surfaces was investigated using a shadow zone shot at a range of 17.8 km and a depth of 244 m. From a previous analysis of the propagation loss, the dominant propagation paths were bottom reflections and the loss measured at the array varied from 85 to 90 dB[4]. This corresponded to SNR values between 8 and 13 dB. The shot signal was processed with a 16-K FFT, corresponding to a time window of 10.6 s that included three bottom reflections. Ambiguity surfaces were determined for 11 frequencies in a 1/6-octave band at 20 Hz. The estimates of the shot position are listed in Table 1 for each frequency and also for averages over the band. Generally, it was not possible to localize the source accurately with a specific frequency component. However, averaging the ambiguity surfaces over the band, using either a dB or a linear average, greatly improved the localization performance. This improvement is obtained because the ambiguous sidelobes are reduced in the process, whereas the central peak representing the source position is frequency independent, and is consequently reinforced. The effect is demonstrated in Figure 2 where we show ambiguity surfaces for a single frequency at 19.23 Hz and for the dB-averaged case.

There is some question of which type of averaging should be used. Our experience with this shot and others indicates that there is very little difference in the source position estimates, over the relatively narrow 1/6-octave band, for either type of averaging. However, the dB-averaged ambiguity surfaces were generally smoother, with fewer and lower sidelobes. Intuitively, there is an appealing argument for the dB or geometric average, since in order for the ambiguous sidelobes to average out, their values should be of the same order of magnitude.

Table 1. Localization by Frequency Averaging for Shadow Zone Shot

Frequency (Hz)	Range (km)	Depth (m)
18.86	15.7	85.0
19.23	19.6	85.0
19.50	19.1	85.0
19.78	40.0	965.0
19.87	11.5	105.0
19.96	14.8	105.0
20.05	47.1	665.0
20.42	40.2	925.0
20.69	16.9	285.0
21.06	17.5	225.0
dB Averaging	17.7	225.0
Linear Averaging	17.0	245.0

2. Partial Mode Sum/Partial Multipath

The related effects of partial mode sum and partial multipath signal were considered using a shot that was deployed at the onset of the convergence zone at a range of 38.3 km and a depth of 244 m. The propagation loss was significantly lower than that for the shadow zone shot, 78 to 82 dB over the array, and the acoustic field was dominated by contributions from refracted paths in the water[4]. The SNR was at least 20 dB, so that it was possible to obtain good localization performance with a single frequency component.

To understand the issues that are presented here, it is useful to consider ray-mode analogies. Each multipath component of the signal can be represented by a sum over a complete set of modes; however, each component will have a different set of mode amplitude coefficients. For instance, waterborne refracted signals will have negligibly small weights for the high-order modes that sample the waveguide like steep-angle, bottom-interacting rays, but will have large amplitudes for the low-order

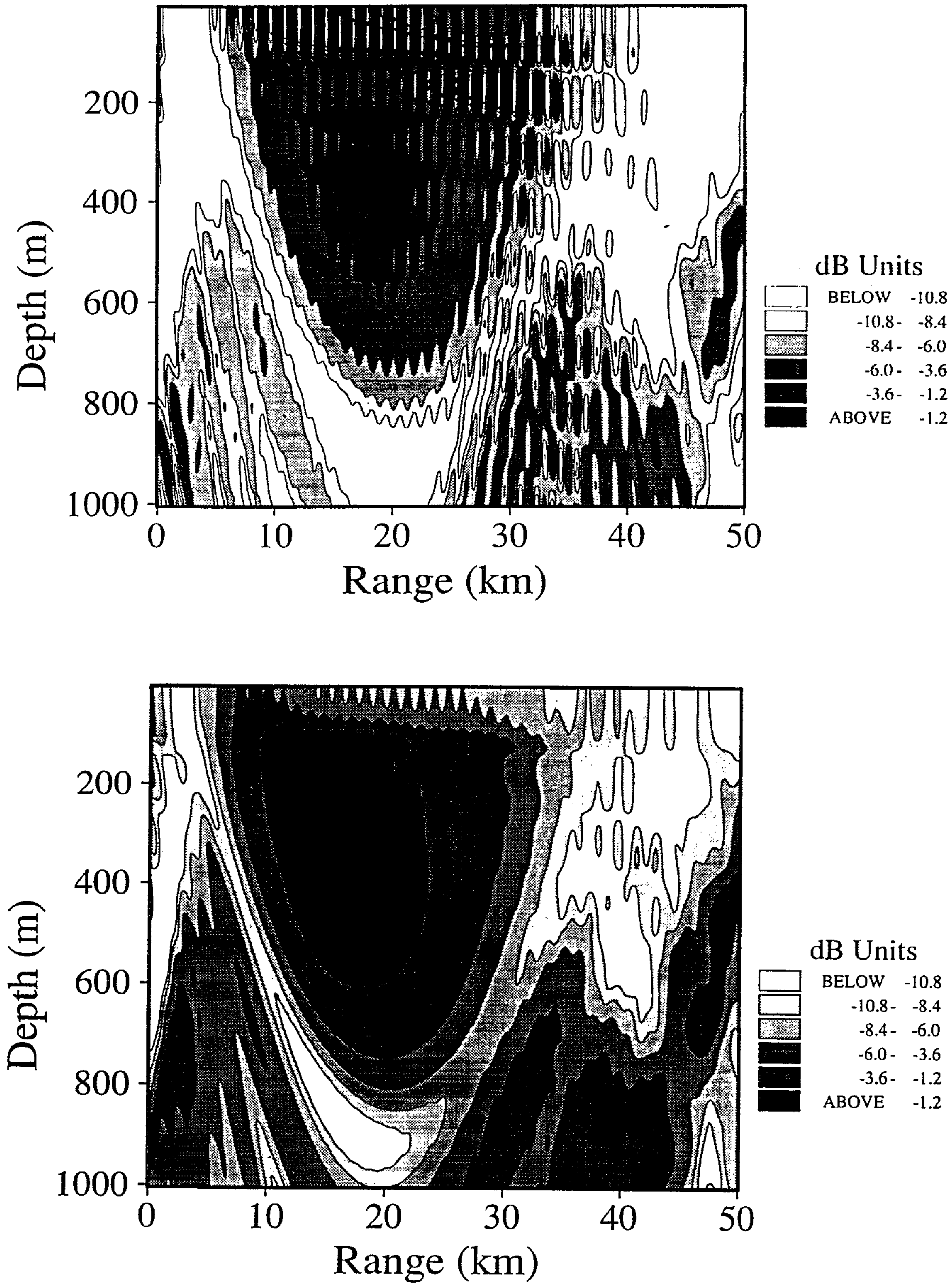

Figure 2. Range/depth ambiguity surfaces for the shadow zone shot. The upper surface is for a single frequency at 19.23 Hz, and the lower surface is for the dB-averaged case.

modes that behave like shallow-angle rays. Thus, it is reasonable to expect that for cases where the propagation is dominated by specific propagation paths, it is possible to construct the replica fields for MFP using a restricted mode sum. In addition, it is also reasonable to expect that the single dominant multipath component can be used to localize the source.

The localizations using the entire multipath signal are presented in Table 2. The data were processed with a 12-K FFT, corresponding to an 8 s time window that included the refracted path and three bottom reflections. Two cases are presented corresponding to MFP with replica fields calculated using the entire mode spectrum, and then with only 40 modes. The restricted mode sum includes only water column and sediment modes, i.e. those with phase speeds from 1480 m/s, equivalent to the minimum sound speed in the water, to 1577 m/s, equivalent to the sediment sound speed. The shot is accurately localized in range and depth for each case, and the processor output is close to the maximum value of 11.5 dB. (For this shot, 2 of the 16 array hydrophones had failed.) This result suggests that it is necessary to use only that part of the mode spectrum which samples the portion of the waveguide where the dominant signal energy is propagating in order to calculate the replica fields. In this case, since the dominant shot energy is waterborne, it is not necessary to include the bottom-interacting modes in processing the data.

Table 2. Localization for Complete Multipath Signal: CZ Shot

Number of Modes	Range (km)	Depth (m)	Processor Power (dB)
118	38.3	265.0	11.4
40	38.4	265.0	11.2

The localizations using only the refracted multipath signal are presented in Table 3. These data were processed with a 1-K FFT, corresponding to a time window of 0.67 s. Included in the Table are MFP results using replica fields calculated with all 118 modes, and then with restricted mode spectra corresponding to modes sampling the water column and sediment layer (40 modes), the water column itself (28 modes), and finally selected depths within the water column. For the cases with restricted depths, the mode spectrum was cut off at the phase speed corresponding to the sound speed at the selected water depth; according to ray-wave analogies this is equivalent to including ray paths with turning points down to the depths shown in the Table.

Table 3. Localization for Refracted Path Signal: CZ Shot

Number of Modes	Ray Turning Depth	Range (km)	Depth (m)	Processor Power (dB)
118	-	38.6	265.0	11.2
40	sediment	38.5	265.0	11.2
28	5000 m	38.2	285.0	11.4
20	4000 m	38.5	285.0	11.4
12	3000 m	38.2	285.0	11.4
6	2000 m	36.9	265.0	11.2

The results indicate that there is excellent performance with the restricted mode spectra; the shot is well-localized using replica fields calculated with as few as 12 modes. This is expected because the waterborne refracted modes are dominant. Moreover, the processing is not degraded when using the complete mode spectrum, since the multipath component can be represented by a sum over all modes.

It is not always possible, however, to obtain good performance when using a partial multipath signal in processing shots deployed in the sound channel. Success generally depends on having a sufficiently large SNR, a condition that may not be satisfied at ranges between the first few convergence zones. In Table 4 we show the results of MFP localization using only the waterborne component of the shadow zone shot considered earlier in this section. The replica fields were calculated using the water column and sediment modes, and the data were frequency-averaged in a 1/6-octave band. The estimated values for the range and depth using only the water column modes are greatly in error from the measured values of 17.8 km and 225 m. This result can be understood by considering the propagation of sound in shadow zones. The refracted signal is actually a leaked arrival from the energy propagating in the sound channel, and there is no equivalent eigenray in conventional ray theory. Consequently, the SNR for the multipath component is generally low, in this case less than 5 dB, and the localization performance is poor.

Table 4. Localization for Partial Multipath: Shadow Zone Shot

Number of Modes	Data	Range (km)	Depth (m)
118	Complete Multipath	17.7	225.0
40	Partial Multipath	13.9	125.0

3. Sound Speed Profile Mismatch

The effect of mismatch has been studied extensively by Tolstoy for VLAs in a deep ocean Pacific profile[8]. The impact of the error due to mismatch depends strongly on the geometry of the experiment, in particular on the source depth, and the greatest sensitivity is obtained for arrays at shallow depths in shadow zones. In this section we demonstrate the effect using the convergence zone shot. The data were processed with replica fields calculated for two different sound speed profiles, one taken near the array at the beginning of the experiment (SSP1) and the other measured at the shooting ship at the time the shot was deployed (SSP2). The profiles are shown in Figure 3. There are subtle differences near the profile minimum, and the gradient for SSP2 is shallower immediately below the minimum down to about 1800 m. These subtle differences result in significantly different acoustic fields calculated for the shot depth in this case. The important feature for this analysis is the cycle distance of the shallow-angle refracted rays; for SSP1 the distance is much smaller, about 33 km, compared to 37 km for SSP2.

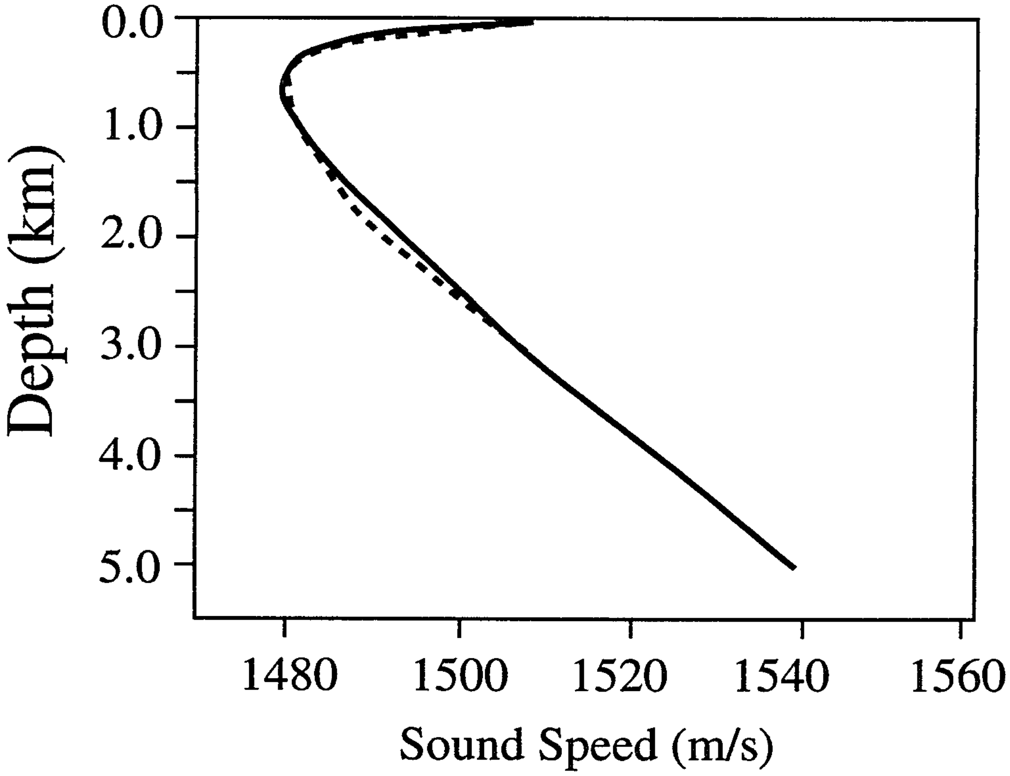

Figure 3. Sound speed profiles measured during the experiment. SSP1 is shown by the solid curve and SSP2 by the broken curve.

The localizations, using the complete multipath signal and all modes, are shown in Table 5. The underestimated range for SSP1 is due to the structure of the profile below the minimum which causes the refracted rays to focus at shorter ranges. This result is consistent with the conclusions obtained by Tolstoy that arrays placed at shallow depths show the greatest sensitvity to mismatch, and in fact provides an example to show that the effect can also be significant at convergence zone ranges.

Table 5. Mismatch in Sound Speed Profile: CZ Shot

Profile	Data	Number of Modes	Range (km)	Depth (m)
SSP1	Complete Multipath	118	33.2	245.0
SSP2	Complete Multipath	118	38.3	265.0

SUMMARY

This analysis has considered several aspects in MFP for broadband shot sources. In general, good localization performance can be obtained with broadband shot sources. For weak signals, frequency averaging improves the localization performance. For strong signals propagating in the sound channel it is possible to use a partial mode sum or a partial multipath signal in processing the data. For the partial multipath case, only the waterborne modes are necessary to localize the source. This can greatly reduce the computation time in calculating the replica fields, and has a significant impact for MF tomography. The effect of mismatch in sound speed profile was also demonstrated. MFP localization performance was significantly degraded by a relatively subtle change in the sound speed gradient near the sound channel axis. This result stresses the importance of adequately sampling the sound speed profile in time and space.

REFERENCES

1. C.S. Clay and S. Li, 'Time domain signal transmission and source location in a waverguide: matched filter and deconvolution experiments', J. Acoust. Soc. Am., **83**, 1377-1383 (1988).

2. W.S. Hodgkiss and R.K. Brienzo, 'Broadband source detection and range/depth localization via full-wavefield (Matched Field) processing', Oceans '90 Proceedings, 2743-2746 (1990)

3. P.C. Mignerey, 'Shot localization using a broadband normal-mode pulse model', Oceans '90 Proceedings, 121-124, (1990).

4. N.R. Chapman and M.L. McKirdy, 'Low frequency sound propagation in a thin sediment North Pacific environment', Proceedings of the 18th

Meeting of TTCP GTP-9 on Sonar Technology, Vol. 3, 275-292, Victoria B.C., (1989).

5. R.G. Fizell, 'Application of high-resolution processing to range and depth estimation using ambiguity function methods', J. Acoust. Soc. Am., **82**, 606-613, (1987).

6. MB. Porter and E.L. Reiss, 'A numerical method for ocean acoustic normal modes', J. Acoust. Soc. Am., **76**, 244-252 (1984) .

7. A.B. Baggeroer, W.A. Kuperman and H Schmidt, 'Matched field processing: source localization in correlated noise as an optimum parameter estimation problem', J. Acoust. Soc. Am., **83**, 571-587 (1988).

8. A. Tolstoy, 'Sensitivity of matched field processing to sound-speed profile mismatch for vertical arrays in a deep water Pacific environment', J. Acoust. Soc. Am., **85**, 2394-2404 (1989).

Matched Field Source Localization with a Horizontal Line Array

N.R. Chapman and M.L. Yeremy
Defence Research Establishment Pacific
FMO Victoria B.C.
V0S 1B0

Abstract

Matched-field processing is used to estimate the range, depth and bearing of a source near aft endfire of a horizontal line array. Simulations carried out for a long surveillance array are used to investigate the effects of uncertainty in experiemental geometry and sound speed profile mismatch on localization performance in deep water. It is shown that the performance is sensitive to the vertical tilt of the array for relatively small tilt angles, less than 5°. However, the horizontal array is robust to mismatch in the gradient of the sound speed profile in the lower portion of the water column. Experimental data for matched field source localization with a towed horizontal array were obtained in the first PACIFIC ECHO sea trial. The source was a 15-Hz CW projector towed at a range of 39 km about 12° off the aft endfire direction. The matched field processor located the source to within 0.6 km in range and within 15 m in depth, and estimated the bearing to within 3° of the true angle. The bearing estimate was obtained by varying the matched field processor through a range of bearings and determining the maximum processor output. By comparison, conventional beamforming located the source at 22° from aft endfire, an error of about 10°.

Introduction

Matched-field processing (MFP) is a generalized beamforming technique that takes advantage of the spatial structure of the sound field of a signal propagating in the ocean to provide improved localization performance compared to that for a conventional plane-wave beamformer. However, because the MF processor is sensitive to the spatial complexities of the field, the performance of the processor can be severely degraded by various types of errors, such as environmental mismatch and uncertainties in experimental geometry. Sensitivity to mismatch in the ocean environment has been investigated by Tolstoy[1] and Porter et al.[2] using simulations, and Tran and Hodgkiss[3] have considered the effect of uncertainty in experimental geometry. All of these investigations have been directed towards applications with vertical arrays operating in deep water.

In this paper we present an investigation of MF source localization performance for a horizontal line array. This type of array is in widespread use in ocean acoustics for a variety of purposes including surveillance and target tracking, and environmental measurements such as bottom profiling.

In the former applications, the array data are processed with a plane-wave beamformer to obtain target bearing information. However, using MFP it is possible to estimate the range and depth of the source as well as the bearing. For MF localization, the horizontal array has significant vertical angle resolution only for near-endfire geometries. However, this geometry is precisely the configuration for which the bearing resolution of a plane-wave beamformer is poorest for a horizontal array, because the endfire beams are generally very broad.

Our investigation of MFP with a horizontal array was carried out using simulations to study the localization performance, and analysis of experimental data. We consider first the effects of uncertainty in array geometry, in particular, the vertical tilt of the array, and mismatch in the sound speed profile. This study was carried out using simulations for a horizontal array in deep water and a source in aft endfire. In the second part of the paper we present the analysis of a source localization experiment carried out in the first PACIFIC ECHO exercise. These experiments were carried out jointly between the Defence Research Establishment Pacific (DREP) and the Naval Research Laboratory (NRL) to investigate MF source localization at very low frequencies. The experiment considered here was a pseudo-stationary localization with a horizontal array and a source in aft endfire.

The paper is organized in the following way. First, the MF processor that was used for the simulations and the experimental analysis is described in the next section. Then the simulation study is described, and results are presented for the effects of mismatch in geometry and sound speed profile. The results from the PACIFIC ECHO experiment are discussed in the third part, and the MF localization performance is compared to that of a plane-wave beamformer.

The Matched-field Processor

The Bartlett or linear processor was used to compute ambiguity surfaces in range and depth for all the MF localizations described in this paper. This processor is defined as

$$B(r,z) = \sum_{i=1,j=1}^{N} p_i^*(r,z) R_{ij} p_j(r,z) \qquad (1)$$

where $R_{ij} = X_i X_j^*$ is the expected value of the cross-spectral matrix of the spectral components of the field at the ith and jth sensors, and $p_i(r,z)$ is the replica field at the ith sensor calculated using a realistic environment model. The calculated pressures are normalized so that the vector of pressures across the array has unit length. If the acoustic environment has been modelled accurately, it can be shown that the Bartlett MF processor achieves the maximum possible signal gain $10 Log N$ for an array of N hydrophones in 2-D isotropic noise[4].

There are a number of methods for modelling the acoustic pressure in order to generate the replica fields at the array. For this work the normal mode model KRAKENC[5] was used to model the propagation in a flat oceanic waveguide with elastic bottom layers. This model computes the pressure field from the sum

$$p_i(r,z) = \alpha \sum_{m=1}^{M} \Phi_m(z_i)\Phi_m(z) \frac{e^{-ik_m r}}{\sqrt{k_m r}} \qquad (2)$$

where z_i is the depth of the ith sensor, and M is the number of modes. Unlike other modal codes which only approximate the effects of attenuation, KRAKENC uses a complex root finder to locate the discrete, complex wavenumbers corresponding to the modes of an elastic waveguide. KRAKENC also computes leaky modes, allowing an approximation to the continuous spectrum (or branch-line integral) portion of the field.

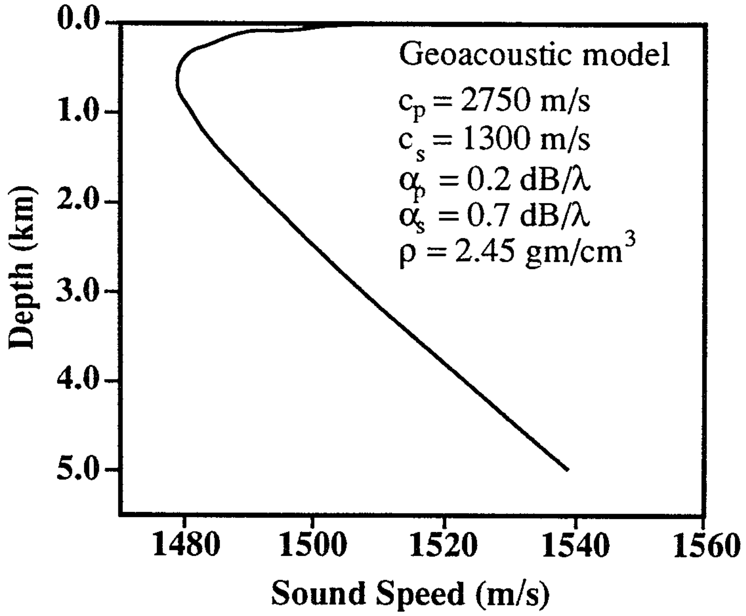

Figure 1. *Sound speed profile and geoacoustic model for the North Pacific site.*

Simulations
1. General

The geometry for the simulations was constructed to model the source/receiver configuration used in the pseudo-stationary localization experiment carried out in PACIFIC ECHO. In the simulated experiment, a very low frequency (VLF) 15-Hz source was located in aft endfire of a long horizontal array. For this geometry sound propagation is in the plane of the source and the array. The array consisted of 40 elements with a spacing of 38.1 m, similar to the DREP horizontal surveillance array COAMS (Canadian Ocean Acoustic Measurement System). The ocean environment was specified by a North Pacific sound speed profile obtained during the PACIFIC ECHO experiment, and a thin-sediment geoacoustic bottom model (Figure 1). The environment was assumed to be independent of range. The range/depth ambiguity surface for each case was calculated on a processing grid defined by a depth step of 20 m (starting from 15 m) and a range step of 38.1 m. The grid was searched over ranges of ± 15 km from the true range, and between 15 m and 1000 m in depth. The location of the maximum peak in this grid was chosen as the best estimate of the source position.

2. Mismatch in array geometry

Knowledge of the array shape is an important consideration in processing data from a towed line array, as it is not uncommon to observe a variation in depth along the array for most experimental systems. In this simulation the effect of vertical tilt was tested using a range of small tilt angles that represented realistic values. Replica fields were calculated assuming that the array was horizontal for localizations with array tilts from 1° to 5°. The source was at a range of 30 km and a depth of 95 m; for this range the source was at the leading edge of the first convergence zone where the intensities of the deep refracted and bottom reflected paths were about equal. The results are presented in Table 1. The first two rows indicate the results of control tests using either horizontal or tilted array geometries for both the measured and modelled fields. In each case the maximum processor gain of 16 dB was obtained for the 40-element array. The results for the tilted arrays indicate that performance, as determined by the position of the maximum processor output, is degraded for the very small tilt angles used in this study. Although the processor gain is only slightly reduced, the estimated positions are greatly in error. This indicates that there are regions of very strong correlation throughout the field that can mask the true source location, at least for a Bartlett processor. Localization performance is also sensitive to an error in the array depth, as demonstrated in the last row of Table 1 where the replica fields were calculated for a vertical shift of 1/3 λ. Although not shown in the Table, the general conclusions were not affected by introducing 10% Gaussian noise in the measured field.

3. Mismatch in Sound Speed Profile

This study was carried out to test the sensitivity to the error in the deep-layer sound speed gradient. Information about this portion of the sound speed profile is generally not measured in experiments that use limited-depth expendable probes (either XBTs or XSVs) to determine the sound speed profile. Livingstone has investigated this effect for a vertical array in a deep

Table 1. *Mismatch in array geometry: vertical tilt and offset.*

	Array Tilt (Data)	Array Tilt (Model)	Processor Gain	Range	Depth
	0°	0°	16 dB	30.0 km	95 m
	5°	5°	16 dB	30.0 km	95 m
	1°	0°	15.7 dB	32.8 km	235 m
	2.5°	0°	14.7 dB	22.0 km	935 m
	5°	0°	14.6 dB	18.9 km	875 m
	0°	0° (1/3 l offset)	15.2 dB	25.3 km	235 m

water Pacific environment, and has noted that source localization performance degrades for very small errors of 0.6 m/s at the ocean bottom, or about 3% error in the sound speed gradient[6]. We have investigated this effect for a horizontal array using mismatches of 3% and 25% for four geometries with source depths of 95 and 295 m and ranges of 18 and 48 km. For the 18-km range, the sources are in the acoustic shadow zone and propagation is primarily by bottom bounce paths, whereas the 48-km sources are within the first convergence zone.

The results, presented in Table 2, indicate that source localization performance (as measured by the estimated source position) is degraded only for large mismatch errors. However, consistent with the results in Table 1, the maximum processor output is not significantly reduced from the optimum value. By comparison with Livingstone's study[6], our results suggest that the horizontal array is more robust than a vertical array to errors in the deep-layer sound speed gradient. The strongest effect due to the mismatch is obtained for the sources at 48 km, because the propagation is predominantly via deep-cycling convergence zone paths that sample the deep layers of the water column at shallow-angles. At shorter ranges in the bottom bounce region, the effect is not as severe because the propagation paths are steeper.

Table 2. *Mismatch in sound speed profile: error in deep-layer sound speed gradient.*

	Mismatch	Source Depth	Processor Gain	Range	Depth
18 km	3%	295 m	16 dB	18.0 km	295 m
	3%	95 m	16 dB	18.0 km	95 m
	25%	295 m	15.8 dB	18.0 km	295 m
	25%	95 m	15.9 dB	18.0 km	95 m
48 km	3%	295 m	16 dB	48.0 km	295 m
	3%	95 m	16 dB	48.0 km	95 m
	25%	295 m	16 dB	54.4 km	915 m
	25%	95 m	15.9 dB	43.0 km	635 m

PACIFIC ECHO data

The experiment considered in this section was a pseudo-stationary source localization carried out using a horizontal line array at a deep water site in the North Pacific near 37.5° N 133° W. The ocean bottom at the site was a relatively smooth thin-sediment/basalt environment, and the average water depth was 5000 m. In the experiment, a 15-Hz VLF source was towed by USNS DESTEIGUER at a depth of 100 m about 39 km astern of the DREP COAMS horizontal array, which was towed at a depth of 240 m by CFAV ENDEAVOUR. Both ships maintained a speed of 4 kts along the track of the run so that the relative distance between the source and receiver was constant. The array shape was monitored by three heading sensors, one at each end and at the mid-point of the array, and six depth sensors spaced evenly along the axis. The aft endfire geometry is optimal for source localization with a horizontal array because the greatest vertical angle resolution is obtained for the various sound propagation paths. Navigation records from the ships indicated that the actual source position during the experiment was about 12° off true aft endfire at a range of 38.8 ± 0.5 km. For this range the source was just within the first convergence zone, and the dominant propagation paths were via relatively shallow angle (12°-15°) refracted rays.

The COAMS VLF aperture, consisting of 40 elements spaced at 38.1 m, was used for the data analysis. Approximately three minutes of array data were processed using 4096-point FFTs to obtain the averaged cross-spectral matrix for the spectral component at 15 Hz. For this data sample, the array was straight to within ± 1°, and the depth variation was less than 10 m along the entire length. The source level was adjusted to produce a signal-to-noise ratio in the processing band of about 20 dB. The ocean environment used for calculating the replica fields was specified by a water column sound speed profile taken by the source ship at the start of the experiment, and by a geoacoustic bottom model. The parameters of the model were estimated from an analysis of bottom reflectivity data measured at the site[7]. Ambiguity surfaces in range and depth were calculated for a grid with spacings of 25 m in range and 20 m in depth (starting from 15 m).

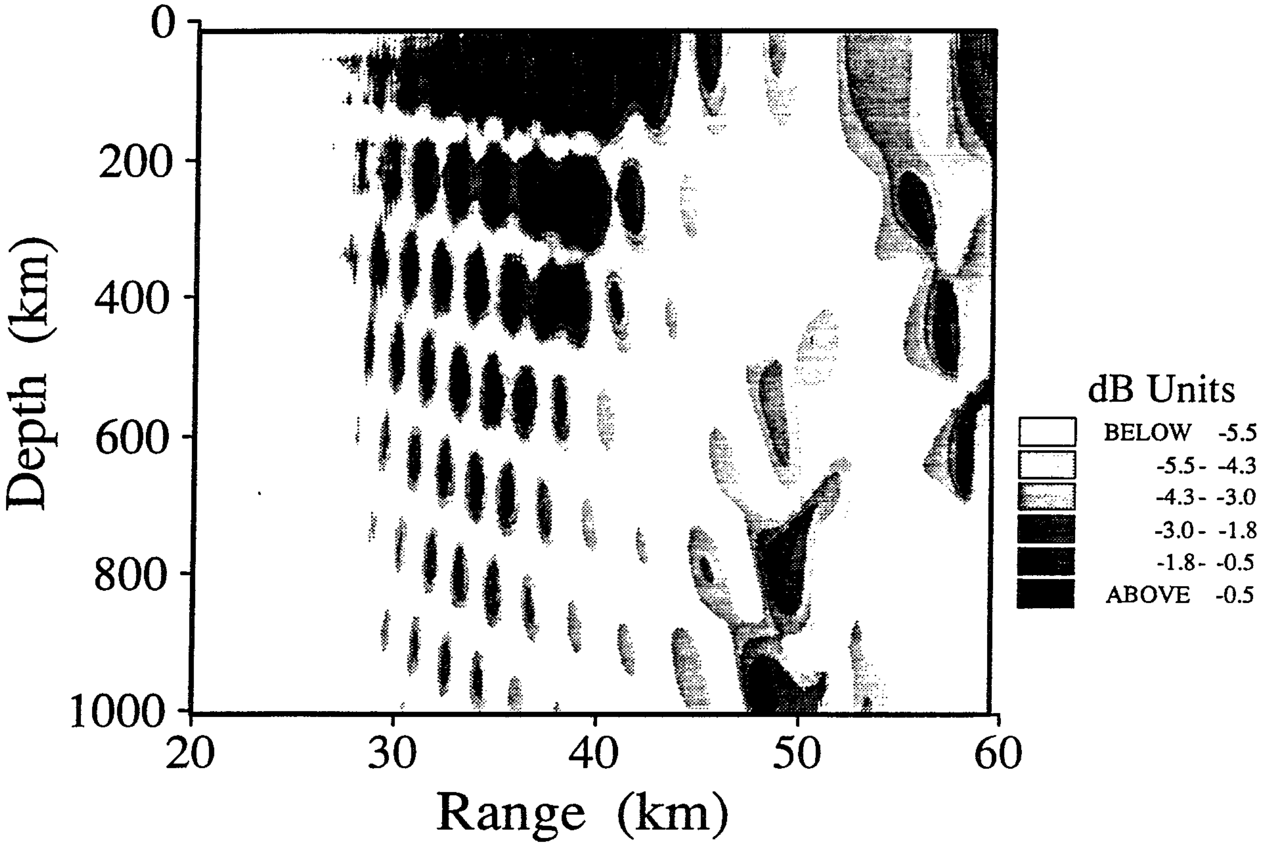

Figure 2. *Ambiguity surface in range and depth for the PACIFIC ECHO data, assuming that the source is in aft endfire. In this case, sound propagation is in the plane of the source and the array.*

The ambiguity surface in range and depth for the true endfire geometry (0° with respect to the array) is shown in Figure 2. There are three main peaks of approximately equal magnitude in the vicinity of the source position, but the maximum peak is at 37.9 km and 235 m. This estimate is within 1 km of the true source range, but the depth is significantly overestimated. In order to improve this estimate, a search was carried out over angles from 0° to 15° off true endfire, and the results are shown in Table 3. From 0° to 7.5° the dominant peak occurs at 37.9 km and 235 m, but a secondary peak exists at 39.2 km and 115 m that becomes the maximum peak at an angle of 9°. This peak estimates the source position within 0.6 km in range and 15 m in depth, and in addition is within 3° of the true bearing. However, there is very little variation in processor gain for the maximum peak over the range of angles. This is not unexpected since the source-receiver range variation with angle is very slow for geometries so close to endfire. In comparison, the same data were processed using a plane-wave beamformer for the 40 element array. For this case the signal was located at an angle of 22° off endfire. This bearing shift towards broadside is due to the effect of the vertical angle of the refracted multipath signal. For this geometry, a bearing of 168° with respect to the array, and using propagation angles of 12-15° for the convergence zone path, the expected beam angle is about 160°, i.e., about 20° off aft endfire.

Table 3. *Bearing estimation for PACIFIC ECHO data*

Bearing	Processor Gain	Range	Depth
0°	15.2 dB 15.0 dB	37.9 km 38.9 km	235 m 115 m
3°	15.2 dB 15.0 dB	37.9 km 38.9 km	235 m 115 m
6°	15.2 dB 15.1 dB	37.9 km 39.1 km	235 m 115 m
7.5°	15.2 dB 15.1 dB	37.9 km 39.2 km	235 m 135 m
9.0°	15.1 dB	39.2 km	115 m
12 °	15.2 dB 14.6 dB	46.8 km 39.2 km	995 m 135 m
15°	15.3 dB	56.0 km	375 m

Summary

Source localization with a horizontal array has been studied using simulations and by analysis of data from a pseudo-stationary localization experiment. The results obtained in this paper are based on matched field processing with a Bartlett processor, using the position of the maximum peak in the amibuity surface as the best estimate of the source location. Simulations were carried out to investigate the effects of mismatch in experimental geometry and the sound speed gradient at the bottom of the water column. Localization performance is sensitve to the vertical tilt of the array for small angles less than 5°. Performance is also sensitive to errors in the deep-layer sound speed gradient, but the effect appears to be not as severe as that for localization with a vertical array. In both types of mismatch, the maximum processor output was not seriously degraded from the optimum value, even for cases in which the estimated position was greatly in error. Good performance was obtained using the experimental data for localization of a source near aft endfire about 39 km astern of the array. The matched field processor estimated the source position within 0.6 km in range and 35 m in depth, and the source bearing within 3° of the true source bearing. This represents a significant improvement over the performance of a plane-wave beamformer which provided an estimate only of the source bearing, and that with significant error.

References

1. A. Tolstoy, 'Sensitivity of matched field processing to sound-speed profile mismatch for vertical arrays in a deep water Pacific environment', J. Acoust. Soc. Am., 85, 2394-2404, 1989.

2. M.B. Porter, R.L. Dicus and R.G. Fizell, 'Simulations of matched-field processing in a deep-water Pacific environment', IEEE J. Oceanic Eng., 12, 173-181, 1987.

3. J.Q.D. Tran and W.S. Hodgkiss, 'Matched field processing of 200-Hz continuous wave data', J. Acoust. Soc. Am., 89, 745-755, 1991.

4. R.G. Fizell, 'Application of high-resolution processing to range and depth estimation using ambiguity function methods', J. Acoust. Soc. Am., 82, 606-613, 1987.

5. M.B. Porter, 'The KRAKEN normal mode program', SACLANT Undersea Research Centre Report, SR-245, 1989.

6. E. Livingstone, 'Effects of sound-speed profile mismatch in the lower water column on matched field processing', J. Acoust. Soc. Am., 91, 2362, 1992.

7. N.R. Chapman and M.L. McKirdy, 'Inversion of geoacoustic profiles in upper oceanic crust by matched field processing of acoustic field data', EOS Supplement, 274, 1992.

Low-SNR Matched Field Processing in a Range-Dependent Environment

by John A. Fawcett, M.L. Yeremy and N. R. Chapman
Defence Research Establishment Pacific
FMO Victoria, B.C.
Canada, V0S-1B0

Abstract

In this paper we present preliminary source localization results obtained by Matched Field (MF) processing of Vertical Line Array (VLA) data from the PACIFIC ECHO III sea trial. The experimental site was located in a region of significant bathymetric variation. The harmonic source for the experiment was towed on a series of arcs, giving data for a sequence of different ranges and azimuths. During the time of the sea trial, there were several freighters and a drilling rig present in the vicinity of the experimental site; thus, the relative levels of the source's spectral lines were often very low in comparison to "noise" levels. In spite of the problems of low SNR and significant bathymetric variation, good MF localization results were obtained for a large fraction of the trial time. In the first part of our analysis it is assumed that the azimuth of the source is known. Substantial improvements in MF localization were obtained by using the range-dependent bathymetry instead of a flat-bottom model to calculate replica acoustic fields. This improvement is demonstrated for data from the longer-range arcs. In the second part of the analysis, we investigate the concept of Environmental Signal Processing, ESP, an enhancement to MF processing that is obtained by making use of the environment's complexity. The azimuthal variation of bathymetry for the source tracks along the arcs was used to obtain estimates of the source bearing from the VLA data. In many instances, the bearing estimates were in reasonable agreement with the known source bearings.

INTRODUCTION

Between 1986 and 1992 the PACIFIC ECHO collaborative sea trials were carried out by Defence Research Establishment Pacific (DREP) and the U.S. Naval Research Laboratory (NRL). These experiments utilized vertical and horizontal arrays and narrowband and broadband sound sources. The data from these experiments have been used to investigate many different aspects of Matched Field (MF) processing such as thin [1] and thick sediment sites, rough sites [1], broadband MF processing [2], the effects of array tilt [1], localization with a horizontal array [3], and the determination of geoacoustic parameters from vertical line array (VLA) data [4].

The PACIFIC ECHO III trial of July 1991 was carried out near a group of large seamounts in the Northeast Pacific where the bathymetry varies significantly. The trial was designed to test experimentally the concepts of Environmental Signal processing [5],[6]. In general, Environmental Signal Processing refers to algorithms for MF processing of acoustic field data that provide enhanced detection and/or localization capabilities by taking advantage of the complexity of the oceanic environment. In particular, we investigate in this paper the estimation of the bearing of the source. Bearing estimation would not be possible for VLA data if the azimuthal variation of the oceanic waveguide was ignored in the acoustic propagation modelling.

In the examples presented in this paper we consider two basic types of MF localization. First, we consider the case where the azimuth of the source is known, and hence the appropriate slice of the three-dimensional bathymetry is also known. In this case, the MF localization corresponds to standard two-dimensional MF processing for a VLA in a range-dependent environment. Second, we consider the more general three-dimensional problem when the azimuth of the source is also estimated. As discussed above, it is only possible to estimate the azimuth of a source from VLA data when the effects of an azimuthally (with respect to the VLA) asymmetric bathymetry are modelled.

I. EXPERIMENTAL SETUP

The sea trial was carried out near the Juan de Fuca Ridge in the Northeast Pacific using two ships, CFAV ENDEAVOUR and USNS DeSTEIGEUR. The vertical line array, consisting of 16 hydrophones spaced 45 m apart with the first hydrophone at a depth of 415 m, was deployed from ENDEAVOUR. DeSTEIGEUR towed a low-frequency sound source on a series of arcs, starting at a short range of 3 nm and ending with an arc at 57 nm. The source depth was approximately 45 m. In Figure 1 we show DeSTEIGEUR's track, the position of the VLA and the underlying bathymetry contours. During the long-range arcs, the source was towed behind a series of seamounts. There was heavy freighter traffic throughout the experiment and also a deep sea drilling rig was operating about 65 nm to the northeast. Thus, the signal-to-noise ratio (SNR) of the source line was at times very low.

II. DATA ANALYSIS

The data were recorded digitally at a sampling rate of 1500 Hz. A 4096 point FFT was applied to each channel and the cross-spectral matrix for the frequency bin of interest was then computed. Each FFT corresponded to 2.73s of data, yielding a frequency resolution of 0.37 Hz. This process was repeated for successive data segments and the cross-spectral matrices for 48 integration periods (131 seconds) were averaged. This averaged result was subsequently used for MF processing.

III. MF PROCESSING AND PROPAGATION MODELLING

For the MF processing of this paper we used the simple Bartlett estimator. An ambiguity surface was produced as a function of range r and depth z, according to the formula

$$B(r,z) = \vec{p}^{\,*}(r,z)\mathbf{R}\vec{p}(r,z) \tag{1}$$

where $\vec{p}(r,z)$ is the vector of modelled pressures at the VLA hydrophones and $\mathbf{R}$ is the data cross-spectral matrix as discussed in the previous section. The model vector was normalized to have unit length. The range and depth (and sometimes azimuth) parameters were searched on a finite, discrete grid of values. In this paper, we typically searched 50 or 100 km in range and 500 m in depth with discrete range steps $\Delta r = 35m$ and depth steps $\Delta z = 10$ or 20 m.

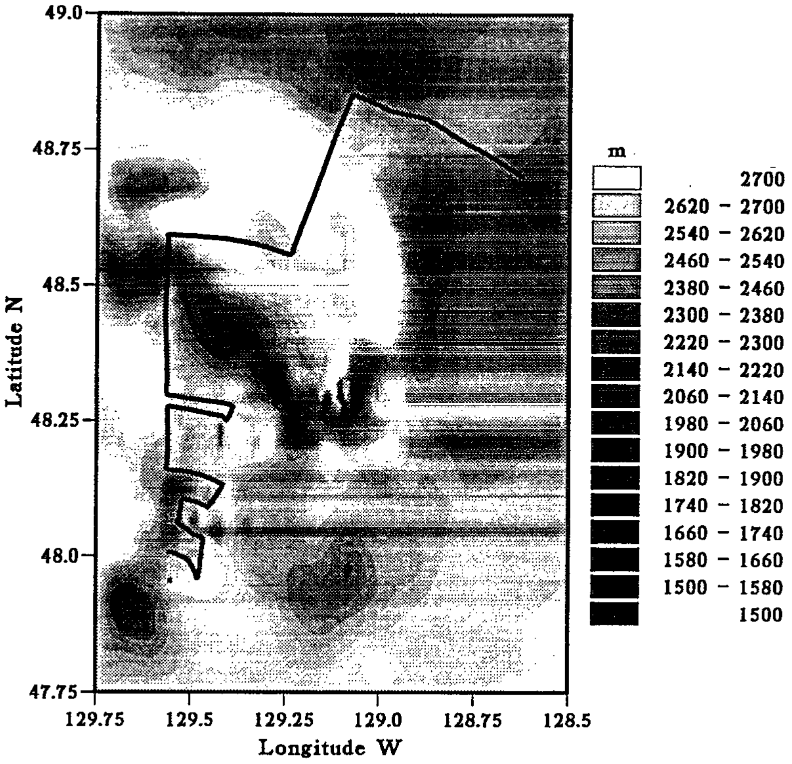

Figure 1. Source track with underlying bathymetry - the location of the VLA array is indicated by the dot

In order to compute the model vector $\vec{p}$ we used the modal model KRAKENC [7]. For a flat waveguide, the modal formula for pressure is

$$p(r,z;z_h) = \alpha \sum_{n=1}^{N_m} \frac{\phi_n(z_h)\phi_n(z)}{\sqrt{k_n r}} exp(-ik_n r) \tag{2}$$

where α is a constant, z is the hypothesized source depth, z_h is the depth of the hth hydrophone, ϕ_n is the mode function of the nth mode and k_n is the associated wavenumber. For a range-dependent environment which is varying sufficiently slowly, it is possible to generalize the expression of Eq.(2) by the adiabatic formula,

$$p(r,z;z_h) = \alpha \sum_{n=1}^{N_m} \frac{\phi_n(z_h;r_a)\phi_n(z;r)}{\sqrt{\int_0^r k_n(u)du}} exp(-i \int_0^r k_n(u)du). \tag{3}$$

Here the modal functions and wavenumbers change implicity as a function of range because of the changing waveguide parameters; however, they are computed for a particular range as if the waveguide was flat at that range. In particular, we note that the modal phase terms are now integrals of the wavenumber over range.

In order to implement Eq.(3) for range-dependent bathymetry we assumed a single sound speed profile for the entire region and considered waveguides of different depths (i.e, range-dependent bathymetry). The sound-speed profile was interpolated or extrapolated to yield values of the sound speed at the bottom of the water column. KRAKENC [7] was used to produce files of modal values and wavenumbers for waveguide depths between 1000 and 3000 m, in increments of 2 m. With these precomputed modal files the numerical implementation of Eq.(3) is straightforward. The integrals were approximated by the trapezoidal rule. For arbitrary bathymetry depths, linear interpolation between the modal files of the two closest precomputed depths was used to obtain accurate modal values.

IV. ENVIRONMENTAL PARAMETERS

In order to accurately compute the wavenumbers k_m and the mode shapes $\phi_m(z)$ of Eqs.(2) and (3) it is, of course, necessary to have an accurate description of the oceanic environment. It is common practice to measure directly the sound speed as a function of depth in the water column during the experiment. However, the geoacoustic parameters of the sediment and basement are much more difficult to measure directly. Furthermore, although in this trial the water depth was monitored by DeSTEIGEUR along its source tow tracks, the bathymetry over the entire region, which is required in detail for modelling purposes, could only be estimated from charts and databases. In Figure 2 we show a sound-speed profile recorded during the experiment near the VLA site. Estimates for the geoacoustic parameters were refined in an iterative process until good MF localization results were achieved for the 3-nm arc. The results are shown in Figure 2, where C_p and C_s denote the compressional/shear speeds, α_p and α_s the compressional/shear attenuations, and ρ the density.

The water depth at the array site was approximately 2640m. A significant amount of effort was devoted to creating a good bathymetric database for the rest of the experimental area. The DBDB5 data base provided a rough bathymetry grid of 5-minute latitude/longitude intervals. However, this proved to be too coarse for our requirements. From the experiment, the depth sounding records from DeSTEIGEUR provided bathymetry values along the arcs. A detailed set of bathymetric values for other parts of the experimental region were obtained from the Pacific Geoscience Centre, Sydney, BC. The bathymetry values from the various sources were combined using gridding and interpolation software of the NAG[8] library to yield a single database of values. This new database was significantly more accurate than that obtained from simply interpolating the DBDB5 database.

V. DATA EXAMPLES

In this section, we present the MF localization results obtained for the arcs at 3, 6, 19 and 38 nm. For the 3-nm arc we used a simple flat-bottom model; for the longer ranges the variation of the bathymetry was more significant and for these data sets we used adiabatic modes to model the propagation of acoustic energy. To illustrate the effects of the range-dependent bathymetry on acoustic propagation, we show in Figures 3a and 3b two-dimensional plots of transmission loss for a flat waveguide (depth 2640 m) and for a slice of bathymetry corresponding to an azimuth through the 38-nm arc. As can be seen,

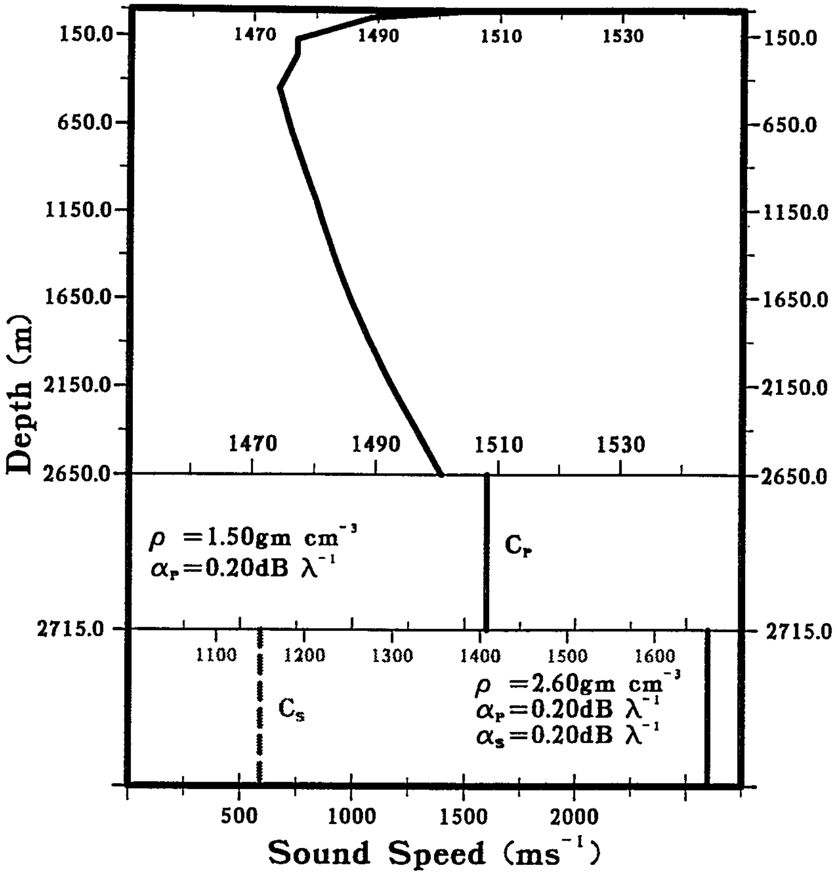

Figure 2. Sound Speed Profile and GeoAcoustic Parameters - Bold and light labels in the basement refer to compressional and shear values respectively.

the effect of the range-dependent bathymetry is to "strip-off " much of the higher-angle energy in the waveguide, and there are significant differences in the acoustic field compared to the flat bottom case.

Initially, in our data analysis, we used the bathymetry appropriate for the known azimuth of the source. However, for some selected data sets we simultaneously estimated the range, depth, and bearing of the source by performing a full three-dimensional MF localization. Once again, we stress that it would not be possible to estimate the azimuth of the source if we did not model the azimuthal variation of the bathymetry.

In Figures 4a-4d we show representative spectra (48 averages) for a single hydrophone for arcs at 3, 6, 19 and 38 nm respectively. The 10 Hz line is clearly evident for the 3- (SNR $\approx$ 10 dB) and 6-nm arcs (SNR $\approx$ 15 dB), although other strong lines and broadband noise are present in the frequency band. We have not shown a spectrum for the 3-nm arc - 7 Hz line but this line also had a high SNR; in fact, its SNR often approached 20 dB. The strengths of the lines for these two arcs did vary with time, but the SNRs were typically in the 10-15 dB range and sometimes higher. However, at longer ranges the projector lines (12.5 Hz (19 nm), 8 Hz (38 nm)) become very weak in comparison to the background noise.

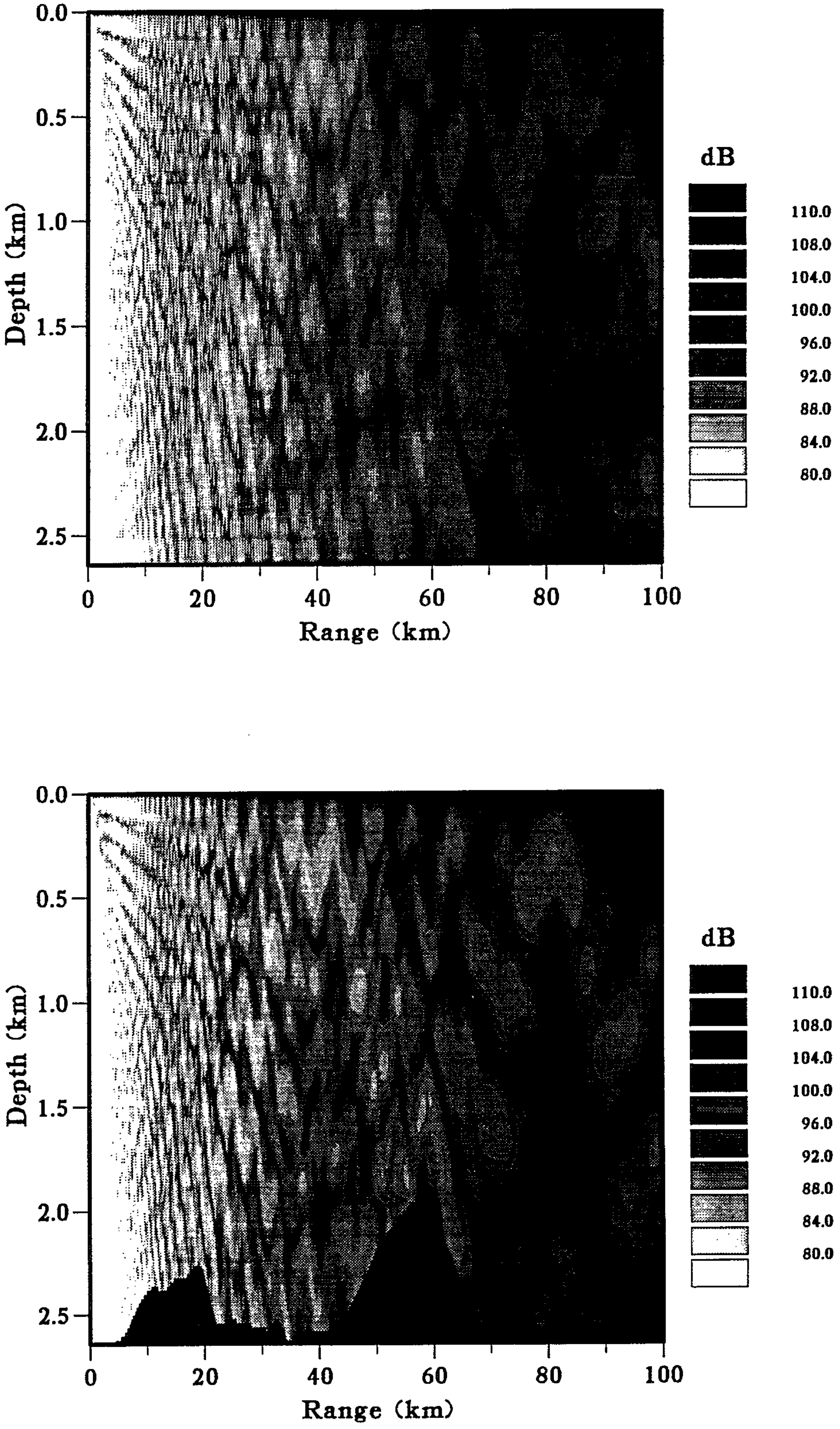

Figure 3. Propagation Loss For a (a) Flat Waveguide (b) Range-dependent Waveguide

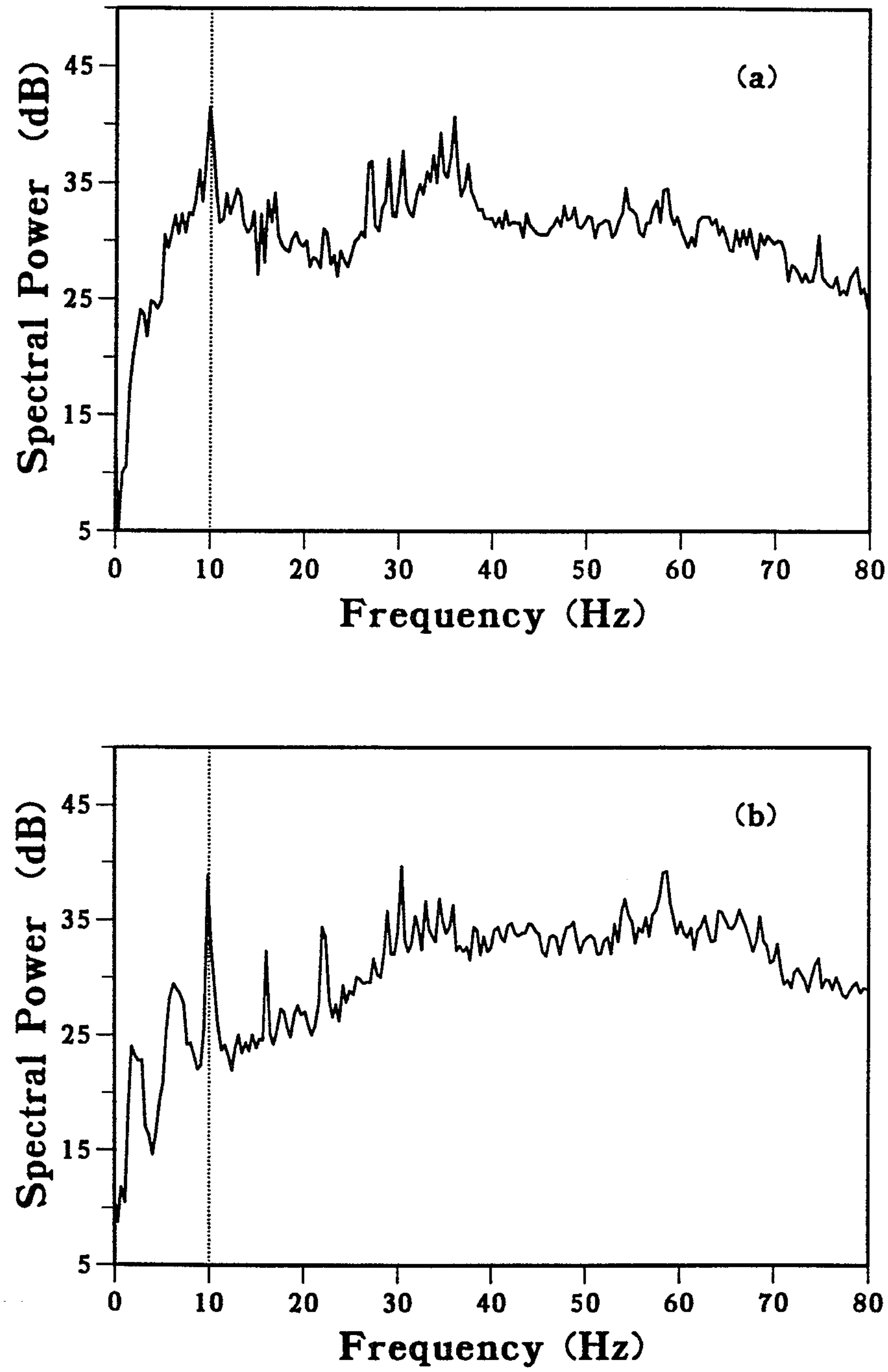

Figure 4. Representative Single-Hydrophone Power Spectrum (Arbitrary Units) From (a) 3-nm arc - 10 Hz (b) 6-nm arc - 10 Hz

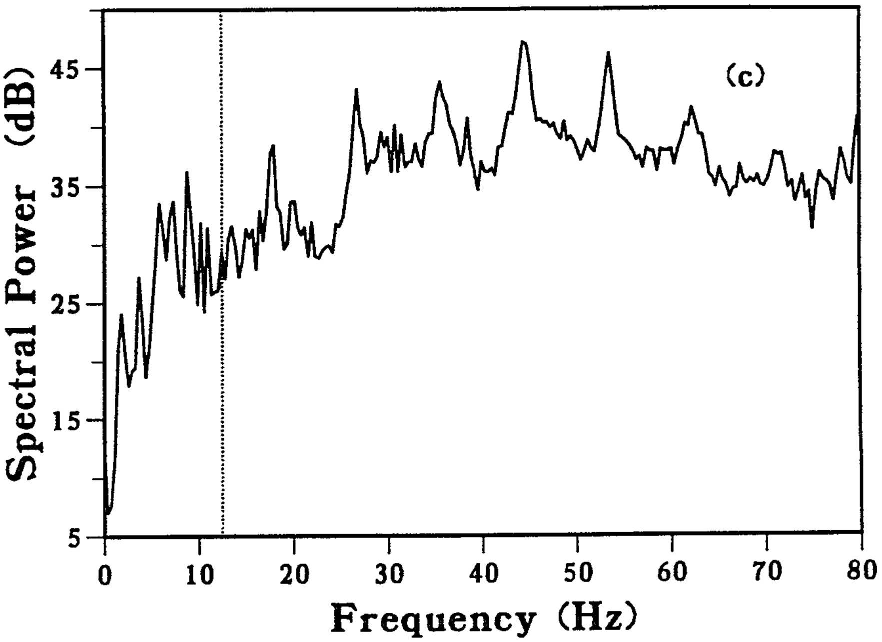

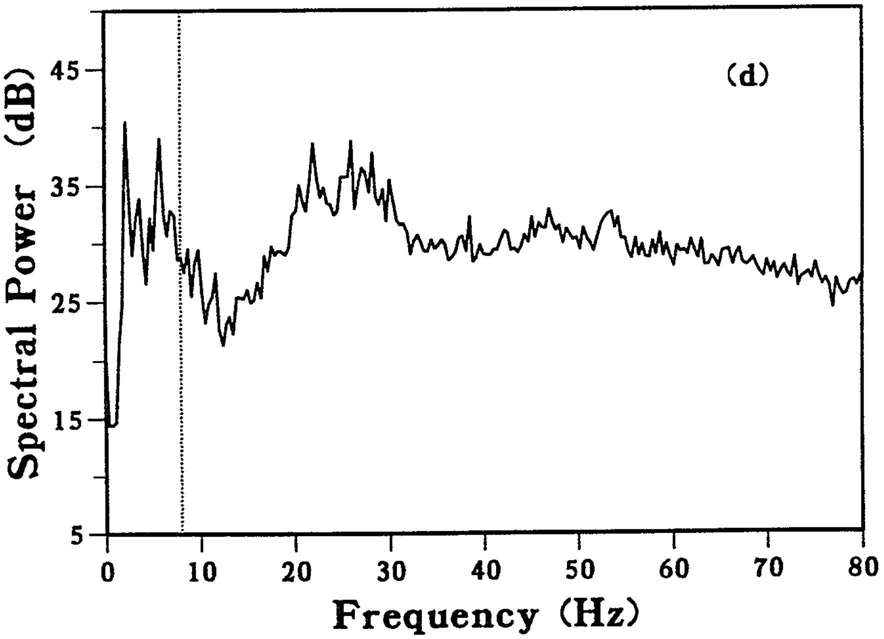

Figure 4. (continued) Representative Single-Hydrophone Power Spectrum (Arbitrary Units) From (c) 19-nm arc - 12.5 Hz (d) 38-nm arc - 8.0 Hz

A. SOURCE AZIMUTH ASSUMED KNOWN

We now consider the MF processing results for the 4 arcs assuming that the azimuth of the source is known.

Case 1: 3-nm arc - 7 and 10 Hz - High SNR

Bartlett ambiguity surfaces were computed for the 7 and 10 Hz signals, for ranges between approximately 0 and 50 km and depths between 0 and 500 m, with a discrete range step of 35 m and a depth spacing of 10 m. For this arc the replica vectors were computed using a flat-bottom model with a depth of 2640 m, the estimated depth at the VLA site. In Figure 5a and 5b we plot the range estimates obtained from MF processing as a function of time along the arc using the 7 and 10 Hz data respectively. The range was estimated as the range corresponding to the peak of the computed ambiguity surface. As can be seen, the range estimates are in excellent agreement with the "true" ranges, often with errors of less than 100 m. These differences are comparable to the experimental error associated with the measured ranges. Also shown in the figure is the correlation of the peak obtained as a function of time; a correlation close to one indicates a good match between the data and model vectors. The relatively low correlation indicates that there is some degree of mismatch between the measured and modelled pressures. The mismatch is likely associated with the geoacoustic model. It is evident from the figure that poor estimates of the range correspond, in general to correlation values below 0.5. In this paper we will concentrate on the range estimates of the source, but, in general, for the 3 nm arc the depth estimates were very good (with errors usually less than 50 m). In Figure 6 we show a typical Bartlett ambiguity surface (7 Hz) for the 3-nm arc. As can be seen the peak is very close to the true source location and the surface is very unambiguous over the entire 50 km range.

Case 2: 6-nm arc - 10 Hz - High SNR

Once again, we computed a series of Bartlett ambiguity surfaces with the same grid parameters as above. In Figures 7a and 7b we show the range estimates obtained as a function of time along the 6-nm arc for the 10 Hz data. In Figure 7a we used the flat-bottom model (2640 m), whereas in Figure 7b we used range-dependent bathymetry and an adiabatic propagation model for computing the replica vectors. For the latter case, a simple approach was used for the model of the bathymetry: we assumed a linear variation between the depth (2640 m) at the array site and the depth recorded on the source ship along the arc.

For the flat-bottom model (Fig. 7a) it can be seen that the range errors are typically about 1 km (or about 10% of the true range). The range estimates are significantly improved for the case of the linear slope model, with errors now usually less than 0.5 km. The depth estimates were also quite good for both models, with depth errors generally less than 50 m. In Figure 8 we show a typical ambiguity surface for this arc computed using the adiabatic model. The peak is near the true source location and the surface is quite unambiguous, but more ambiguous than that of Figure 6 for the 3-nm arc.

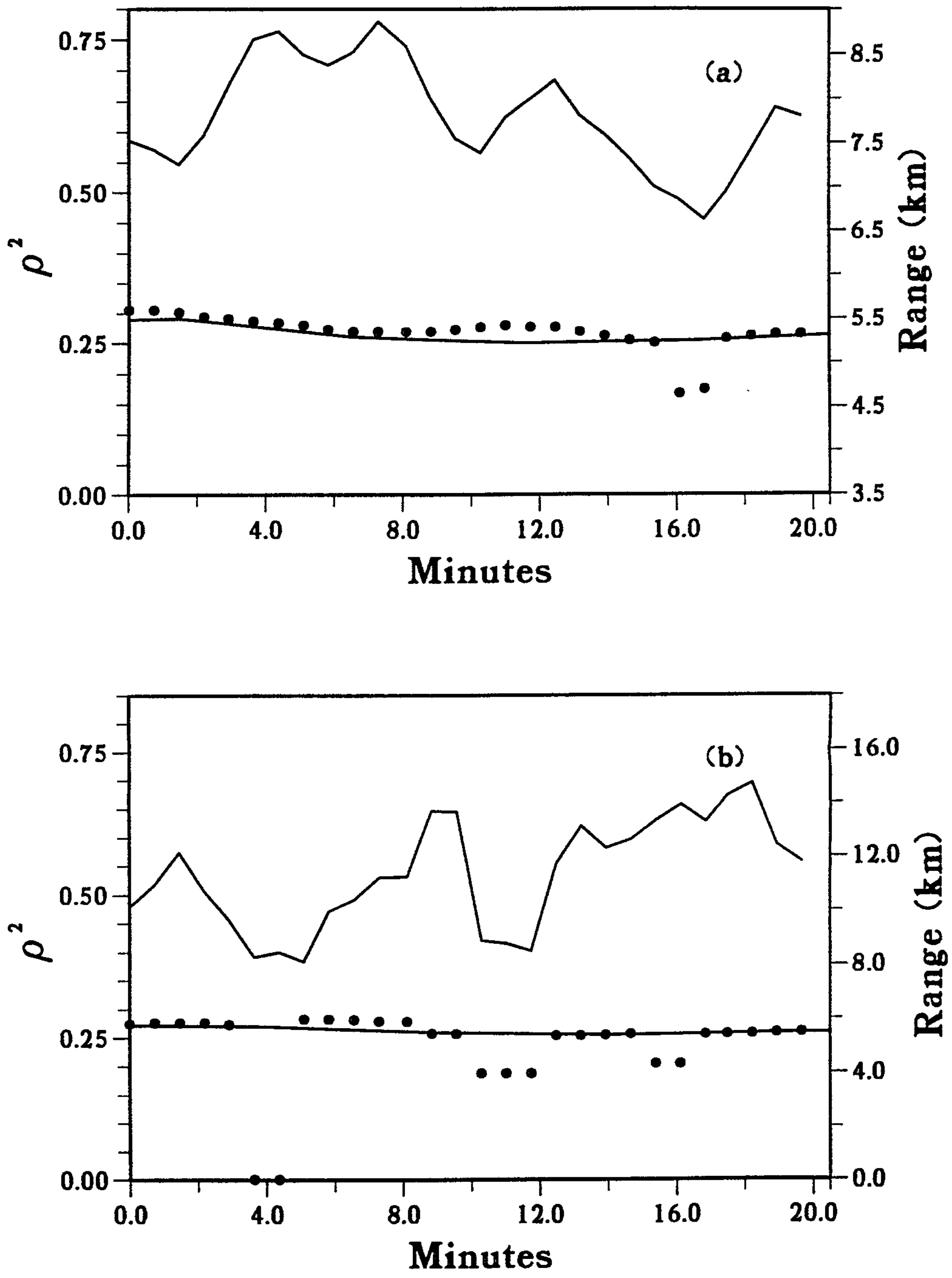

Figure 5. MF Range Estimates and Correlation for the 3-nm arc for (a) 7 Hz Data (b) 10 Hz Data - Lower Solid Line is "true " range, Upper curve is correlation, Dots are MF estimates

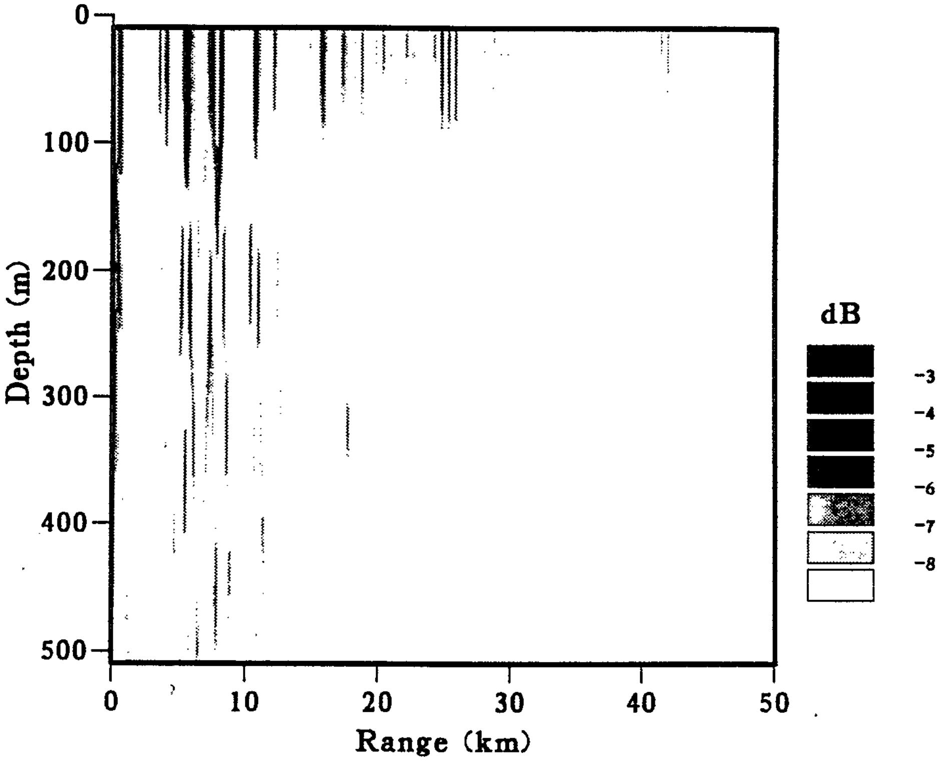

Figure 6. Representative Ambiguity Surface for 3-nm Arc - 7 Hz

Case 3: 19-nm arc - 12.5 Hz - Low SNR

For the cross-spectral matrices from the 19-nm arc we computed a series of Bartlett ambiguity surfaces for ranges between 0 and 100 km, with the same depth and grid spacing as that used previously. In Figures 9a and 9b we show the MF range estimates (range of the peak of the ambiguity surface) as a function of time along the 19-nm arc with first a flat-bottom model and then with the range-dependent adiabatic model. When using the adiabatic model, we used our data base to generate the range/bathymetric variation along the slices. As can be seen for the flat-bottom model the range estimates are very erratic with only a few clustered about the true value. Modelling the range-dependent bathymetry significantly improved the range estimates with most values clustering near the true value. The remaining very poor range estimates correspond generally to times of relatively poor peak correlation values (although this is not so at the 16 minute mark). The depth estimates, using either the flat or adiabatic model, are much poorer for this arc than for the previous two. There is a large amount of variation of the depth estimates as a function of time and the errors often exceeded 300 m. In Figure 10 we show a typical ambiguity surface (range-dependent model). The peak location is accurate and the surface is fairly unambiguous with respect to range but the power lobe associated with the peak is quite extended in depth.

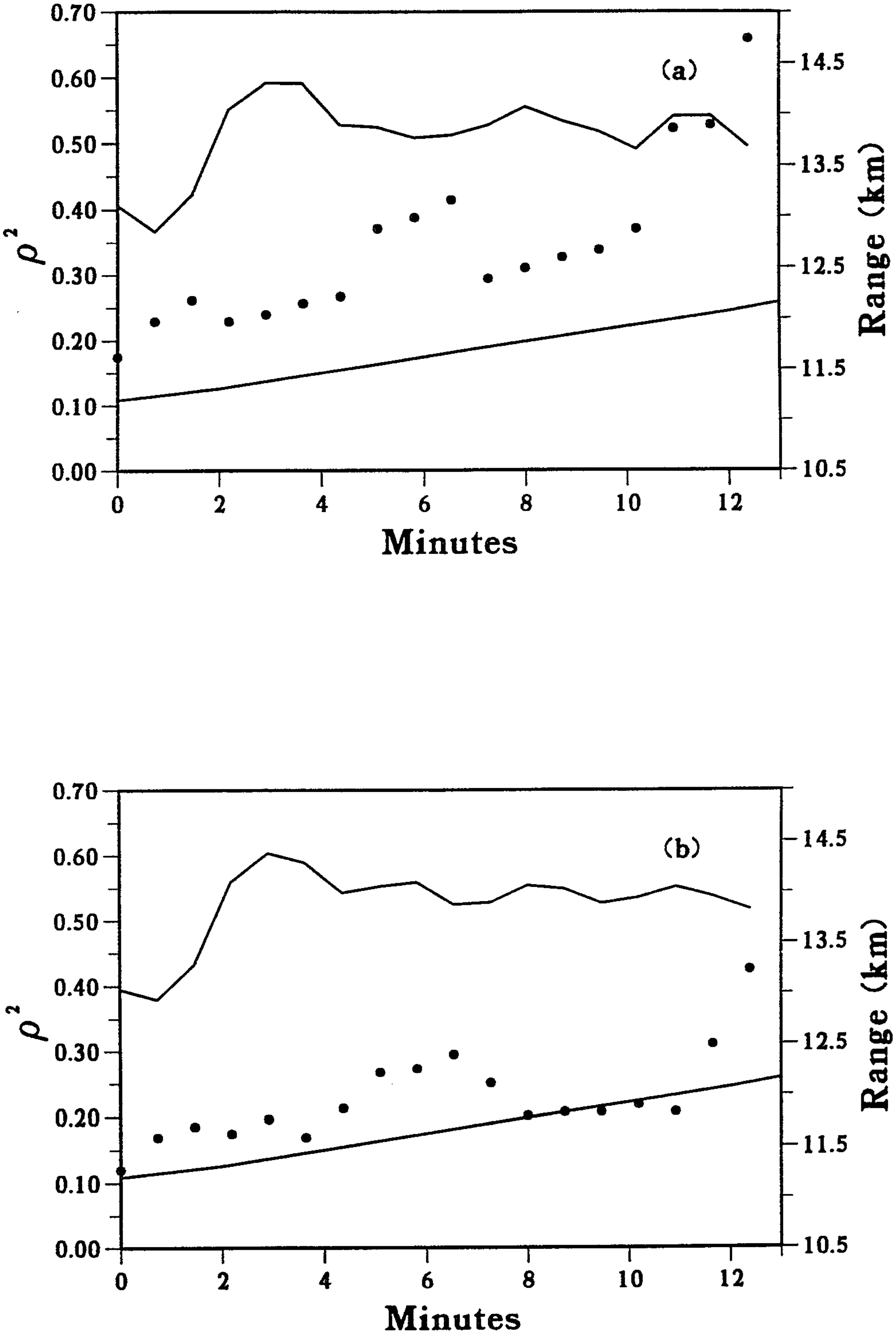

Figure 7. MF Range Estimates and Correlation for the 6-nm Arc for (a) Flat Waveguide Model (b) Range-dependent Model

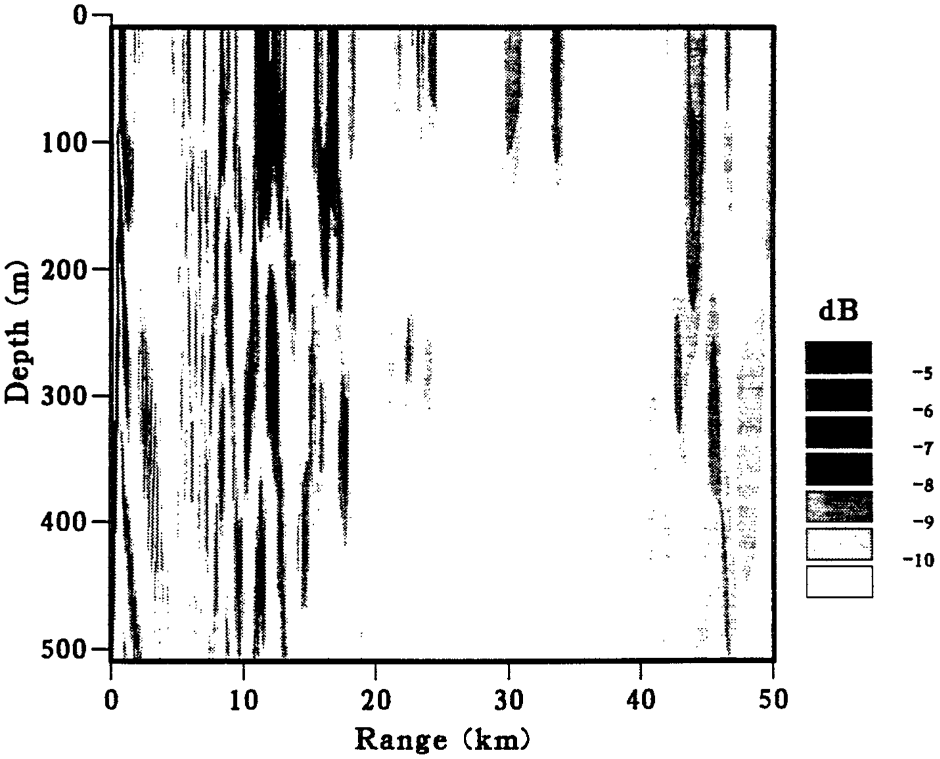

Figure 8. Representative Ambiguity Surface for 6-nm Arc - 10 Hz

Case 4: 38-nm arc - 12.5 Hz - Low SNR

In the case of the 38-nm arc the source ship passed behind some significant bathymetric features. In Figure 11a it can be seen that the MF estimates, using simply a flat bottom model, are quite self-consistent, but constantly underestimate the range by about 5 km. Overall, the adiabatic model corrects this bias as can be seen by the results of Fig. 11b; however, it does poorer than the flat model for a 20 minute period near the 30 minute mark. We feel that there are at least two possible explanations for the poor behaviour of the adiabatic model during this time period: (1) the bathymetry values we used were only estimates and our knowledge of the bathymetry between the 38-nm arc and the VLA location was somewhat incomplete; (2) the bathymetry slopes on the latter part of the arc were more severe than those on the first part of the arc and consequently the adiabatic modelling of the acoustic pressure field along the propagation paths for this arc may not be sufficiently accurate.

In Figure 12 we show a representative ambiguity surface for this arc. The surface is very ambiguous and, although the range of the peak is accurate, the depth estimate is very poor. Once again, this is probably due to inaccurate modelling of the range-dependent propagation. In general, for both the flat and adiabatic model, the depth estimates were consistently too deep. For the flat model the estimated depths were usually near 400 m

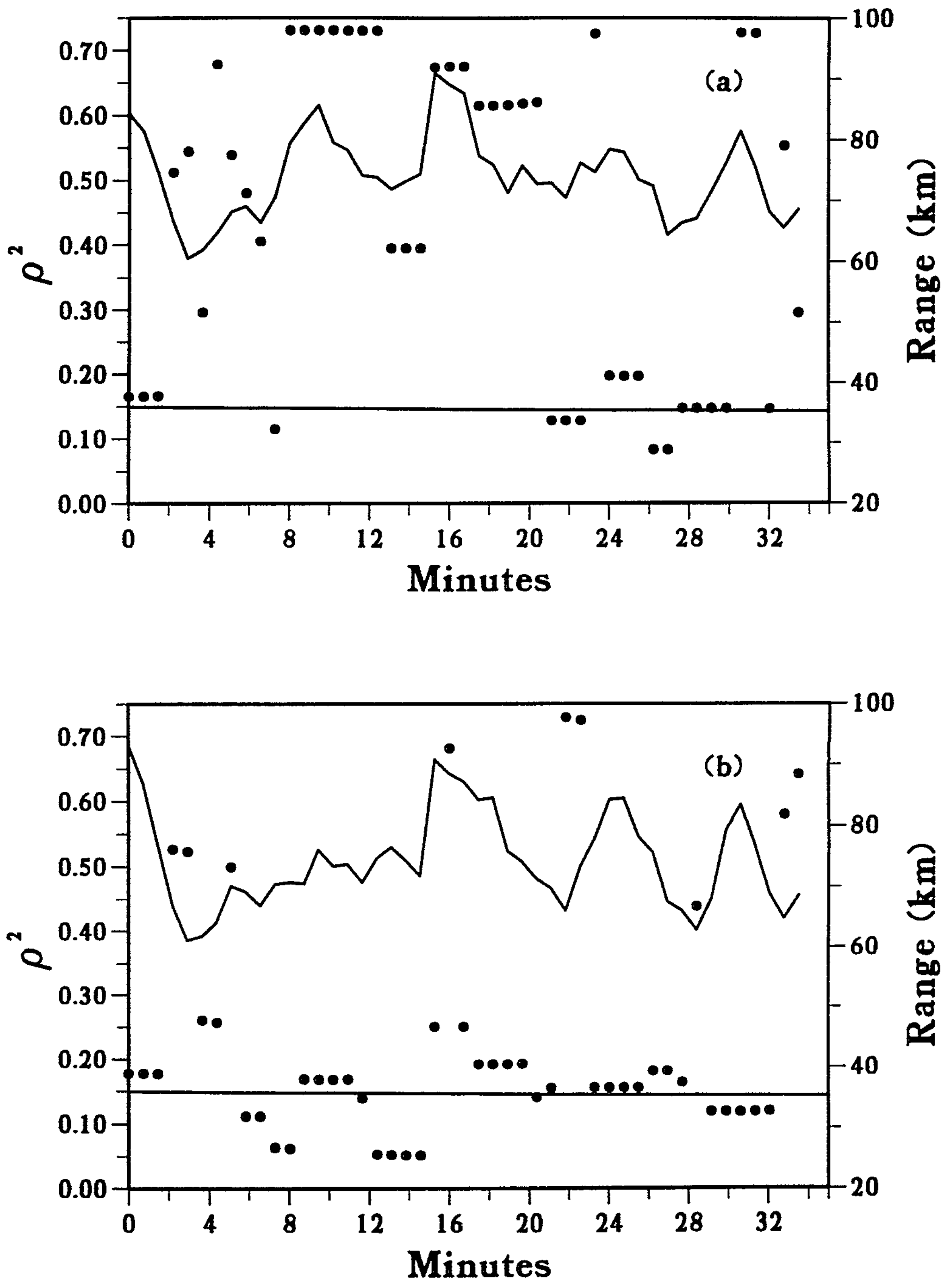

Figure 9. MF Range Estimates and Correlation for the 19-nm Arc for (a) Flat Waveguide Model (b) Range-dependent Model

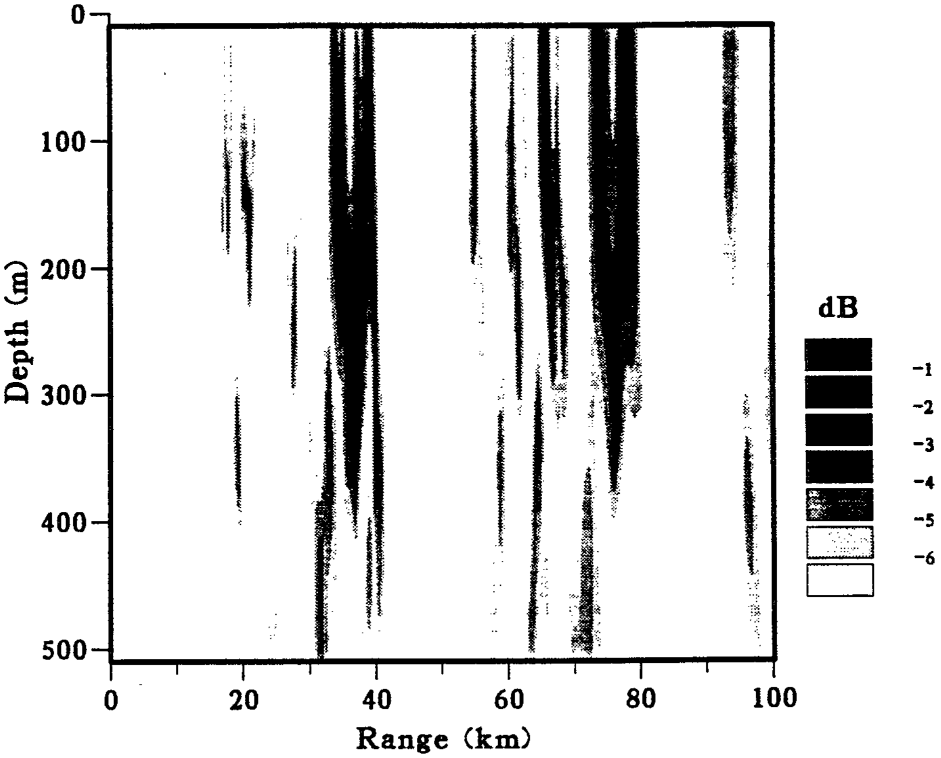

Figure 10. Representative Ambiguity Surface for 19-nm Arc - 12.5 Hz

and for the adiabatic model the depth estimates were consistently near the deepest allowed value (for our search grid) of 500 m. It is interesting to note that despite the poor depth estimates, the correlation values for the peak estimates are higher than for the shorter range arcs. This is probably due to the fact that the amount of acoustic energy which interacts with the bottom is less for the longer ranges; hence, the amount of mismatch due to errors in the geoacoustic model is also less.

B. RANGE, DEPTH, AND BEARING ESTIMATION

We now consider the estimation of azimuth from the VLA data. In addition to the estimation of source range and depth, we also search over a set of hypothesized bearings for the source. In the examples below, we used data from the 6- and 19-nm arcs.

Case 1. 6-nm Arc - High SNR - 10 Hz

Using the cross-spectral matrices from the 6-nm arc, Bartlett ambiguity surfaces were computed as a function of range, depth and bearing. The range was searched from 0 to 30 km in steps of 35 m and the depth from 0 to 500m in steps of 10 m. The bearings were searched in the interval $[-10°, 46°]$ in steps of 2°. In Figure 13 we show a typical range/bearing plot of correlation using one of the averaged cross-spectral matrices. For each value of range and bearing shown in Figure 13, the correlation values plotted are the

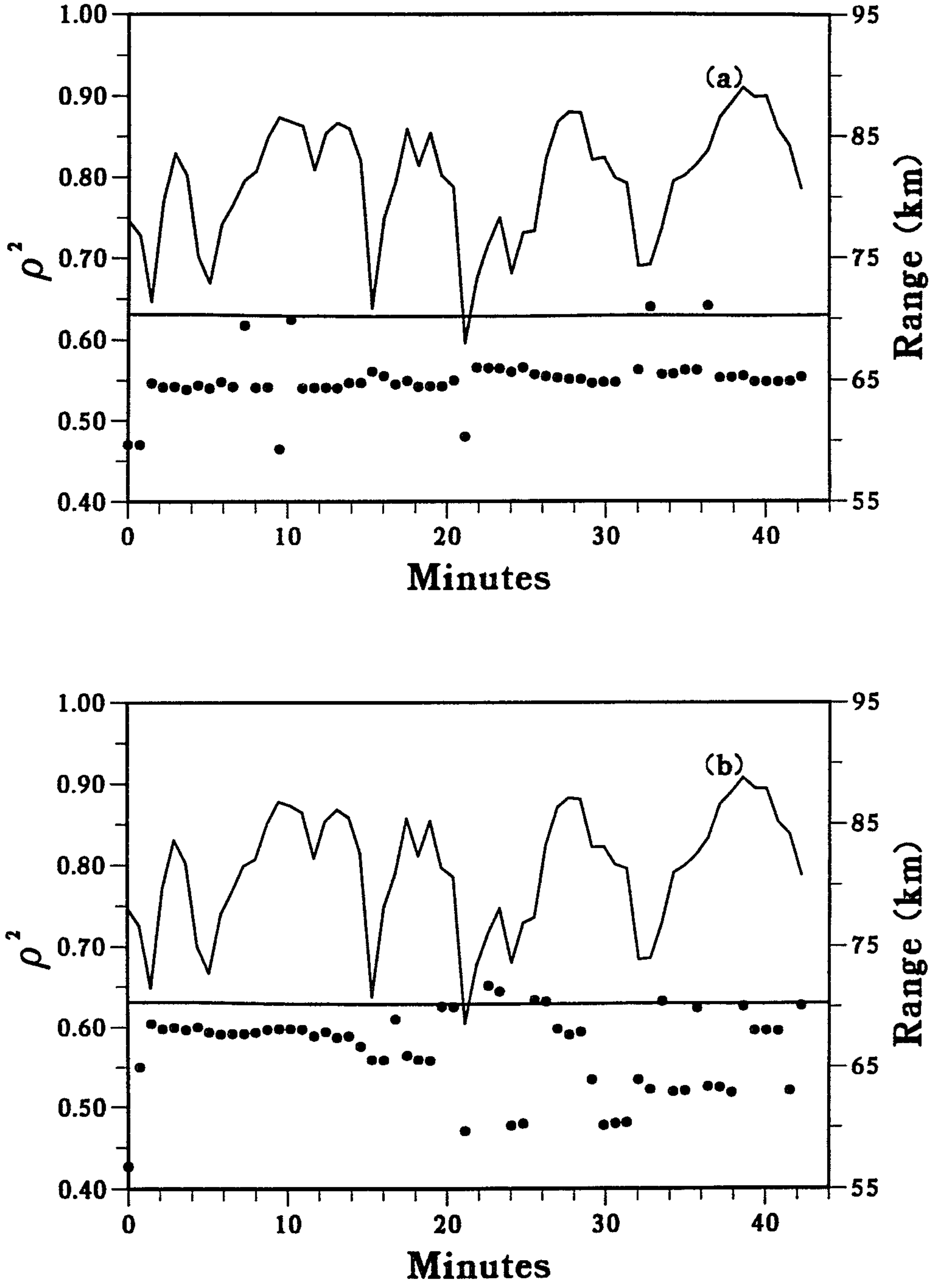

Figure 11. MF Range Estimates and Correlation for the 38-nm Arc for (a) Flat Waveguide Model (b) Range-dependent Model

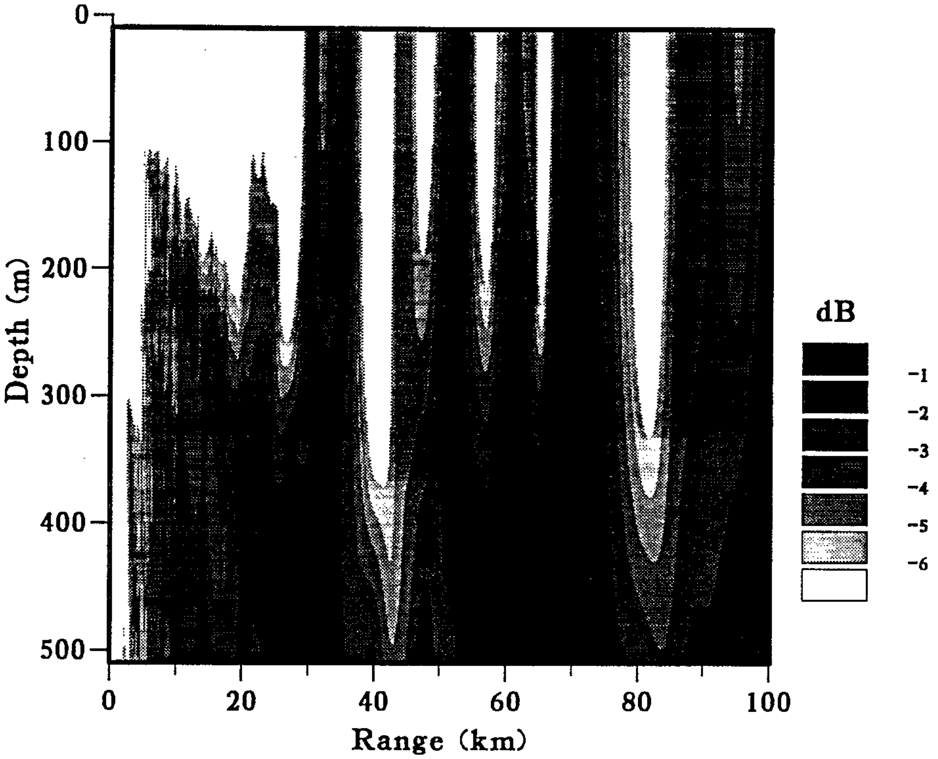

Figure 12. Representative Ambiguity Surface for 38-nm Arc - 8.0 Hz

maximum values as a function of the depth variable. There is a peak at 8 − 10° and a range of 11.76 km which is in excellent agreement with the true value of 10° and 11.70 km.

We now consider the sequential estimation of bearing from consecutive data sets along the 6-nm arc. In Figure 14 we show the bearing peak estimates obtained as a function of the time along the arc. The line in the plot represents the true value of bearing as a function of time. As can be seen there is a large amount of scatter in the estimates. However, the values do cluster about a value of 8.0° which is a good average bearing estimate. This result is very encouraging because initially it was expected that the cumulative effects of the range-dependent bathymetry would be too small to allow effective bearing estimation for this case.

Case 2. 19-nm arc - Low SNR - 12.5 Hz

In Figure 15 we show a representative range/bearing ambiguity surface for the 19-nm arc (the values shown have been optimized with respect to depth). The Bartlett surfaces were computed for ranges between 0 and 50 km in steps of 35 m and depths between 0 and 500 m in steps of 20 m. For this arc we considered bearings in the interval $[-10°, 38°]$ in steps of 2°. In this case there is a well-defined, broad, peak centred at a bearing of 5° and a range of 37.59 km (the peak value is at 0°). There is also a secondary peak at about 20°. The true bearing and range for this case were at 6.2° and range 35.39 km.

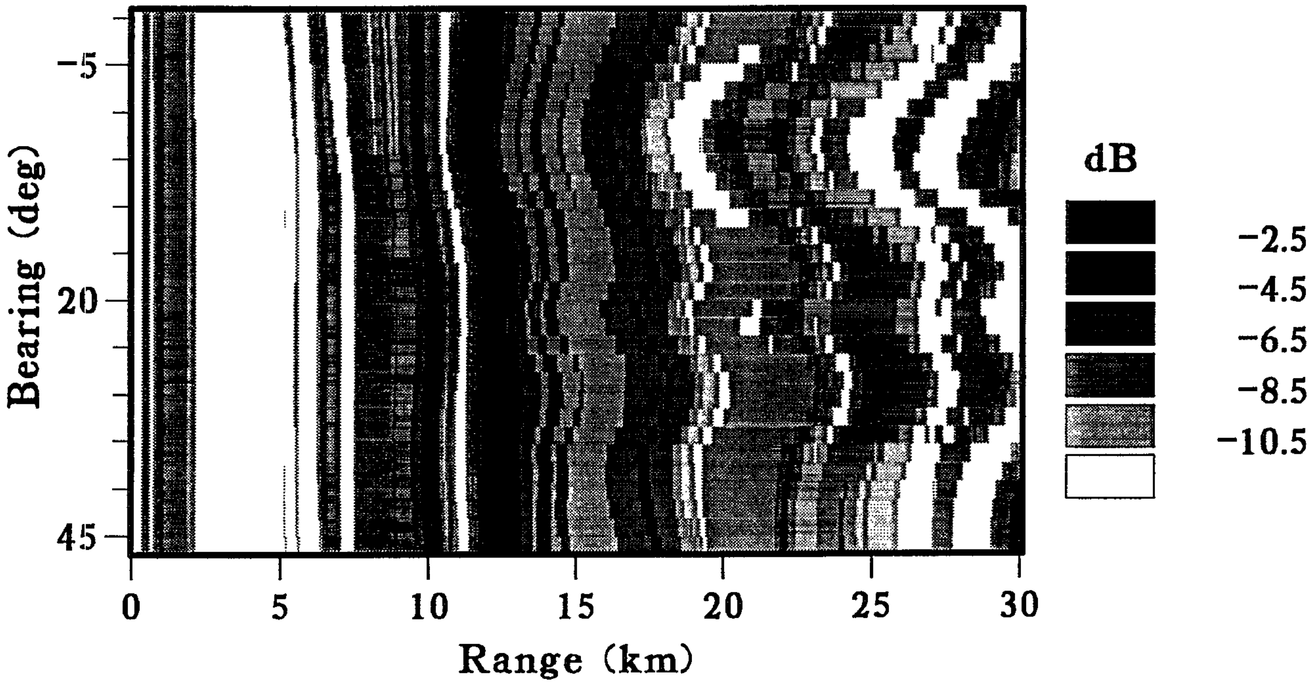

Figure 13. Representative Range/Bearing Ambiguity Surface for 6-nm arc

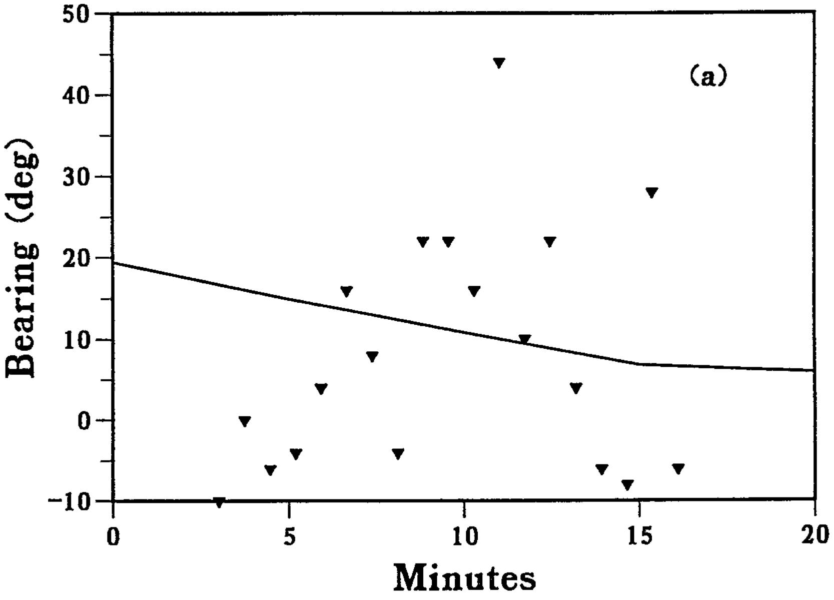

Figure 14. Peak bearing estimates for 6-nm arc

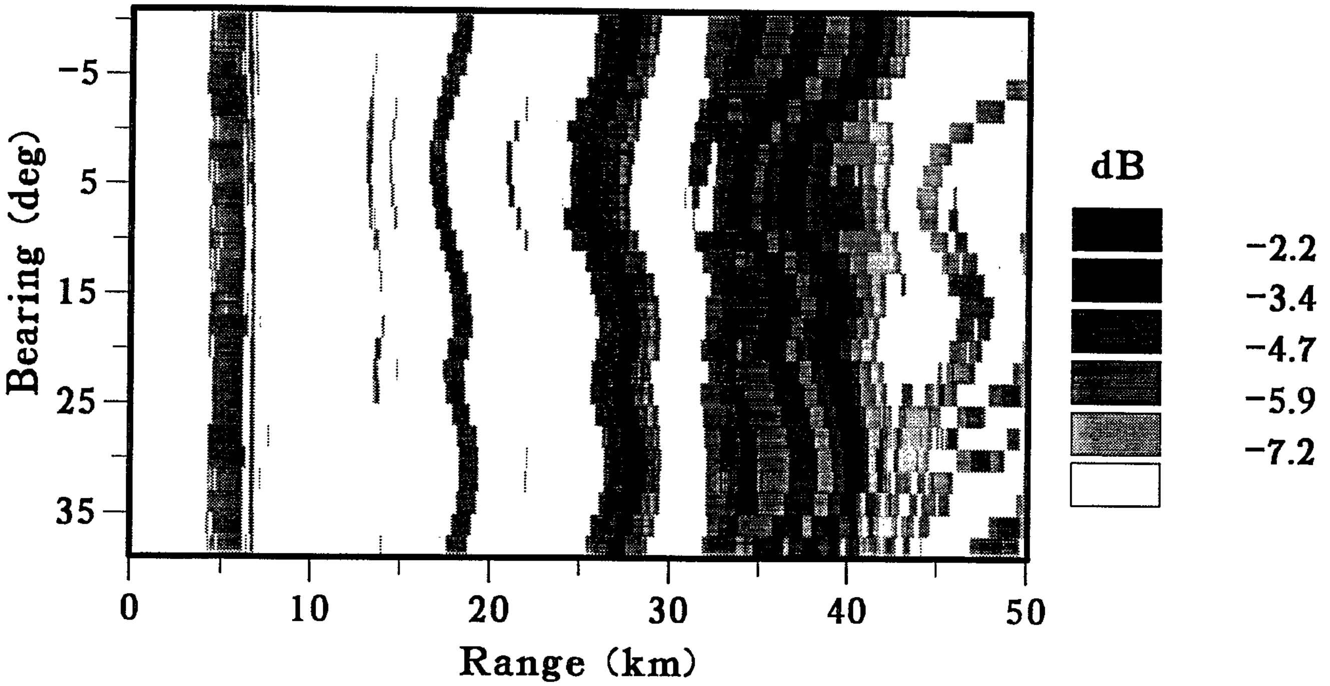

Figure 15. Representative Range/Bearing Ambiguity Surface for 19-nm arc

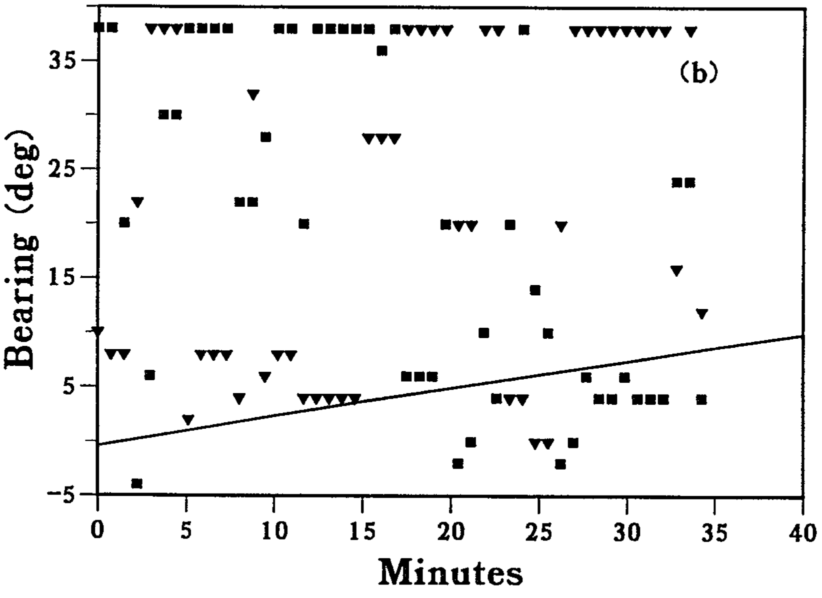

Figure 16. Peak bearing estimates for 19-nm arc
(triangles) primary peaks (squares) secondary peaks

In Figure 16 we show the sequential results for the 19-nm arc. Here we have reduced the bearing search interval to $[-4°, 38°]$. For this case there are often two peaks with nearly the same correlation values. We plot the locations of both the primary peaks (triangles) and the secondary peaks (squares). The peak values cluster around the true curve of values and the 38° line. It should be noted that 38° was the maximum bearing searched during these computations so that, in fact, the upper peak estimates are clipped. There were certain periods of time, e.g., between 10 and 15 minutes, during which the bearing estimates were very good.

Overall, our estimation of bearing is erratic for the two arcs. However, it did appear possible to obtain a reasonable average estimate of the source bearing. It should be noted again that our knowledge of the bathymetry and the geoacoustic model is far from complete and hence we would not expect very accurate bearing estimates. It would seem that the 38-nm arc should provide an excellent data set for the determination of source bearing, due to the longer ranges, and the significant bathymetric variation which occurs along the source/VLA propagation paths. However, as as indicated in Figure 12, we were unable to obtain good depth estimates for this particular arc. Thus, not surpisingly, we were also unable to obtain good bearing estimates. We hope, in the future, to investigate whether a more accurate propagation model, such as a Parabolic Equation code, might improve the MF results for these data.

VI. SUMMARY AND DISCUSSION OF RESULTS

In this paper we have successfully demonstrated that it is possible to localize a source accurately and consistently with MF processing in a low-SNR, range-dependent environment. Modelling the range-dependent bathymetry using an adiabatic mode model improved on the results obtained from simply using a flat-bottom model. For the range-dependent computations it was assumed that we had a good knowledge of the bathymetry between the array and the source. The relatively poor performance of the MF estimates for the 38-nm arc may be due, in part, to the breakdown of this assumption. When we allowed the bearing of the source to be an unknown parameter, we were able to obtain rough estimates of the source azimuth which corresponded reasonably well to the true values. This is a successful demonstration of one of the ideas of environmental signal processing, namely, that by exploiting knowledge of the three-dimensional bathymetry it is possible to determine the bearing of the source. This would not be possible if a flat bottom had been used in the propagation modelling.

In the future we would like to investigate whether our present results can be improved by using a propagation model other than adiabatic modes, in particular, a parabolic equation code. We would also like to consider focalization [9] techniques to see if we can reduce the localization errors due to inaccurate bathymetric information.

REFERENCES

1. J.A. Fawcett, N.R. Chapman, and M. McKirdy "Matched Field Processing Experiments with PACIFIC ECHO Sea Trial Data", Proceedings of the 19th Meeting of TTCP Technical Panel GTP-9, WSRL Salisbury, Australia, 1990.

2. N.R. Chapman and M. L. McKirdy, "Matched Field Source Localization with PACIFIC ECHO Broadband Shot Data", Proceedings of the 20th Meeting of TTCP Technical Panel GTP-9, NUSC, New London, U.S.A., 1991.
3. N. R. Chapman and M. Yeremy, "Matched Field Processing with a Horizontal Array", Proceedings of the 21st Meeting of TTCP Technical Panel GTP-9, DRA, Portland, U.K., 1992.
4. N. R. Chapman and M. McKirdy, "Low Frequency Sound Propagation in a Thin-Sediment North Pacific Environment", Proceedings of the 18th Meeting of Technical Panel GTP-9, DREP, Victoria, B.C., Canada, 1989.
5. John S. Perkins and W. A. Kuperman, "Environmental signal processing: Three-dimensional matched-field processing with a vertical array", *J. Acoust. Soc. Am.*, **87**, pp. 1553-1556 (1990).
6. John S. Perkins, L. T. Fialkowski, M. D. Collins, M.D, L. Hall, R. Marrett, L. J. Kelly, A. Larsson, and J. Fawcett, "TESPEX: INITIAL PROCESSING RESULTS", Presented at 22nd Meeting of TTCP Technical Panel GTP-9, DREA, Dartmouth, N.S., Canada, October 1993.
7. M. Porter, "The KRAKEN normal mode program", SACLANTCEN MEMORANDUM, SM-245, September 1991.
8. NAG Fortran Library, Mark 15, Numerical Algorithms Group (1991)
9. M. D. Collins and W. A. Kuperman, "Focalization: Environmental focusing and source localization", J. Acoust. Soc. Am., **90**, 1410-1422 (1991).

Matched field inversion for geoacoustic profiles of upper oceanic crust

N. R. Chapman and M. L. Yeremy

Defence Research Establishment Pacific, FMO Victoria, B.C., Canada V0S 1B0

The geoacoustic properties of the upper oceanic crust have a significant effect on low-frequency sound propagation in large regions of the Pacific where the sediment layer is thin. This paper describes the inversion of acoustic field data using a method based on matched field processing with simulated annealing to obtain the geoacoustic profile for the upper crust. The data were obtained in an experiment with a vertical line array at a thin-sediment site in the North Pacific. The inversion method is demonstrated using simulated data for an upper crust model consisting of a basalt layer with constant sound speed gradients, and then the inversion of the experimental data is presented. The estimated values compare very well with the results obtained from a reflection coefficient amplitude inversion.

1. INTRODUCTION

The effect of crustal age on the elastic properties of the upper crust was investigated in a series of experiments designed to measure the ocean bottom reflectivity at thin-sediment sites in the North Pacific. The data from these experiments provide the basis for estimating geoacoustic bottom profiles, and a number of different inversion techniques have been developed for this purpose[1]. These generally fall into two categories, those based on travel time inversion and those based on amplitude inversion. In this paper, we describe the results of an inversion using a different approach for inverting the geoacoustic profile based on matched field processing.

Matched field (MF) inversion is a nonlinear optimization technique that has been applied to various types of inverse problems in underwater acoustics [2]. For inverting geoacoustic profiles [3,4], the method proceeds by specifying the form of the geoacoustic model, and then searching the multi-dimensional model parameter space for the set of values that optimizes a cost function. The cost function is based on the MF correlation between measured and replica acoustic fields that are calculated for a specific experimental geometry. Simulated annealing is used to provide an efficient method for searching the parameter space, which can be very large for realistic models. Because MF inversion is based on accurate modelling of wave propagation in the elastic media that define the environment, the data for each source/receiver position provide an estimate of the geoacoustic profile. In contrast, other techniques [1] in widespread use for seismic inversion involve a set of measurements that are made as the relative distance between the source and receiver is changed.

2. EXPERIMENT

The experiment was carried out using two ships at a thin-sediment site near 37° N 133.5° W in the North Pacific, where the crustal age was 42 million years, and the water depth was ~5000m. The bottom topography was characteristic of abyssal hills, with local rms roughness from 5–15m and sediment thickness from <5–20m over the experimental track. The data were obtained in a shot run using 0.8 kg charges deployed at nominal depths of 244m out to a range of 40 km. The shot spacing was designed to provide measurements of the bottom reflectivity at intervals of 2° from 80° to <10°. The shot signals were recorded digitally at a 16-element vertical line array suspended in the sound channel; the hydrophone spacing was 45m, and the topmost element was at a depth of 377m. Ranges between the shots and the array were determined from measurements using a radio trisponder system on the ships.

The MF inversion for the geoacoustic profile of the upper oceanic crust is based on the acoustic field measurements obtained at the vertical line array for a shot at a range of 16.8 km. The array data were processed using an FFT processor to obtain the cross-spectral matrix for the spectral component at 20 Hz. This very low frequency was used to minimize the effect of experimental uncertainty in the range and hydrophone depths, and to reduce the computational load on calculating the acoustic fields.

3. MATCHED FIELD INVERSION

The components of the MF inversion method include 1) a geoacoustic model, 2) a propagation model for calculating replica acoustic fields, 3) a cost function based on a MF processor for assessing specific models, and 4) an efficient search algorithm for searching the model parameter space. For this work, the geoacoustic model consisted of three layers: a water layer, an elastic upper crust layer with constant sound speed gradients, and an underlying homogeneous elastic substrate. The model parameters for the upper crust included the thickness, h, the density, ρ, the sound speeds, c, and their gradients, g, and attenuations, α, of the compressional (p) and shear (s) waves propagating in the layer (Fig. 1). This model is a realistic approximation to the layer 2A upper crust environment in the Pacific [5].

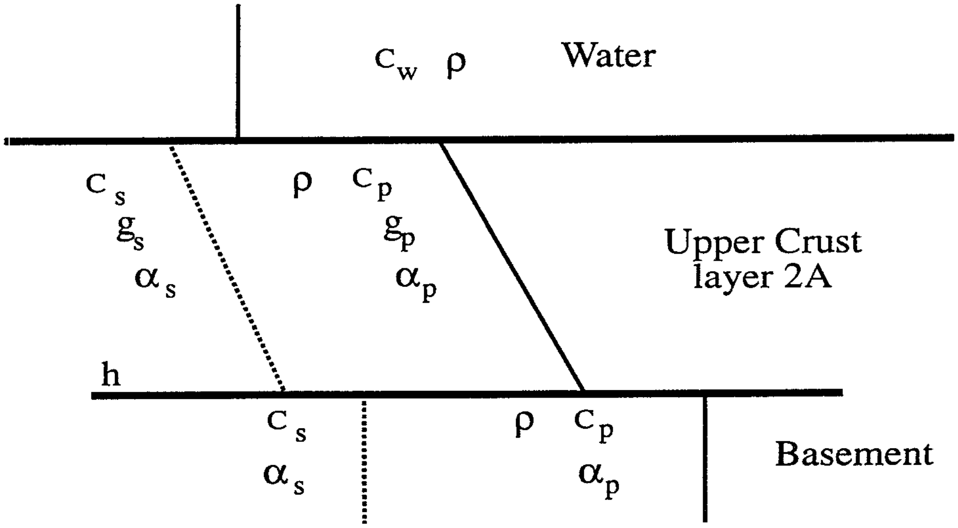

Figure 1. Geoacoustic model for the upper oceanic crust.

The cost function, E(m), is based on the Bartlett MF processor which describes the correlation between the measured and replica acoustic fields. It is given by

$$E(m) = 1 - p^*(m) R p(m) \quad (1)$$

where R is the cross-spectral matrix for the data and p(m) is the replica field calculated for a specific model, m. The replicas were calculated using the normal mode model KRAKENC [6]; this model uses a complex root finder to locate the discrete complex wavenumbers corresponding to the modes of an elastic waveguide.

To estimate the model parameter values, simulated annealing was used to search the model parameter space for the optimum solution. The search was initiated with random values for the parameters chosen within the imposed bounds; the inversion then proceeded through a series of iterations involving random perturbations of the model parameters, as a control parameter analogous to the temperature was reduced. Perturbations that decreased the cost function were accepted unconditionally. Those that increased the cost function were accepted conditionally, with probability of acceptance given by the Boltzmann distribution

$$P(\Delta E_i) = \exp(-\Delta E_i / s_i T) \tag{2}$$

where s_i is a scale factor for the i^{th} parameter and T is the control parameter. The scale factor accounts for the different sensitivities of the model parameters, so that all parameters converge at about the same rate. The temperature was reduced according to the schedule

$$T_{j+1} = \gamma^{j+1} T_0, \text{ with } \gamma \leq 1 \tag{3}$$

and at each temperature step the inversion cycled through the set of parameters twice. The parameter perturbations were selected according to

$$m_i = m_i + a^{j-1} \xi \delta_i, \qquad j=1,2,\ldots \tag{4}$$

where ξ is a random number from a uniform distribution on [-1,1], δ_i is the maximum perturbation for the i^{th} parameter and $a \leq 1$ is a scale factor to gradually decrease the size of the perturbations as the temperature decreases.

3. SIMULATION

Prior to the analysis of the experimental data, a simulation was carried out at a frequency of 20 Hz to determine the sensitivity of the thirteen geoacoustic model parameters. The water layer was described by a sound speed profile measured during the experiment, and a canonical geoacoustic profile was used for the upper crust. The annealing process consisted of 200 temperature steps using a cooling schedule with $T_0 = 0.23$, $\gamma = 0.94$, and $a = 0.98$. Keeping in mind that the propagating modes must be determined in each iteration, the annealing process was computationally intensive. This simulation took over 12 hours on a VAX 9000.

The cooling curve for E(m) shown in Fig. 2a indicates that a high degree of correlation was obtained after about 3000 iterations. Similar results are presented in Fig. 3a where the accepted model parameter values are plotted versus iteration number for three of the most sensitive parameters; the horizontal line corresponds to the true value.

The most sensitive parameters were the layer thickness, the upper crust sound speeds and gradients, and the substrate sound speeds. For these parameters, the estimated values were within ± 3% of the true values, indicating very close agreement . Other parameters such as the densities, and all the attenuations were increasingly less sensitive, although in some cases good results were obtained. In general, however, stable values had not been frozen out for these latter parameters even after nearly 5000 iterations.

4. EXPERIMENTAL DATA

4.1 MF inversion

The inversion method was applied to the shot data using the same cooling schedule as described above. The parameter bounds, the maximum perturbation size, and the sensitivities (based on the simulation results) are listed in Table 1. For this set of parameter values, the North Pacific environment supported ~120 modes. The cooling curve shown in Fig. 2b for the cost function indicates that a stable result corresponding to a matched field correlation of ~0.7 was obtained after 2000 iterations. This relatively low correlation is likely associated with mismatch in the experimental geometry. The best results were obtained for the thickness, and the sound speeds and gradients of the upper crust. For these parameters, stable values were obtained after around 2500 iterations, as shown in Fig. 3b for the upper crust thickness and sound speeds. The final model is listed in Table 1; the errors were estimated from the variance of the cooling curves for each parameter. These results are consistent with estimates from recent seismic experiments designed to study the structure of the upper crust in the Pacific [5].

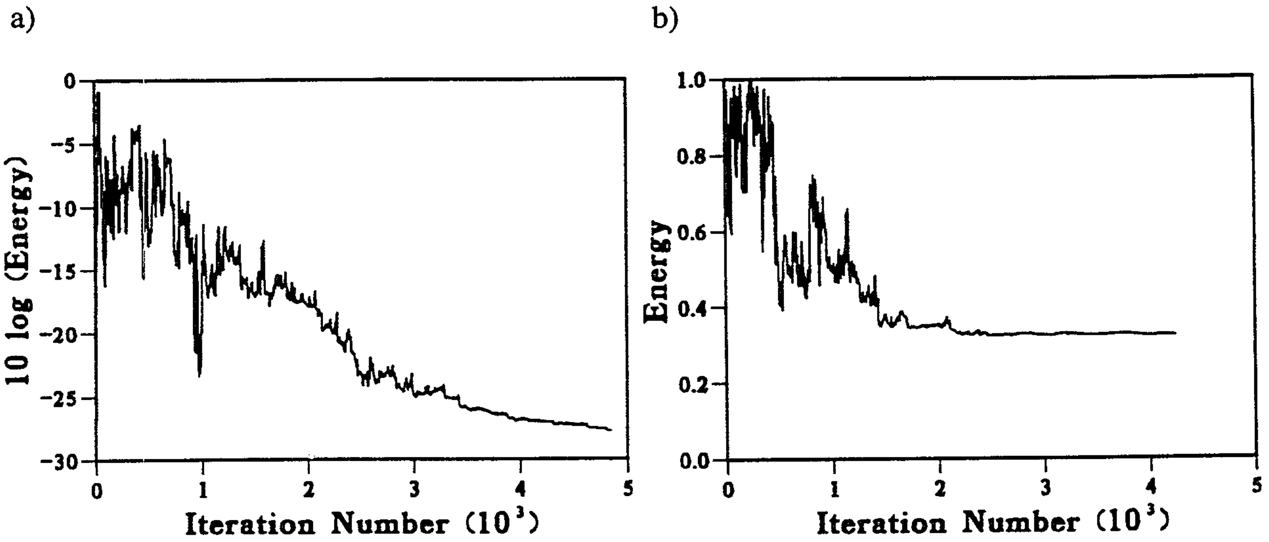

Figure 2. Cooling curves for the cost function E(m): (a) simulation; (b) data.

Table 1. Summary of matched field inversion results using experimental data: m_i represents the model parameters, s_i are the temperature scale factors, and δ_i are the maximum pertubations.

m_i	Bounds	s_i	δ_i	Estimated value
Upper Crust				
h (m)	(0, 350)	1.0	100	180 ± 10
c_p (m/s)	(2500, 3000)	1.0	100	2690 ± 25
c_s (m/s)	(1250, 1500)	1.0	100	1340 ± 25
g_p (1/s)	(0.3, 1.0)	1.0	0.3	0.9 ± 0.1
g_s (1/s)	(0.3, 2.5)	1.0	0.3	0.8 ± 0.1
ρ (gm/cm^3)	(2.0, 2.4)	0.8	0.15	2.3 ± .15
α_p(dB/λ)	(0.1, 0.4)	0.6	0.2	0.3 ± 0.2
α_s(dB/λ)	(0.3, 0.9)	0.6	0.2	0.8 ± 0.2
Substrate				
c_p (m/s)	(3500, 4000)	1.0	100	3550 ± 100
c_s (m/s)	(1700, 2000)	1.0	100	1940 ± 100
ρ (gm/cm^3)	(2.4, 2.7)	0.6	0.2	2.5 ± 0.2
α_p(dB/λ)	(0.1, 0.4)	0.6	0.2	0.3 ± 0.2
α_s(dB/λ)	(0.3, 0.9)	0.6	0.2	0.7 ± 0.2

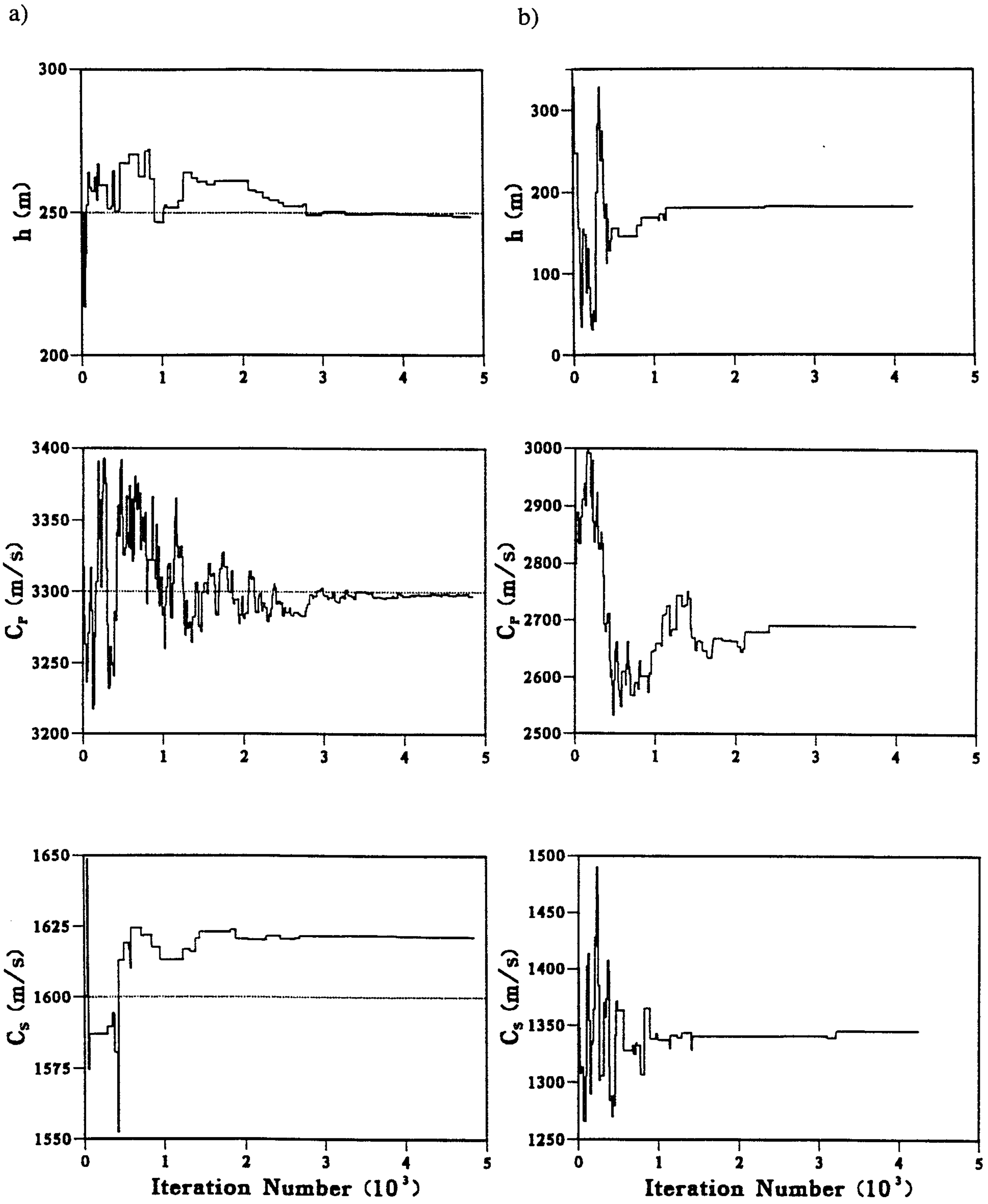

Figure 3. Convergence of geoacoustic model parameters. The accepted values for the upper crust thickness, and the p and s wave sound speeds are plotted versus iteration number for: (a) simulation; (b) data.

4.2 Comparison with amplitude inversion

The model presented in Table 1 was compared with estimates based on an inversion of reflection loss versus angle data that were obtained in the same experiment. This inversion is sensitive to the properties of the topmost portion of the upper crust, and is based on an elastic half-space geoacoustic model [7]. The estimated values for the upper crust p and s wave sound speeds were 2.7 km/s and 1.3 km/s, respectively, and 2.4 gm/cm^3 for the density. These results are in very close agreement with those from the MF inversion.

5. SUMMARY

Matched field inversion with simulated annealing has been applied to VLA data from an experiment in the North Pacific in order to estimate the geoacoustic profile for the upper oceanic crust. Stable estimates were obtained for the p and s wave sound speeds and gradients and for the layer thickness. The results were in close agreement with estimates from a reflection coefficient amplitude inversion, and were generally consistent with results from recent seismic studies of the upper crust.

REFERENCES

1. P. Carrion, Inverse Problems and Tomography in Acoustics and Seismology, Penn Publishing, Atlanta, 1987.
2. A. Tolstoy, Matched Field Processing for Underwater Acoustics, World Scientific Monograph, New York, 1993.
3. M.D. Collins, W.A. Kuperman, and H. Schmidt, J. Acoust. Soc. Am., 92, 2770-2783, 1992.
4. S.E. Dosso, M.L. Yeremy, J.M. Ozard, and N.R. Chapman, IEEE J. Oceanic Eng., 18, 232-239, 1993.
5. R.S. Jacobson, Reviews of Geophysics, 30, 23-42, 1992.
6. M.A. Porter and E.L. Reiss, J. Acoust. Soc. Am., 77, 1760-1767, 1985.
7. N.R. Chapman and K. Rohr, pp 537-544, in Shear Waves in Marine Sediments, J.M. Hovem, M.D. Richardson and R.D. Stoll, (eds), Kluwer Academic Press, Dordrecht, 1991.

MATCHED FIELD INVERSION FOR GEOACOUSTIC PROPERTIES OF YOUNG OCEANIC CRUST

N. R. CHAPMAN and K. S. OZARD
Defence Research Establishment Pacific
FMO Victoria, B.C. Canada
V0S 1B0

ABSTRACT A geoacoustic profile for young oceanic crust has been estimated from experimental data using matched field inversion with simulated annealing. The effect of errors in experimental geometry was investigated, and the inversion performance was significantly improved by including geometrical parameters such as range in the simulated annealing search algorithm.

Introduction

Matched field (MF) processing has been applied to a wide variety of inverse problems in underwater acoustics [1]. Geoacoustic properties of the ocean bottom have been estimated by MF inversion using acoustic field data for specific experimental geometries [2,3]. The inversion proceeds by specifying a set of geoacoustic models, and then searching the model parameter space to obtain the best correlation between measured and modelled acoustic fields. The practical application of the inversion depends in part on having an efficient method for searching the multi-dimensional space of ocean bottom models. In this paper, simulated annealing is used as the search algorithm in an investigation using MF inversion of vertical line array (VLA) data to determine geoacoustic profiles for young oceanic crust. The inversion is capable of estimating both the compressional and shear properties of the basalt.

Successful inversion requires that the experimental geometry be accurately known, however, there is usually some degree of uncertainty in the measurements of the variables that define the experimental arrangement. In general, the inversion performance is sensitive to mismatch in the range, water depth, and array tilt. The effect of errors in the experimental geometry on the model parameter estimation was investigated in a simulation study using a range-independent ocean bottom consisting of a fluid sediment layer over an elastic basement. The relatively high sensitivity to geometrical mismatch indicated that the experimental uncertainties could be tolerated in the inversion by including variables such as the range and depth as parameters in the search process. This approach is an application of the concept of 'focalization' [4].

In the remainder of the paper, the method for MF inversion is described, and the results of the simulation study on the effect of geometrical errors are presented. Following this, the MF inversion method, including focalization, is applied to experimental data that were obtained at a deep water site near the Juan de Fuca Ridge, and the results are summarized.

Matched Field Inversion

The components of the matched field inversion method include a geoacoustic model, a propagation model for calculating the acoustic field at the receiver, a cost function based on a matched field processor for assessing specific models, and an efficient search algorithm for searching the model parameter space. For this work, the geoacoustic model consisted of three layers; a water layer, a homogeneous fluid sediment layer, and an underlying homogeneous elastic upper crust. The sediment layer was described by the thickness, h, the density, ρ, and the sound speed, c, and attenuation, α; the upper crust was descibed by the density and the sound speed and attenuation of the compressional (p) and shear (s) waves propagating in the layer (Fig. 1). The form of this model is a realistic approximation to the layer 2A upper crust environment for the experimental site [5].

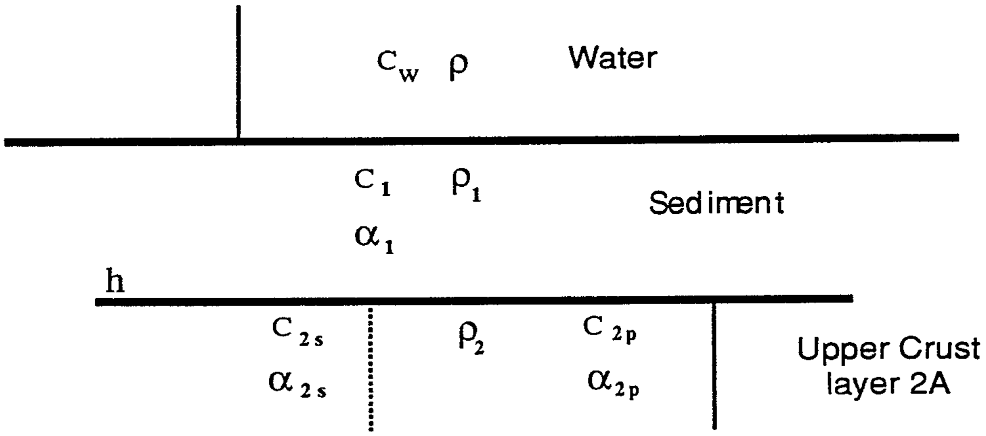

Fig. 1. Geoacoustic model for the upper crust at the experimental site.

The cost function, $E(m)$, is based on the Bartlett matched field processor which describes the correlation between the measured and modelled acoustic fields. It is given by

$$E(m) = p^{*}(m)Rp(m) \tag{1}$$

where R is the cross-spectral matrix and $p(m)$ is the modelled field calculated for a specific model, m. Although the Bartlett processor has low resolution and high sidelobes, it is robust under conditions of noise and mismatch. The modelled fields were calculated using the normal mode model KRAKENC [6]; this model uses a complex root finder to locate the discrete complex wavenumbers corresponding to the modes of an elastic waveguide.

To estimate the model parameter values, simulated annealing was used to search the model parameter space for the optimum solution. The search was initiated with random values for the parameters chosen from the imposed bounds; the inversion then proceeded through a series of iterations involving random perturbations of the model parameters, as a control parameter analogous to the temperature was reduced. Perturbations that decreased the cost function were accepted unconditionally. Those that increased the cost function were accepted conditionally, with probability of acceptance given by the Boltzmann distribution

$$P(\Delta E_i) = \exp(-\Delta E / s_i T) \qquad (2)$$

where s_i is a scale factor for the i$^{\text{th}}$ parameter and T is the control parameter. The scale factor accounts for the different sensitivities of the model parameters, so that all parameters converge at about the same rate. The temperature was reduced according to the schedule

$$T_{j+1} = \gamma^{j+1} T_0, \text{ with } \gamma \leq 1, \text{ and } j = 0,1,... \qquad (3)$$

The parameter perturbations were selected according to

$$m_i = m_i + \xi^3 \delta_i \qquad (4)$$

where ξ is a random number from a uniform distribution on [-1,1], and δ_i is the maximum perturbation for the i$^{\text{th}}$ parameter.

Simulations

The simulations were carried out for a VLA consisting of 16 hydrophones spaced 45 m apart, with the top element at a depth of 200 m. The array was located 2 km from a 10-Hz CW sound source at a depth of 46 m. The geoacoustic profile was designed to model the ocean environment at the experimental site. The ocean bottom consisted of two homogeneous layers: a sediment layer that was 75 m thick, with density 1.8 g/cm^3, sound speed 1600 m/s, and attenuation 0.2 dB/λ; and an elastic half-space upper crust with density 2.4 g/cm^3, p-wave speed 2700 m/s, s-wave speed 1250 m/s and both attenuations 0.1 dB/λ. The sound speed profile for the water column was a profile measured during the experiment, which was truncated at a depth of 1000 m. For this environment, there were 14 modes at 10 Hz.

Initially a study was carried out to determine the sensitivity of the Bartlett processor to the model parameters. Each parameter was tested separately, while all the others were fixed at their true values. The sediment layer thickness and the upper crust p-wave speed were the most sensitive, followed by the sediment sound speed and the upper crust s-wave speed. The least sensitive parameters were the densities and attenuations for both layers; the attenuations were fixed at their true values for all the inversions. Similar tests indicated that the sensitivities for geometrical parameters such as the range, ocean depth and array depth were equivalent to those for the most sensitive geoacoustic parameters. The results for an inversion under ideal conditions of no mismatch are shown in Table 1. The final correlation after 2500 iterations was 0.9961.

The effect of range errors was investigated in inversions for which the modelled fields were calculated at array locations that were shifted by 1/3, 2/3 and 4/3 wavelengths from the true range. The results are shown in Table 2. Using the final MF correlation and the error in the estimate for the most sensitive parameter as a measure of the effect, it is evident that both the correlation and the accuracy are significantly decreased. The high sensitivity to range error indicated that the uncertainty could be tolerated in the inversion by including the range as a search parameter. In this approach, the inversion simultaneously localizes the source and estimates the optimum parameters of the waveguide model [4]. A simulation was carried out to search the range over a 50-m range mismatch, and the results are shown in the last column of Table 2. The range was estimated to within 3 per cent of the error, and the final MF correlation and the errors in the model parameter estimates were comparable to those for the ideal case.

Table 1. MF inversion estimates for the ideal case of no mismatch.

m_i	**True Value**	**Bounds**	**s_i**	**Estimate**
h (m)	75	(50 - 100)	1.0	77.8
c_1 (m/s)	1600	(1500 - 1700	10.0	1596
c_{2p} (m/s)	2700	(2500 - 2900)	1.0	2658
c_{2s} (m/s)	1250	(1050 - 1450)	10.0	1285
ρ_1 (g/cm^3)	1.8	(1.6 - 2.0)	100	1.8
ρ_2 (g/cm^3)	2.4	(2.1 - 2.7)	100	2.2

Table 2. Effect of range error on MF inversion estimates.

m_i	**1/3 λ**	**2/3 λ**	**4/3 λ**	**Range Search**
Correlation	0.9527	0.8476	0.6495	0.9977
h (m)	67.0	59.3	56.6	78.0
c_1 (m/s)	1608	1530	1700	1580
c_{2p} (m/s)	2751	2893	2895	2766
c_{2s} (m/s)	1097	1264	1119	1201
ρ_1 (g/cm^3)	1.6	1.7	1.6	1.8
ρ_2 (g/cm^3)	2.2	2.4	2.2	2.2
Range (km)	-	-	-	2.00

Experimental Data Inversion

The data were obtained in an experiment carried out using two ships at a site near the Juan de Fuca Ridge in the Northeast Pacific. One ship monitored a 16-element, 675-m VLA that was suspended at a depth of 413 m, and the other ship towed a 10-Hz CW sound source at a depth of 46.3 m in an arc at a radius of 5.5 km from the VLA. The range was determined from GPS navigation measurements that were recorded on each ship, and the ocean depth was measured using a 3.5-kHz profiler on the source ship. The VLA data were processed using a 4K FFT to obtain the spectral components at 10 Hz, and cross spectral averages were then formed for a two minute time period.

The inversion was performed for a range independent waveguide of depth 2660 m using the geoacoustic model in figure 1. Based on the results of the simulations, the range was included as a search parameter, and four other model parameters were estimated. The insensitive parameters were held fixed at values of $\rho_1 = 1.55$ g/cm^3, $c_1 =$ 1550 m/s, and $\alpha_1 = 0.2$ dB/λ for the sediment, and $\alpha_2 = 0.1$ dB/λ for both attenuations in the upper crust. There were approximately 35 modes for this environment. The estimated values after 10000 iterations are listed in Table 3, along with the sensitivity scale factors. The accepted values for each parameter are plotted versus iteration number in Fig. 2; for this case, the search converged after about 6000 iterations. The VLA range is in excellent agreement with the GPS measurement of 5.45 km. The sound speeds are consistent with recent data for young crust of age 1-2 million years [7], and the density is also within expected limits [8]. The relatively low value for the final MF correlation,

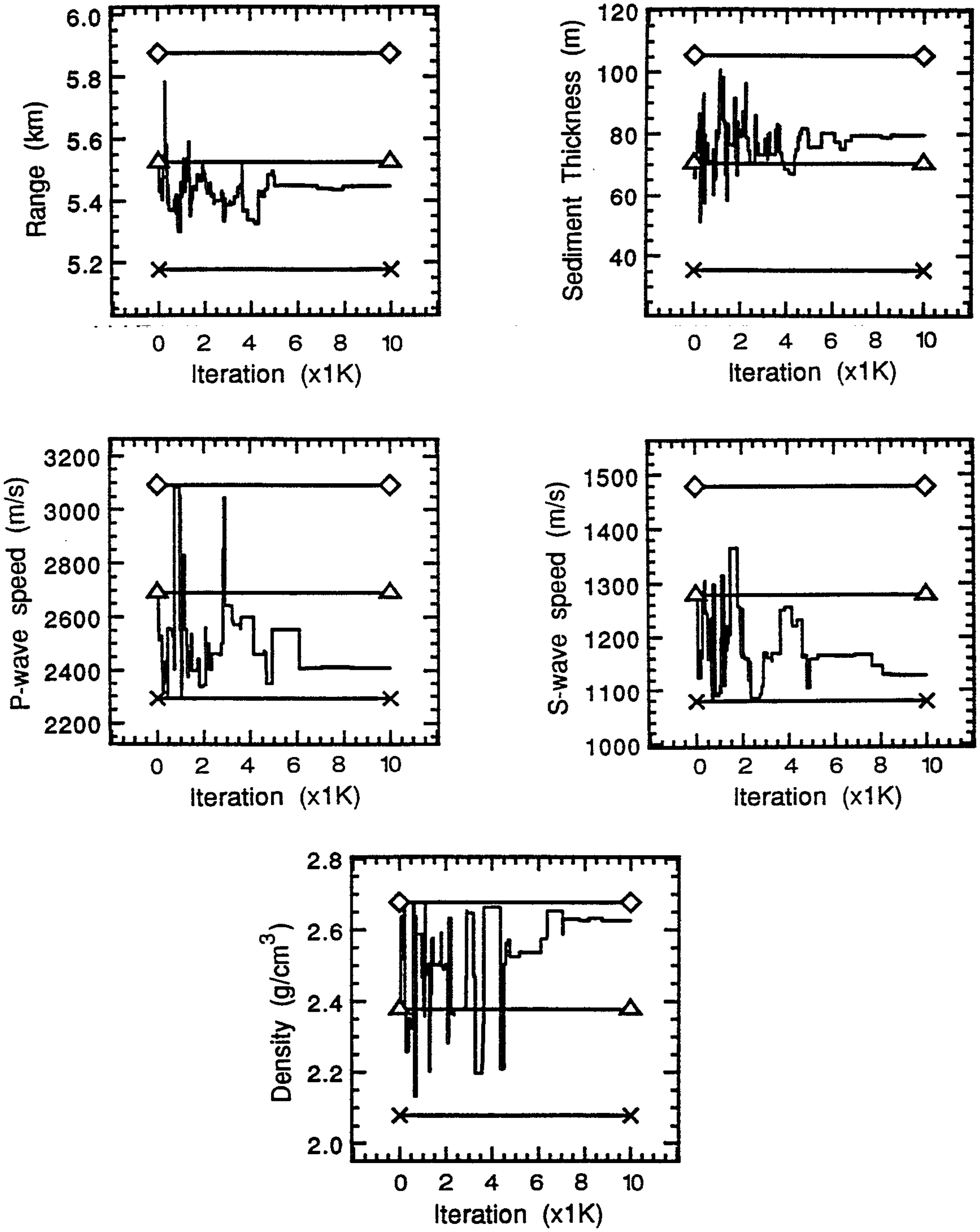

Fig. 2. Accepted values for the range, sediment thickness, and the upper crust p-wave speed, s-wave speed and density. Search limits are shown by the horizontal bars.

0.58, indicates that there is some degree of mismatch. This could be due to effects such as array tilt and range dependence in the waveguide.

Table 3. MF inversion for data from young crustal site.

m_i	Bounds	s_i	Estimate
Range (km)	(5.2 - 5.9)	0.4	5.44
h (m)	(35 - 110)	1.0	79.0
c_{2p} (m/s)	(2300 - 3100)	1.1	2410
c_{2s} (m/s)	(1050 - 1500)	3.0	1128
ρ_2 (g/cm^3)	(2.1 - 2.7)	48.6	2.6

Summary

The effect of uncertainties in experimental geometry has been investigated for matched field inversion for geoacoustic properties of the ocean bottom. Simulations that were carried out for a VLA indicated that the inversion performance was highly sensitive to range errors. However, the uncertainty could be tolerated in the inversion by including the range as a parameter in the simulated annealing search process. The inversion, including the concept of focalization, was applied to estimate a geoacoustic profile for upper oceanic crust at a site near the Juan de Fuca Ridge where the age of the basalt is very young. The estimate for the p-wave speed is consistent with the low values that have been observed for young crust at other sites. In addition, the method provides a means of estimating the shear wave speed.

References

1. Tolstoy, A. (1993) *Matched Field Processing for Underwater Acoustics*, World Scientific Monograph, New York.
2. Collins, M.D., Kuperman, W.A., and Schmidt, H. (1992) Nonlinear inversion for ocean-bottom properties, *J. Acoust. Soc. Am.*, **92**, 2770-2783.
3. Dosso, S.E., Yeremy, M.L., Ozard, J.M. and Chapman, N.R. (1993) Estimation of ocean bottom properties by matched field inversion of acoustic field data, *IEEE J. Oceanic Eng.*, **18**, 232-239.
4. Collins, M.D. and Kuperman, W.A. (1991) Focalization: Environmental focussing and source localization, *J. Acoust. Soc. Am.*, **90**, 1410-1422.
5. Cudrak, C.F. and Clowes, R.M. (1993) Crustal structure of Endeavour Ridge segment, Juan de Fuca Ridge, from a detailed seismic refraction survey, *J. Geophys. Res.*, **98**, 6329-6349.
6. Porter, M.A. and Reiss, E.L. (1985) A numerical model for bottom interacting ocean acoustic normal modes, *J. Acoust. Soc. Am.*, **77**, 1760-1767.
7. Jacobson, R.S. (1992) The impact of crustal evolution on changes of the seismic properties of the uppermost ocean crust, *Reviews of Geophysics*, **30**, 23-42.
8. Hamilton, E.L. (1980) Geoacoustic modelling of the sea floor, *J. Acoust. Soc. Am.*, **68**, 1313-1340.

DISTRIBUTION

REPORT NUMBER: 94 - 151

TITLE: The PACIFIC ECHO Sea Trials
DREP/NRL: 1986-92

AUTHORS: N.R. Chapman, J.A. Fawcett and M.L. Yeremy

DATED:

1 -	DSIS	
1 -	DRDM	
1 -	DMCS-3	
1 -	DMOR	
3 -	DREA	Library D.M.F. Chapman D.D. Ellis
14 -	DREP	Library J. Kennedy G. Brooke N.R. Chapman (5) S.E. Dosso G. Ebbeson D.J. Thomson J.M. Ozard M.L. Yeremy G. Heard
10 -	SACLANTCEN Undersea Research Centre	A. Caiti O. Diachok J.P. Hermand S. Jesus D. Bradley F. Jensen D. Gingras P. Gerstoft J. Fawcett W. Roderick
1 -	ARPA	W. Carey

3 -	NRL	A. Tolstoy P. Mingerey J. Perkins
3 -	ONR	T. Goldsberry M. Badiey R.S. Jacobson
4 -	NRaD	M. Morrison N. Booth H. Bucker J. Rice
2 -	NUWC	E. Sullivan D. Lee
2 -	Woods Hole Oceanographic Institution	G.V. Frisk J. Doutt
2 -	Massachusetts Institute of Technology	A. Baggeroer H. Schmidt
3 -	Marine Physical Laboratory	W. Hodgkiss W.A. Kuperman M. Buckingham
2 -	ARL:UT	E. Westwood N. Bedford
1 -	Centre for Applied Math and Statistics	M. Porter
1 -	Thomson Sintra ASM (France)	G. Bienvenu
1 -	NDRE (Norway)	J. Glattetre
2 -	Institute of Applied and Computational Math (Greece)	M. Taroudakis N. Kampanis
1 -	DSE (New Zealand)	R. Marrett

2 - WSRL (Australia)
R. Barrett
L. Kelly

DOCUMENT CONTROL DATA

(Security classification of title, body of abstract and indexing annotation must be entered when the overall document is classified)

1 ORIGINATOR (the name and address of the organization preparing the document. Organizations for whom the document was prepared, e.g. Establishment sponsoring a contractor's report, or tasking agency, are entered in section 8.) Defence Research Establishment Pacific FMO Victoria, B.C. VOS 1BO	2. SECURITY CLASSIFICATION (overall security classification of the document including special warning terms if applicable) Unclas

3. TITLE (the complete document title as indicated on the title page. Its classification should be indicated by the appropriate abbreviation (S,C or U) in parentheses after the title.)

The Pacific Echo Sea Trials DREP/NRL: 1986 - 92 (U)

4 AUTHORS (Last name, first name, middle initial)

Chapman, N.R., Fawcett, J.A. and Yeremy, M.L.

5 DATE OF PUBLICATION (month and year of publication of document) December 1994	6a. NO. OF PAGES (total containing information. Include Annexes, Appendices, etc.) 115	6b. NO. OF REFS (total cited in document) 20

7 DESCRIPTIVE NOTES (the category of the document, e.g. technical report, technical note or memorandum. If appropriate, enter the type of report, e.g. interim, progress, summary, annual or final. Give the inclusive dates when a specific reporting period is covered.)

Technical Memorandum

8. SPONSORING ACTIVITY (the name of the department project office or laboratory sponsoring the research and development. Include the address.)

DRDM

9a PROJECT OR GRANT NO. (if appropriate, the applicable research and development project or grant number under which the document was written. Please specify whether project or grant) DRDM-08	9b. CONTRACT NO. (if appropriate, the applicable number under which the document was written)
10a. ORIGINATOR'S DOCUMENT NUMBER (the official document number by which the document is identified by the originating activity. This number must be unique to this document.) DREP TM 94-151	10b. OTHER DOCUMENT NOS. (Any other numbers which may be assigned this document either by the originator or by the sponsor)

11. DOCUMENT AVAILABILITY (any limitations on further dissemination of the document, other than those imposed by security classification)

(X) Unlimited distribution
( ) Distribution limited to defence departments and defence contractors; further distribution only as approved
( ) Distribution limited to defence departments and Canadian defence contractors; further distribution only as approved
( ) Distribution limited to government departments and agencies; further distribution only as approved
( ) Distribution limited to defence departments; further distribution only as approved
( ) Other (please specify):

12. DOCUMENT ANNOUNCEMENT (any limitation to the bibliographic announcement of this document. This will normally correspond to the Document Availabilty (11). However, where further distribution (beyond the audience specified in 11) is possible, a wider announcement audience may be selected.)

13. ABSTRACT (a brief and factual summary of the document. It may also appear elsewhere in the body of the document itself. It is highly desirable that the abstract of classified documents be unclassified. Each paragraph of the abstract shall begin with an indication of the security classification of the information in the paragraph (unless the document itself is unclassified) represented as (S), (C), or (U). It is not necessary to include here abstracts in both offical languages unless the text is bilingual).

The PACIFIC ECHO sea trials comprised a series of collaborative experiments between the Defence Research Establishment Pacific and the Naval Research Laboratory from 1986-92. The general objective of the experiments was to investigate matched field processing for source localization and geoacoustic inversion. The experiments were carried out in thin sediment environments in the North Pacific. Much of the data analysis carried out at DREP over the years has been reported primarily at meetings of Technical Panel TTCP GTP-9, and has not been widely distributed. This report provides a brief summary of the PACIFIC ECHO sea trials, and includes the collection of DREP papers on the analysis of the PACIFIC ECHO data in appendices.

14. KEYWORDS, DESCRIPTORS or IDENTIFIERS (technically meaningful terms or short phrases that characterize a document and could be helpful in cataloguing the document. They should be selected so that no security classification is required. Identifiers, such as equipment model designation, trade name, military project code name, geographic location may also be included. If possible keywords should be selected from a published thesaurus. e.g. Thesaurus of Engineering and Scientific Terms (TEST) and that thesaurus-identified. If it is not possible to select indexing terms which are Unclassified, the classification of each should be indicated as with the title.)

PACIFIC ECHO
Matched Field Processing
Source Localization
Vertical Line Arrays
Horizontal Line Array
Ocean Bottom Reflectivity
Geoacoustic Inversion

#150979

NO. OF COPIES NOMBRE DE COPIES 1	COPY NO. COPIE N° 1	INFORMATION SCIENTIST'S INITIALS INITIALES DE L'AGENT D'INFORMATION SCIENTIFIQUE JC
AQUISITION ROUTE FOURNI PAR ▶	DREP	
DATE ▶	31 Mar 95	
DSIS ACCESSION NO. NUMÉRO DSIS ▶		

DND 1158 (6-87)

National Defence Défense nationale

PLEASE RETURN THIS DOCUMENT TO THE FOLLOWING ADDRESS:

DIRECTOR
SCIENTIFIC INFORMATION SERVICES
NATIONAL DEFENCE
HEADQUARTERS
OTTAWA, ONT. - CANADA K1A 0K2

PRIÈRE DE RETOURNER CE DOCUMENT À L'ADRESSE SUIVANTE:

DIRECTEUR
SERVICES D'INFORMATION SCIENTIFIQUES
QUARTIER GÉNÉRAL
DE LA DÉFENSE NATIONALE
OTTAWA, ONT. - CANADA K1A 0K2